INVESTIGATIONS ON IMP2-2 AND KUPFFER CELLS IN STEATOHEPATITIS

Dissertation

zur Erlangung des Grades
des Doktors der Naturwissenschaften
der Naturwissenschaftlich-Technischen Fakultät
der Universität des Saarlandes

von

Dipl.-Biol. Beate Martha Czepukojc

Saarbrücken

2019

Tag des Kolloquiums: 24.10.2019

Dekan: Prof. Dr. G. Kickelbick

1. Berichterstatter: Prof. Dr. A. K. Kiemer

2. Berichterstatter: Prof. Dr. J. E. Walter

Vorsitz: Prof. Dr. U. Müller

Akad. Mitarbeiter: Dr. M. Engel

Table of content

Abbreviations

(v/v)	Volume per volume		DOR	Differentially open chromatin region
(w/v)	Weight per volume		DW	Drinking water
A	Ampere		ECM	Extracellular matrix
aa	Amino acids		EDTA	Ethylenediamine-N,N,N,N'-tetra acid
AFL	Alcoholic fatty liver		ER	Endoplasmic reticulum
AFLD	Alcoholic fatty liver disease		ESI-MS/MS	Electrospray ionization tandem mass spectrometry
ALT	Alanine-aminotransferase		EU	Endotoxin units
AMPK	Adenosine monophosphate-activated protein kinase		FA	Fatty acid
APS	Ammonium persulfate		FDR	False discovery rate
ASH	Alcoholic steatohepatitis		FFA	Free fatty acids
AST	Aspartate transaminase		Gilz	Glucocorticoid-induced leucine zipper
bp	Base pair		GO	Gene ontology
c	Concentration		h	Hour
cDNA	Complementary DNA		HCC	Hepatocellular carcinoma
CE	Cholesteryl ester		HDL	High-density lipoprotein
CER	Ceramides		HE	Hematoxylin and eosin
clo	Clodronate liposome		HFD	High-fat diet
co	Control		HSC	Hepatic stellate cells
CpG	Undermethylated 5'-CG-3' sequences		i.p.	Intraperitoneal
CSC	Cancer stem cell		IGF	Insulin-like growth factor
DEG	Differentially expressed gene		Il1β	Interleukin 1 beta
DEN	Diethylnitrosamine		Il6	Interleukin 6
DEPC	Diethyl dicarbonate		IMP	IGF2 mRNA binding protein
DMR	Differentially methylated region		IR	Insulin resistance
DNA	Deoxyribonucleic acid		KCs	Kupffer cells
DNase	Deoxyribonuclease		kcal	Kilocalories
DNMT	DNA methyltransferase		kDa	Kilo Dalton
dNTP	Deoxyribonucleosidtriphosphate		KEGG	Kyoto Encyclopedia of Genes and Genomes

KH	hnRPN K homology domain	RNA	Ribonucleic acid
LDC	Lieber-DeCarli	ROS	Reactive oxygen species
LPC	Lysophosphatidylcholine	RRBS	Reduced representative bisulfite sequencing
LPS	Lipopolysaccharide	RRM	RNA recognition motif
m	Mass	s	Seconds
M	Molar	SAM	S-adenosylmethionine
MCD	Methionine-choline-deficient	sat	Saturated species
miRNA	microRNA	SDS	Sodium dodecyl sulfate
mRNA	Messenger ribonucleic acid	SEM	Standard error of mean
n.s.	Not significant	SM	Sphingomyelin
NAFL	Non-alcoholic fatty liver	SNP	Single nucleotide polymorphism
NAFLD	Non-alcoholic fatty liver disease	TBE	Tris-boric acid-EDTA buffer
NASH	Non-alcoholic steatohepatitis	TE	Tris-EDTA buffer
NPC	Non-parenchymal cell	TG	Triglyceride
OGC	Observed gene count	tg	Transgenic
PAGE	Polyacrylamide gel electrophoresis	TLC	Thin-layer chromatography
PBS	Phosphate buffered saline	TLR4	Toll-like receptor 4
PBST	Phosphate buffered saline with Tween 20	Tnfα	Tumor necrosis factor alpha
PC	Phosphatidylcholine	Tris	A,α,α-tris-(hydroxymethyl)-methylamine
PE	Phosphatidylethanolamine	U	Units
PE P	PE-based plasmalogens	unsat	Unsaturated species
PG	Phosphatidylglycerol	UPR	Unfolded protein response
PI	Phosphatidylinositol	V	Volt
PPAR	Peroxisome proliferator-activating receptors	VLDL	Very-low-density lipoprotein
PS	Phosphatidylserine	wk	Weeks
qPCR	Quantitative polymerase chain reaction	wt	Wild type
RBB	Rockland blocking buffer	*g*	gravitational force

Abstract

Alcoholic and non-alcoholic steatohepatitis (ASH and NASH) represent risk factors for the development of hepatocellular carcinoma. The prevalence of ASH and NASH is strongly increasing worldwide. Within this work, different mechanisms responsible for steatohepatitis disease progression were elucidated in murine models.

The insulin-like growth factor 2 (*IGF2*) mRNA binding protein (IMP) p62/IMP2-2 was shown to promote progenitor or dedifferentiated cell populations in a model of NASH and thereby amplify fibrosis.

In diet-induced steatohepatitis, epigenetic alterations strongly affected genetic regions playing a role in lipid metabolism and liver morphology.

Depletion of Kupffer cells, the resident macrophages of the liver, induced liver damage and attenuated hepatic accumulation of storage lipids, while hepatotoxic lipids were incorporated.

Taken together, this work provides evidence that p62 promotes the appearance of undifferentiated or dedifferentiated cells and thereby disease progression and furthermore that macrophages are crucial in hepatic lipid homeostasis and protection of lipotoxicity.

Zusammenfassung

Die alkoholische und nicht-alkoholische Steatohepatitis (ASH und NASH) stellen Risikofaktoren für die Entwicklung eines hepatozellulären Karzinoms dar. Die Verbreitung von ASH und NASH nimmt weltweit stark zu. Innerhalb dieser Arbeit wurden verschiedene Mechanismen in Mausmodellen aufgeklärt, die für das Fortschreiten der Steatohepatitis Erkrankung verantwortlich sind.

Es wurde gezeigt, dass das Insulin-ähnliche Wachstumsfaktor 2 (IGF2) mRNA bindende Protein (IMP) p62/IMP2-2 das Auftreten hepatischer Progenitorzellen oder dedifferenzierter Zellpopulationen in einem NASH Modell fördert und dadurch eine Fibrose begünstigt.

In Diät-induzierter Steatohepatitis beeinflussten epigenetische Veränderungen genetische Regionen, die eine Rolle im Lipidstoffwechsel und in der Morphologie der Leber spielen.

Die Depletion von Kupffer-Zellen, den Makrophagen der Leber, rief Leberschäden hervor und verringerte die Menge an Speicherlipiden in der Leber, während hepatotoxische Lipide eingelagert wurden.

Zusammengefasst bietet diese Arbeit Hinweise darauf, dass p62 das Auftreten von undifferenzierten oder dedifferenzierten Zellen und damit den Krankheitsverlauf fördert und dass Makrophagen von entscheidender Bedeutung in der Lipidhomöostase der Leber und im Schutz vor Lipotoxizität sind.

1 BACKGROUND

1.1 NAFLD/AFLD - definition and prevalence

The liver contributes to a wide range of functions and possesses the capacity to regenerate. It is a central organ and gland for digestion, detoxification, and metabolism. One of its key roles is the lipid metabolism. Under healthy circumstances, excess lipids are exported out of the liver and transported *via* the circulation to adipose tissue. However, under pathological conditions, disruption of the normal mechanism for synthesis, transport, oxidation, and storage of lipids causes an accumulation of lipids in hepatocytes (Bradbury *et al.*, 2004).

An excessive accumulation of fat in the liver in more than 5% of hepatocytes according to the guidelines is termed steatosis (EASL, EASD, EASO, 2016), the main feature of fatty liver disease (FLD). According to its etiology, the FLD can be distinguished into non-alcoholic and alcoholic fatty liver disease. In both cases, a secondary cause of hepatic lipid accumulation, such as steatogenic medication, hereditary disorders, or virus infections, need to be excluded (Chalasani *et al.*, 2018).

Non-alcoholic fatty liver disease (NAFLD) was first described in 1980 and is nowadays diagnosed when heavy alcohol consumption can be excluded, as it is the case when daily intake is less than 20 g of ethanol for women and 30 g for men (Ludwig *et al.*, 1980; Ratziu *et al.*, 2010). The disease is commonly associated with metabolic comorbidities, such as obesity, type 2 diabetes, hypertension, and dyslipidemia. These features of the metabolic syndrome are highly prevalent in patients with NAFLD (Vernon *et al.*, 2011). Furthermore, an existing metabolic syndrome increases the risk of developing NAFLD, proposing it as the hepatic manifestation of the metabolic syndrome (Neuschwander-Tetri, 2005; Younossi *et al.*, 2011; Byrne *et al.*, 2015).

Alcoholic fatty liver disease (AFLD) is caused by excessive alcohol consumption (Mann *et al.*, 2003; Adachi *et al.*, 2005). Several risk factors for AFLD have been identified, including obesity, cigarette smoking, genetic factors, and sex. Females have an increased propensity toward alcohol-induced liver injuries than men (Gramenzi *et al.*, 2006). A possible reason for the increased risk in females results from the presence of estrogen, a higher proportion of body fat, lower levels of gastric alcohol dehydrogenase, and therefore higher blood ethanol levels than men (Frezza *et al.*, 1990; Eagon, 2010).

NAFLD and AFLD range among the most prevalent liver diseases in developing as well as in developed countries (Rehm *et al.*, 2013; Younossi *et al.*, 2016). They have similar pathogenesis but different

etiology and epidemiology. They are umbrella terms for a histological spectrum of diseases ranging from steatosis to steatohepatitis, advanced fibrosis, and cirrhosis (Figure 1) (Angulo, 2002).

Alcoholic and non-alcoholic fatty liver (AFL/NAFL) is a simple hepatic steatosis, whereas alcoholic and non-alcoholic steatohepatitis (ASH/NASH) represent advanced stages of AFLD/NAFLD, characterized by steatosis coexisting with hepatocellular injury and inflammation with or without fibrosis (EASL, 2012; EASL, EASD, and EASO, 2016). The prevalence of developing simple steatosis ranges from 15% to 30% for non-alcoholic steatosis and from 90% to 95% for alcoholic steatosis in people with chronic alcohol abuse with more than 60 g of alcohol per day (EASL, 2012; Schuppan *et al.*, 2013). Only 10% to 15% of patients develop steatohepatitis or a more severe outcome of the disease, like cirrhosis or hepatocellular carcinoma (HCC) (Figure 1) (EASL, 2012).
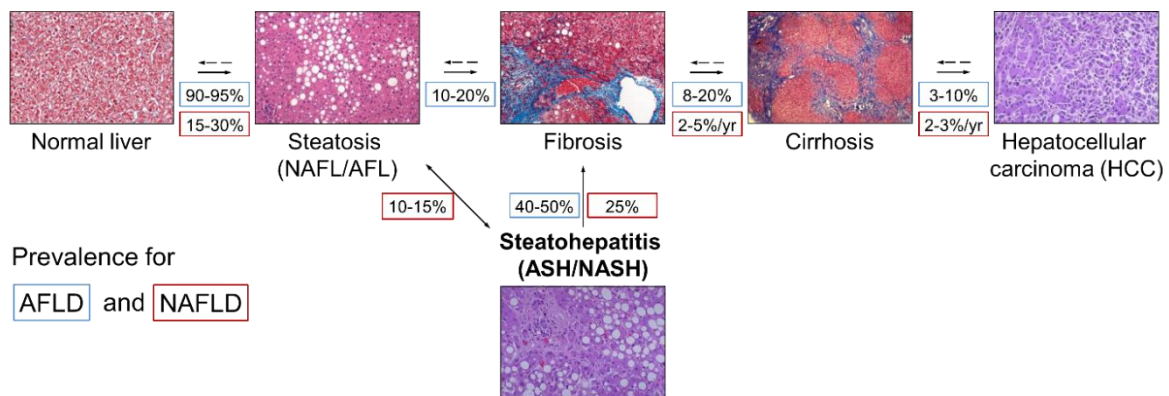
Figure 1: *Spectrum of alcoholic and non-alcoholic fatty liver disease (AFLD/NAFLD) progression. Estimated risks of progression are displayed in blue for AFLD and red for NAFLD. AFL/NAFL: alcoholic/non-alcoholic fatty liver; ASH/NASH: alcoholic, non-alcoholic steatohepatitis. (Adapted from the European Association for the Study of the Liver, 2012; Schuppan and Schattenberg, 2013).*

1.2   Pathogenesis of NAFLD/AFLD

The European Association for the Study of the Liver (EASL) distinguishes NAFLD into "two pathologically distinct conditions with different prognoses": NAFL and NASH, while the latter also includes fibrosis and cirrhosis (EASL, EASD, and EASO, 2016). According to the traditional view, widely known as the 'two-hit' theory, a hepatic fat accumulation is a 'first hit' that sensitizes the liver to the development of hepatocyte injury. The 'second hit' (e.g. lipid peroxidation, reactive oxygen species, gut-derived endotoxin) results in inflammation and fibrosis (Day *et al.*, 1998; Day, 2002). However, this theory has been challenged and fails to explain why steatosis is a benign process in the majority of patients in contrast to NASH. Therefore, the initial theory has been modified by a 'multiple parallel hits' hypothesis. This model suggests many hits acting in parallel and leading to an inflammation that may precede steatosis in NASH, supporting the separation of NAFL and NASH as two diseases (Tilg *et al.*, 2010; Yilmaz, 2012).

1.2.1   Lipotoxicity and impaired triglyceride export

Dysregulation of the lipid environment or the intracellular composition is called lipotoxicity and can possibly lead to organelle dysfunction, cell injury or cell death. Although triglycerides represent the

main lipid class, their accumulation can be considered as protective. In particular, blocking of triglyceride synthesis by inhibition of diacylglycerol acyltransferase 2 caused a reduction of steatosis associated with increased inflammation and fibrosis (Yamaguchi *et al.*, 2007). Besides the total amount of lipids, the lipid composition may be more important (Cortez-Pinto *et al.*, 2006; Puri *et al.*, 2007, 2009). Higher levels of free fatty acids (FFA), particularly saturated FFA, or of ceramide (CER), free cholesterol, and lysophosphatidylcholine (LPC) are associated with lipotoxicity and cell damage. Stress associated mechanisms are activated resulting in hepatic inflammation or apoptosis as shown in Figure **2** (Mota *et al.*, 2016). Here the stress-associated mechanism can be oxidative stress by production of reactive oxygen species (ROS) or endoplasmic reticulum (ER) stress with activation of the unfolded protein response (UPR).

Another impaired mechanism in AFLD/NAFLD is the export of triglycerides (TG) *via* very-low-density lipoprotein (VLDL) particles made of TG, cholesterols, phosphatidylcholines (PC), and apolipoproteins. *In vivo* and *in vitro* studies showed an impaired VLDL secretion after ethanol administration (Venkatesan *et al.*, 1988; Kharbanda *et al.*, 2009; McVicker *et al.*, 2012), which may inhibit the synthesis of PC, and therefore VLDL formation and TG export (Wehr *et al.*, 1993). The link between choline deficiency and hepatic steatosis has been known for many years, leading to the establishment of choline-deficient diets modeling NAFLD in animals (Vance *et al.*, 1985; Yao *et al.*, 1990).
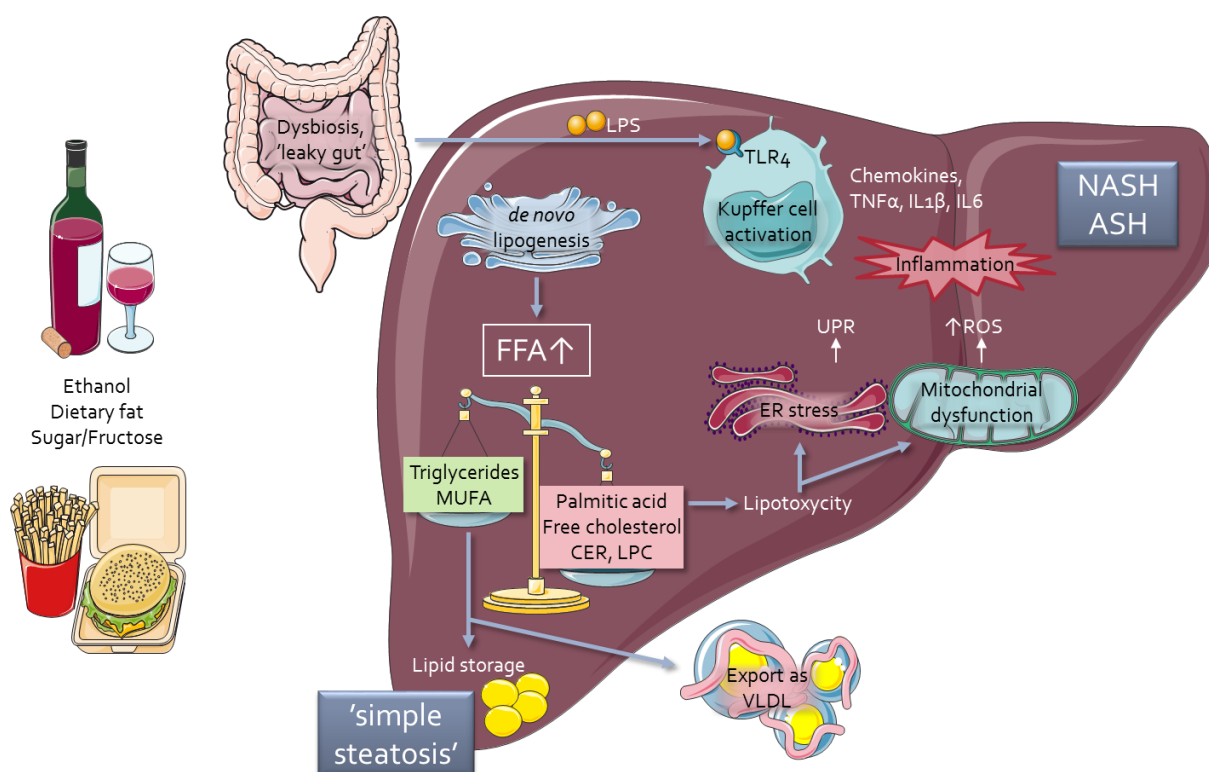
Figure 2: *Influences of fatty diet and ethanol consumption on the liver. CER: ceramides; ER: endoplasmic reticulum; FFA: free fatty acids; IL: interleukin; LPC: lysophosphatidylcholine; LPS: lipopolysaccharides; MUFA: monounsaturated fatty acid; NASH/ASH: non-alcoholic/alcoholic steatohepatitis; ROS: reactive oxygen species; TLR4: toll-like receptor 4; TNF: Tumor necrosis factor; UPR: unfolded protein response; VLDL: very-low-density lipoprotein. Created with elements from Servier Medical Art (https://smart.servier.com/), licensed under a Creative Commons Attribution 3.0 Unported License.*

1.2.2 Leaky gut, endotoxemia, and endogenous ethanol

The cross-talk between the intestine and the liver plays an important role in the pathogenesis and progression of liver disease (Schnabl *et al.*, 2014; Tripathi *et al.*, 2018). In AFLD and NAFLD not only enteric dysbiosis (compositional changes of the gut microbiota) and bacterial overgrowth occur, but also increased gut permeability (Farhadi *et al.*, 2008; Yan *et al.*, 2011). This permeability might be due to a disruption of intercellular tight junctions in the intestine, as observed in NAFLD patients (Miele *et al.*, 2009). Studies in germ-free mice showed modulation of hepatic lipid homeostasis through the gut flora, thus, inducing lipotoxicity (Turnbaugh *et al.*, 2006).

In patients with NAFLD as well as AFLD increased serum levels of bacterial endotoxins, such as lipopolysaccharides (LPS), can be detected, supporting the 'leaky gut' approach and the translocation of gut-derived bacterial endotoxins to the liver (Rao, 2009; Harte *et al.*, 2010; Wong *et al.*, 2015). The first evidence that LPS might play a role in the pathogenesis in steatohepatitis was already demonstrated in 1987. Rats receiving a liquid ethanol diet, the Lieber-DeCarli (LDC) diet, developed a fatty liver, while littermates challenged with an additional LPS injection developed necrosis with associated inflammatory changes (Bhagwandeen *et al.*, 1987). LPS can activate Kupffer cells (KCs), the liver resident macrophages, *via* interaction with the toll-like receptor 4 (TLR4). This concludes in consequent activation of the inflammatory cascade, leading to the production of pro-inflammatory mediators, such as TNFα, IL1β, IL6, chemokines, and ROS (see Figure 2) (Liu *et al.*, 2002; Hritz *et al.*, 2008). LPS also directly stimulates the activation of hepatic stellate cells or sinusoidal endothelial cells. Hence, liver non-parenchymal cells (NPCs) may play a pivotal role in the pathogenesis of NAFLD and AFLD (Seki *et al.*, 2007; Jagavelu *et al.*, 2010).

The exposure to ethanol and its metabolites distinguishes AFLD from NAFLD. Nevertheless, in NASH patients and also in murine NASH models elevated endogenous ethanol produced by gut bacteria was found (Cope *et al.*, 2000; Nair *et al.*, 2001; Baker *et al.*, 2010; Zhu *et al.*, 2013). These findings support the hypothesis that NAFLD might be an endogenous AFLD, explaining the similar histopathology and molecular biology of both diseases (de Medeiros *et al.*, 2015).

1.3 Role of inflammatory cells in AFLD and NAFLD

The liver is comprised of parenchymal and non-parenchymal cells working together in cohesion. For the understanding of the pathogenesis of AFLD and NAFLD, it has become of great importance to study their interaction and crosstalk.

Hepatocytes represent the main liver cell type, which constitutes two-third of the total cell population (approx. 70%) (Gao *et al.*, 2007). They fulfill the metabolic and detoxifying functions of the liver. The remaining cells are NPCs, including KCs, liver sinusoidal endothelial cells, biliary cells, lymphocytes, and hepatic stellate cells (HSCs). These HSCs play an unequivocal role in hepatic fibrosis and are generally quiescent cells that become activated during liver injury. They undergo morphological changes and differentiate into myofibroblasts producing collagen (Tsuchida *et al.*, 2017).

The activation of inflammatory pathways is crucial in the progression of AFLD and NAFLD. One hallmark is the infiltration of inflammatory cells. However, this process and the involved inflammatory cells play a dual role: On one hand, inflammation is proposed to play a key role in promoting the progression towards steatohepatitis; on the other hand, an inflammation can have beneficial effects, such as host defense and liver regeneration (Gao *et al.*, 2016).

The first line of defense against injury are macrophages. KCs represent the largest population of tissue macrophages within the body. Their main role is the clearance of pathogen-associated molecular pattern molecules and translocated gut-derived bacteria. Still, their role in the pathogenesis of AFLD and NAFLD is controversially discussed, because they can have detrimental as well as beneficial effects, indicated in Figure 3. As described earlier, endotoxins activate KCs *via* TLR4. The importance of KCs and the TLR4 signaling in the development of NAFLD was demonstrated by Rivera and colleagues: mice lacking TLR4 or KCs are resistant to diet-induced hepatic inflammation and NASH (Rivera *et al.*, 2007). In early and chronic stages of AFLD and NAFLD, where infiltrations of macrophages and lymphocytes are a prominent feature, inactivation or depletion of macrophages prevented experimental AFLD and NAFLD (Adachi *et al.*, 1994; Lanthier *et al.*, 2011).

In contrast to these findings, KCs can also adopt an anti-inflammatory phenotype and release e.g. IL-10 (Byun *et al.*, 2013; Wan *et al.*, 2014). Released cytokines and chemokines from hepatic macrophages can promote the transmigration of neutrophils in ASH and NASH for assistance in the defense against bacteria (Ebe *et al.*, 1999). Nevertheless, neutrophils are supposed to promote progression of steatohepatitis by inducing hepatocyte injury (Ramaiah *et al.*, 2007; Chang *et al.*, 2015).
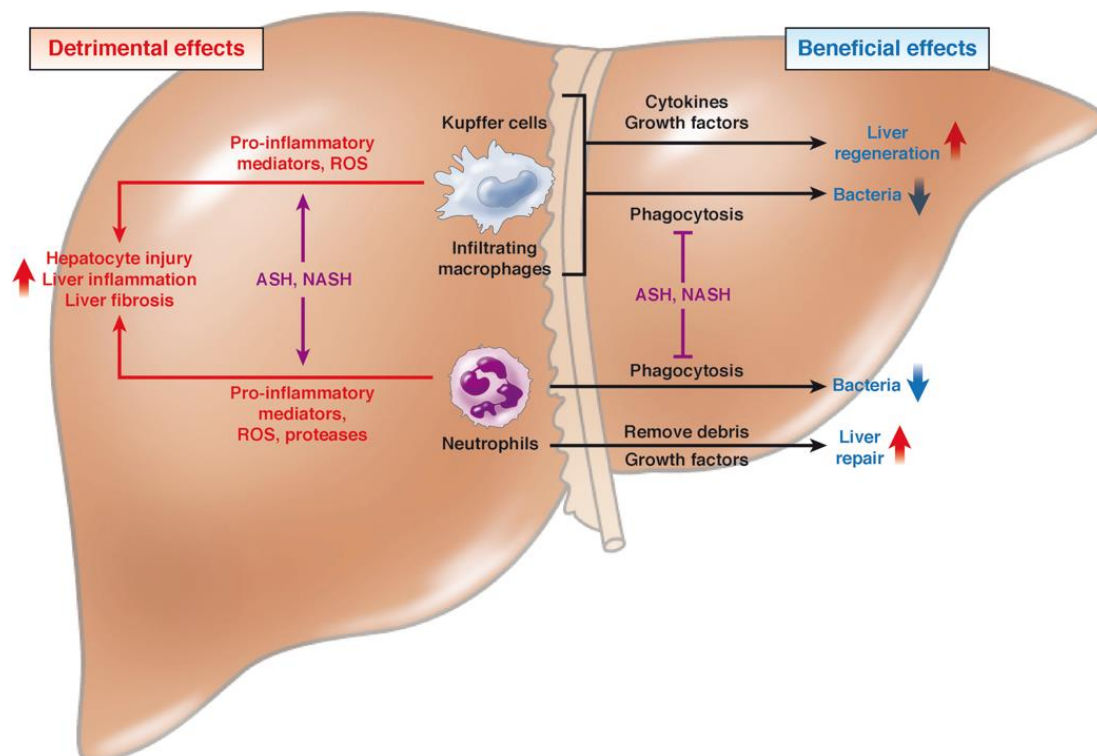
Figure 3*: Adverse and favorable effects of hepatic macrophages and neutrophils in AFLD and NAFLD. Pro-inflammatory functions are activated during ASH and NASH, while phagocytic functions can be suppressed (Gao* et al.*, 2016).*

1.4 Kupffer cell depletion

One method to study the function of KCs in the progression of steatohepatitis is the selective *in vivo* depletion by "the liposome-mediated macrophage 'suicide' technique" (Van Rooijen, 1989).

Liposomes consist of amphipathic phospholipid molecules. In aqueous solutions, the phospholipids organize themselves into concentric phospholipid bilayers with aqueous compartments (Figure 4 A). Hence, strongly hydrophilic molecules, such as the bisphosphate clodronate (dichloromethylene-bisphosphate), when solved in an aqueous solution, can be encapsulated within the liposomes. Clodronate itself is a non-toxic drug originally developed for the treatment of osteolytic bone diseases and cannot pass phospholipid bilayers of cell membranes or liposomes. These clodronate liposomes are used as a Trojan horse to be ingested by phagocytosis of macrophages (Figure 4 B: no. 1). Once ingested, the phospholipid bilayer is lysosomally digested (Figure 4 B: no. 2 and no. 3) and the clodronate is released within the cell and accumulates (Figure 4 B: no. 4). At a certain threshold concentration, irreversible damage causes the programmed cell death (apoptosis) of the macrophage (van Rooijen *et al.*, 1996). The released clodronate has a short half-time and is rapidly cleared from the renal system.
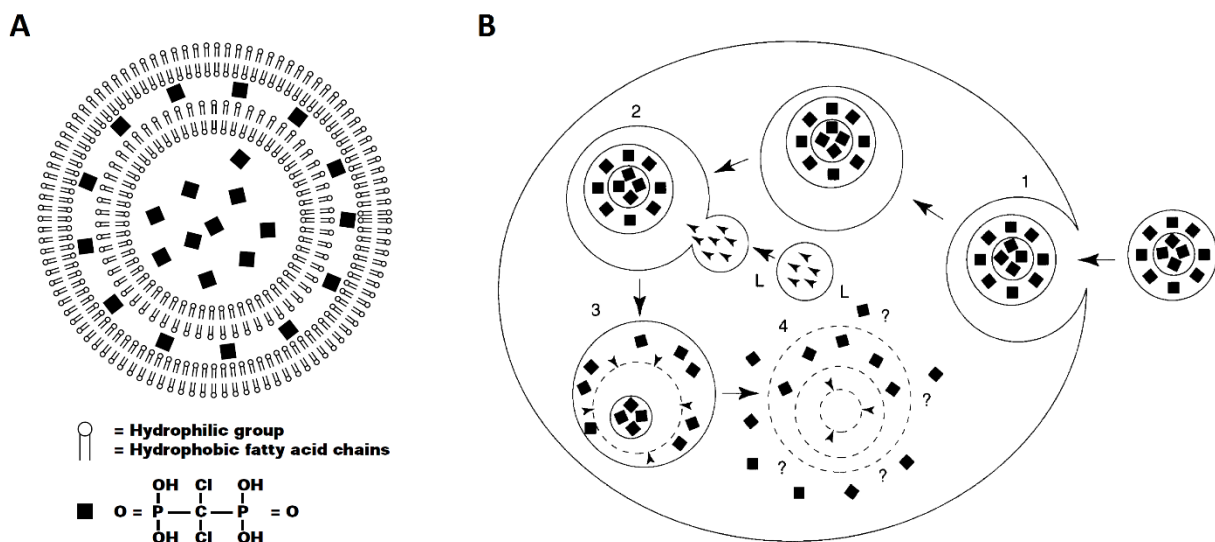
Figure 4: *Illustration of a clodronate liposome and the macrophage 'suicide' mechanism. A: Clodronate liposomes consist of multilamellar phospholipid bilayers (ϖ) with encapsulated clodronate (■) separated by aqueous compartments (Rooijen and Sanders, 1994). B: The clodronate liposome is ingested by macrophages via endocytosis (1) and fuses with the lysosome (L) (2). Lytic enzymes like phospholipases disrupt the bilayers and digest the liposomes (3). The encapsulated clodronate is released within the cell (4). Clodronate is accumulated within the cell until a certain threshold concentration leads to cell apoptosis (van Rooijen, Bakker and Sanders, 1997).*

An intraperitoneal (i.p.) injection of clodronate liposomes depletes macrophages in the peritoneal cavity. *Via* the lymph flow, they are carried to the blood circulation and lead to a depletion of macrophages in the liver (KCs), spleen, and bone marrow. Since the lymph flow circulation is a passive form of transport, i.p. administered clodronate liposomes may last approx. 3 days before depleting macrophages in the liver. For a longer depletion period than 5 days, injections have to be repeated in

order to avoid the replacement of depleted macrophages with new ones. Other immune cells like dendritic cells as well as neutrophils are not depleted by clodronate liposomes (Claassen *et al.*, 1990; Qian *et al.*, 1994).

1.5 Role of liver progenitor cells in chronic liver disease

Liver progenitor cells were discussed in the past years as a possible source of liver tumor development. Liver progenitor cells are quiescent cells and considered bipotential with the capacity to differentiate and carry markers for hepatocytes and cholangiocytes (Miyajima *et al.*, 2014). Under persistent liver injury, when the ability of mature hepatocyte proliferation is compromised, liver progenitor cells are activated and expand in patients as well as in experimental injury models (Español–Suñer *et al.*, 2012; Tarlow *et al.*, 2014; Lu *et al.*, 2015).
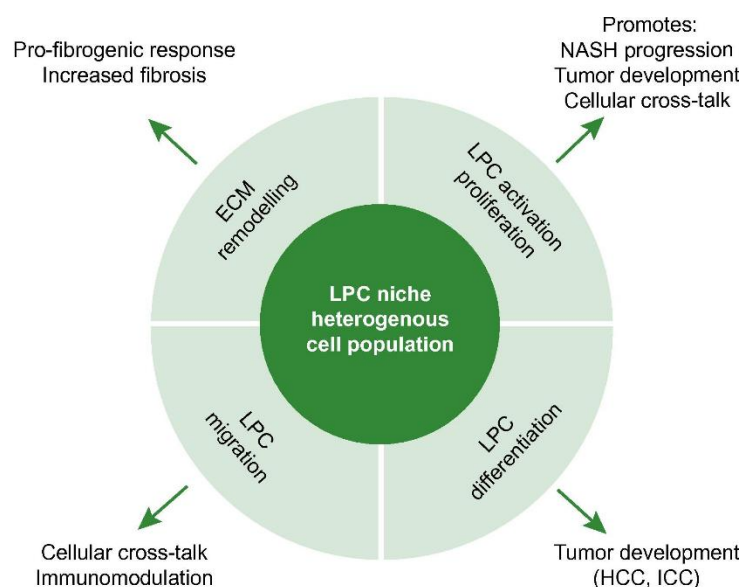
Figure 5: *Different functions of liver progenitor cells (LPCs) in chronic injured liver diseases, where liver regeneration is impaired. Liver progenitor cells can give rise to hepatocytes, but their activation, proliferation, and differentiation are reported to be involved in tumor development and NASH progression. Furthermore, the process requires extracellular matrix (ECM) remodeling and is associated with increased fibrosis (Lukacs-Kornek et al., 2017).*

Liver progenitor cell activation is accompanied by the ductular reaction, where ductules are formed, which may arise from existing cholangiocytes or liver progenitor cells (Roskams *et al.*, 2004; Gouw *et al.*, 2011). Additionally, liver progenitor cell activity is often accompanied by extracellular matrix (ECM) remodeling and pro-fibrogenic responses in animal models (Figure 5) (Van Hul *et al.*, 2009; Kuramitsu *et al.*, 2013; Peng *et al.*, 2016). Moreover, liver progenitor cell activation and ductular reaction have been observed in several human chronic liver diseases including NASH, ASH, and HCC, where the degree of activation and ductular reaction correlates with their severity (Lowes *et al.*, 1999; Roskams *et al.*, 2003; Roskams, 2006; Richardson *et al.*, 2007; Sancho-Bru *et al.*, 2012; Gadd *et al.*, 2014).

1.6   Epigenetic factors in AFLD and NAFLD

AFLD and NAFLD comprise diseases, which are ranging from steatosis to steatohepatitis, advanced fibrosis, and cirrhosis. Despite their different etiology and epidemiology, they share similar underlying pathomechanisms. Susceptibility to and progression of AFLD/NAFLD is influenced by genetic as well as environmental factors (Figure 6) (Day, 2006; Eslam *et al.*, 2018).
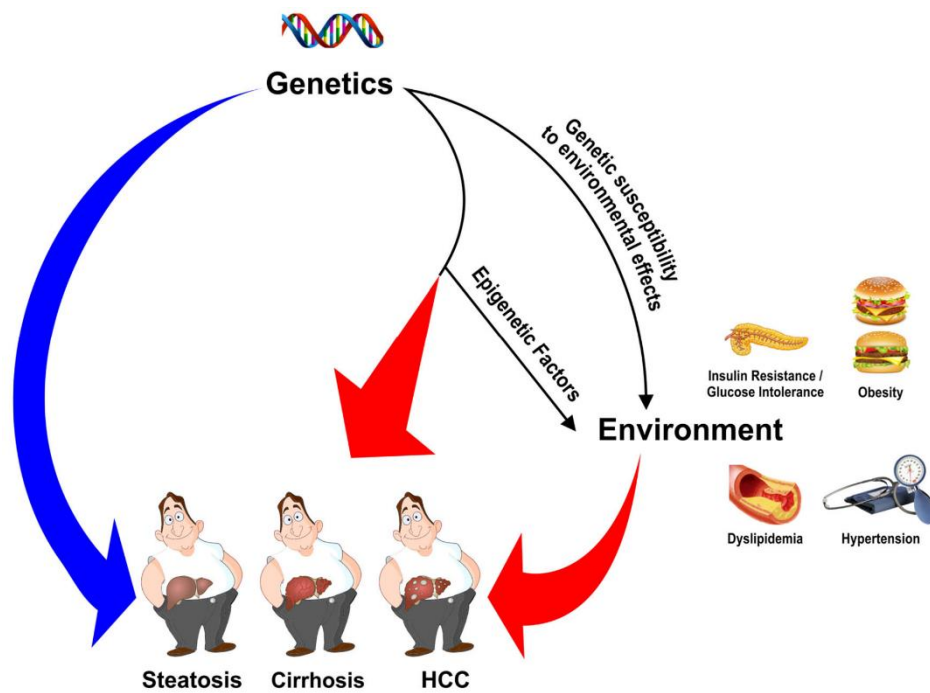
Figure 6*: Interaction of genetic and environmental factors in the susceptibility and progression of AFLD and NAFLD* (Eslam *et al.*, 2016)*.*

Epigenetic changes have gained much interest in recent studies on the pathogenesis of liver diseases. The epigenome is involved in reversible changes in gene expression through modification of the secondary or tertiary structure of DNA, the chromatin, without altering the underlying DNA sequence and is representative for the cell phenotype. The epigenome is influenced by the genome through the presence of SNPs, by environmental factors such as diet or smoking, and also by age and gender (Figure 6) (van Dongen *et al.*, 2016). The underlying mechanism comprises histone modification, DNA methylation, and non-coding RNA mediated actions (Figure 7).

Post-translational modifications of histones have an impact on gene transcription, making the DNA either more or less accessible to transcription and regulatory factors. Aberrant histone modifications have been shown to be associated and involved in the development of insulin resistance and consequently NAFLD (Ling *et al.*, 2009). Ethanol exposure is linked to an imbalance of histone acetylation and deacetylation enzymes in hepatocytes, where H3K9 acetylation correlates with a transcriptional increase of the alcohol dehydrogenase (ADH1) (Park *et al.*, 2005). Furthermore, ethanol might also be a stimulator of fibrosis by altering histone-modifying enzymes in HSCs, resulting in increased expression of extracellular matrix proteins including elastin (Page *et al.*, 2015).
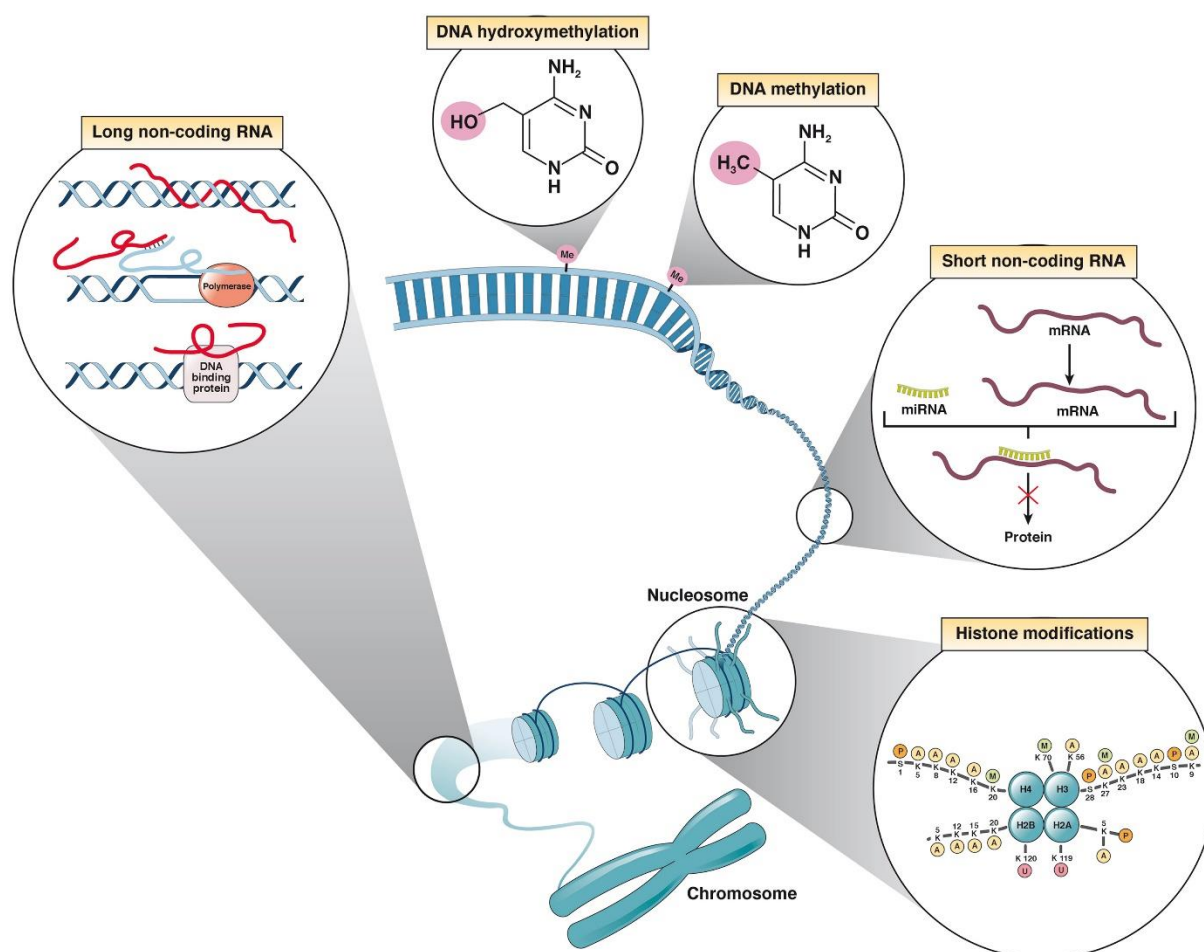
Figure 7: *Epigenetic mechanisms important in the control of gene expression: histone modifications, non-coding RNAs, DNA methylation and hydroxylation (Moran-Salvador and Mann, 2017).*

DNA methylation takes place at the 5'-position of cytosines in CpG dinucleotides (Figure 7) and is catalyzed by DNA methyltransferases (DNMTs). CpG islands, clusters of CpG sequences, are found in an unmethylated state in promoters and are associated with a transcriptionally active state. Methylation, on the other hand, leads to chromatin condensation, inhibiting the binding of transcriptional activators, and therefore to transcriptional silencing (Edwards *et al.*, 2010; Stadler *et al.*, 2011). Different methylation patterns are proposed to distinguish different stages of NAFLD or fibrosis (Zeybel *et al.*, 2015). Comparing mild to advanced NAFLD in liver biopsies of patients, Murphy and colleagues found general hypomethylated CpG sites in advanced NAFLD (Murphy *et al.*, 2013). Additionally, it was shown in hepatoma cells that genes coding for the alcohol-metabolizing enzymes are regulated by DNA methylation (Dannenberg *et al.*, 2006).

In addition to histone modification and DNA methylation, endogenous non-coding RNA (ncRNA) molecules are important regulators of gene expression (Figure 7). They are classified by their size and functional mechanism. Aberrant profiles of microRNAs (miRNAs) have been found in NAFLD and AFLD and might be involved in NAFLD progression (Bala *et al.*, 2012; Szabo *et al.*, 2013; Ferreira *et al.*, 2014). Characteristic plasma miRNA profiles have also been suggested as potential novel biomarkers for NAFLD and AFLD (Momen-Heravi *et al.*, 2015; Pirola *et al.*, 2015). Inflammatory responses are modified as well: Chronic alcohol feeding induced an increase of *miR-155* in KCs and promoted TNFα productions

via increased mRNA stability, demonstrating an important role of *miR-155* to promote liver inflammation (Bala *et al.*, 2011). This was further supported by *miR-155* knock-out mice, which were protected from alcohol-induced increased serum endotoxin and TNFα levels (Lippai *et al.*, 2014).

1.7 Insulin-like growth factor 2 mRNA binding protein p62

The insulin-like growth factor 2 (*IGF2*) mRNA binding protein (IMP/IGF2BP) family represents a group of highly conserved RNA binding proteins, comprising three members (IMP1-3). They participate in posttranscriptional RNA processing i.e. by mediating RNA splicing, localization, stability, and translation of their target mRNA transcripts, such as *IGF2* and *H19* (Nielsen *et al.*, 1999; Runge *et al.*, 2000; Bell *et al.*, 2013). IMPs have a conserved structure of two N-terminal RNA-recognition motifs (RRMs) and four hnRNP K homology (KH) domains in the C-terminal region, which has been shown to be critical for their RNA-binding capacity (Farina *et al.*, 2003). The IMP2 gene is located on chromosome 3 q27.2 and encodes 16 exons. As shown in Figure 8 p62/IMP2-2/IGF2BP2-2 (NM_001007225.2) represents a human splice variant of IMP2. Compared to IMP2, p62 lacks exon 10 corresponding to 43 amino acids between the KH2 and KH3 domain.
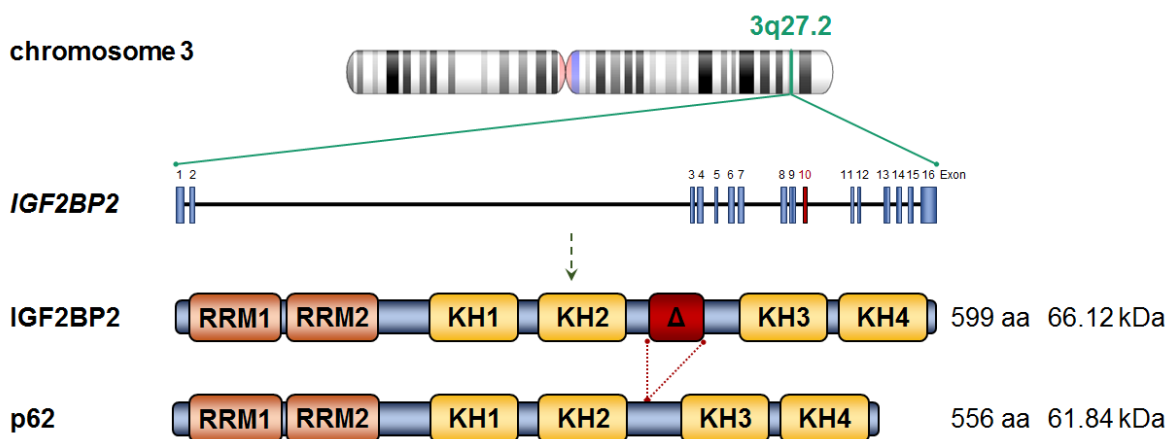
Figure 8: *Chromosomal location of the IGF2BP2/IMP2 and the p62 gene and the structure of the transcribed and spliced protein, giving the number of amino acids (aa) and the size (kDa) (chromosome created by the Genome Decoration Page/NCBI; adapted from Christiansen* et al*., 2009; Cao, Mu and Huang, 2018).*

IMP1 and 3 are classified as oncofetal proteins, whereas the expression of IMP2 in the adult liver has been controversially discussed. p62/IMP2-2 was originally identified in 1999 as an autoantigen in HCC (Zhang *et al.*, 1999). In following studies, *p62/IMP2-2* was not only found to be upregulated in human HCC but also to promote hepatocarcinogenesis and correlate with a poor outcome in human HCC (Kessler *et al.*, 2013, 2015).

1.8 Murine models to study NAFLD and AFLD

NAFLD and AFLD are very complex diseases and yet not fully understood. Therefore, animal models are being used to elucidate their pathogenesis. However, the 'available' animal models are only able to mirror single hallmarks of the diseases and do not fully display the complete pathophysiology of human NAFLD or AFLD. The animal models can be distinguished into dietary and genetic models.

1.8.1 Models of NAFLD

To investigate the pathophysiology of NAFLD the models presented in Table 1 are used.

Thereby, the **p62 transgenic mouse** is a genetic model, expressing the human *p62/IMP2-2* specifically in the liver. The *p62* transgenic mouse was described in our group as a model for non-inflammatory steatosis with elevated lipid classes and fatty acids (Tybl *et al.*, 2011; Laggai *et al.*, 2013, 2014). Accordingly, other studies employing *IMP2*-deficient mice resist diet-induced obesity and fatty liver (Dai *et al.*, 2015). *p62* transgenic mice display steatosis and mild inflammation but neither obesity nor insulin resistance (IR) (Kessler *et al.*, 2014; Laggai *et al.*, 2014). With an additional diet e.g. the methionine-choline-deficient diet hepatic *p62* expression was shown to amplify fibrosis (Simon, Sonja M Kessler, *et al.*, 2014).

A nutrient-deficient model is the **methionine-choline-deficient** (MCD) diet. The lack of methionine and choline leads to the hepatic accumulation of lipids through impairment of fat export from the liver *via* VLDL and increased fatty acid uptake (Rinella *et al.*, 2008). Furthermore, the diet can model inflammation and liver fibrosis. However, it causes weight loss and does not display features of the metabolic syndrome, such as insulin resistance (Anstee *et al.*, 2006).

Overnutrition can be modeled by **high-fat diet** (HFD) feeding. Available diets vary in their relative carbohydrate and fat content ranging from 20% to more than 70% of total calories. Moreover, HFDs also differ in the saturation of the nutritional fatty acids, and the content of nutritional cholesterol. This inconsistency makes it difficult to compare the current literature. The HFD feeding induces obesity, insulin resistance, steatosis, and to some extent inflammation (Table 1) (Anstee *et al.*, 2006). The outcome depends not only on the type of diet and the duration of diet exposure but also on the susceptibility of the mouse strain.

Table 1: *Animal models of NAFLD. IR: insulin resistance; MCD: methionine-choline-deficient diet; ✓: occurs; ✗: not detected.*

Model	IR	Obesity	Steatosis	Inflammation	Fibrosis
Genetic model					
p62 transgenic mice	✗	✗	✓	✓	✗ (diet inducible)
Feeding model					
MCD	✗	✗	✓	✓	✓
High-fat diet	✓	✓	✓	✓ (mild)	✓ (mild, after at least 1 year of treatment)

1.8.2 Models of AFLD

The pathogenesis of AFLD is studied by using two feeding models presented in Table 2.

Table 2:   *Animal models of AFLD. DW: drinking water; ✘: not detected; ✓: occurs.*

Model	Steatosis	Inflammation	Fibrosis
Feeding model			
Ethanol in DW	✓ (mild)	✓ / ✘	✘
Lieber-DeCarli diet	✓	✓ / ✘	✘

The **ethanol in drinking water** (DW) method represents the simplest way of ethanol administration. Here, increasing concentrations of ethanol from 10% up to 40% (v/v) are supplemented into the drinking water as the only drinking source. This ad libitum approach has been shown to cause mild steatosis and inflammation but no progression to fibrosis (Table 2) (Keegan *et al.*, 1995; Cook *et al.*, 2007; Brandon-Warner *et al.*, 2012).

One of the first diets used for studying the effects of alcohol *in vivo* was the liquid **Lieber-DeCarli** (LDC) diet. This diet derives up to 36% of its calories from alcohol (DeCarli *et al.*, 1967; Lieber *et al.*, 1982). The LDC diet has been reported to induce steatosis and mild inflammation (Table 2). Pritchard et al. demonstrated that female C57BL/6 mice developed micro- and macrovesicular steatosis with a significant increase in liver triglycerides after a feeding period of 6 weeks (Pritchard *et al.*, 2007). Furthermore, the liver to body weight ratios were elevated and the alanine-aminotransferase (ALT) activity in the serum was increased (Pritchard *et al.*, 2007). Moreover, they also observed low inflammation with elevated liver cytokines, such as TNFα or IL6. Further hepatic injury can only be induced by an additional factor, such as injections of LPS or CCl_4 (Pritchard *et al.*, 2007).

1.9 The aim of the present work

Steatohepatitis is characterized by an inflammation-associated storage of excessive lipids in the liver. In the progression of the disease, liver-resident macrophages, i.e. Kupffer cells (KCs), play a crucial role. They can have both adverse as well as favorable effects, and their function is controversially discussed. *p62/IMP2-2*, the human splice variant of IMP2 was found to induce steatosis in a liver-specific *p62* transgenic mouse model and to promote other liver pathologies, such as fibrosis and liver cancer. The IMP family is a group of highly conserved RNA-binding proteins, comprising three members. IMP1 and IMP3 are classified as oncofetal proteins, whereas the expression of IMP2 in the adult liver is controversially discussed.

Aim of this work was an in-depth characterization of the role of KCs in steatohepatitis and the impact of a liver-specific overexpression of *p62* in a murine mouse model of steatohepatitis. The following aspects were investigated:

1. The hypothesis that IMP2 is an oncofetal protein is aimed to be confirmed. Further, the influence of p62/IMP2-2 on progression towards fibrosis is characterized.

2. The role of resident macrophages, i.e. KCs, in epigenetically regulated changes in gene expression was investigated in a murine steatohepatitis model.

3. A potential role of *p62* overexpression on the epigenome of hepatocytes was explored and how it impacts steatohepatitis dependent on the presence or absence of KCs.

2 CHAPTER I

IMP2-2/p62 promotes the occurrence of liver progenitor cells

2.1 Introduction

The IMP/IGF2BP family members IMP1 and IMP3 are regarded as oncofetal proteins, whereas the expression of IMP2 in adult liver is controversially discussed (Zhang *et al.*, 1999; Dai *et al.*, 2011; Bell *et al.*, 2013), not least due to the lack of quantitative data on IMP2 expression. Therefore, it was aimed to reliably quantify the expression of Imp2 at different stages of embryonic development and at different ages (Figure 9).

Figure 9*: Overview of embryonic (E12.5), neonatal (P0), infant (2 weeks), and adult (10 and 85 weeks) mice analyzed for hepatic IMP2 expression in a time-dependent course. Created with elements from Servier Medical Art (https://smart.servier.com/), licensed under a Creative Commons Attribution 3.0 Unported License.*

IMP2 was found to be highly expressed in glioblastoma cancer stem cells, where it is responsible to preserve their maintenance (Janiszewska *et al.*, 2012). Undifferentiated liver progenitor cells are known to be activated in chronic liver diseases including NASH and HCC accompanied by a ductular reaction. Their degree of activation and the extent of ductular reaction correlates with the severity of liver disease (Roskams, 2006; Richardson *et al.*, 2007; Gadd *et al.*, 2014). Therefore, it was aimed to test the hypothesis that IMP2 is an oncofetal protein in the liver and that IMP2-2/p62 can promote cell stemness.

2.2 Results

IMP2 gene and protein expression in embryonic and adult livers were analyzed to test the hypothesis of an oncofetal protein. Publicly available RNA sequencing data sets (PRJNA66167, PRJNA280600; Yue *et al.*, 2014) showed a high *IMP2* expression in fetal mouse and human liver compared to the respective adult liver (Figure 10 A). Embryonic markers, such as *IGF2* and *H19*, were also highly expressed in fetal livers (Figure 10 A). The low expression in adult, but high expression in fetal liver of *Imp2*, *Igf2*, and *H19* was confirmed by qPCR in a time-dependent course of embryonic (E12.5), neonatal (P0), and adult (2, 10, and 85 weeks) mice (Figure 10 B, C, and D). The age-dependent pattern of murine *Imp2* expression was confirmed on protein level by Western Blot analysis (Figure 10 E, F).
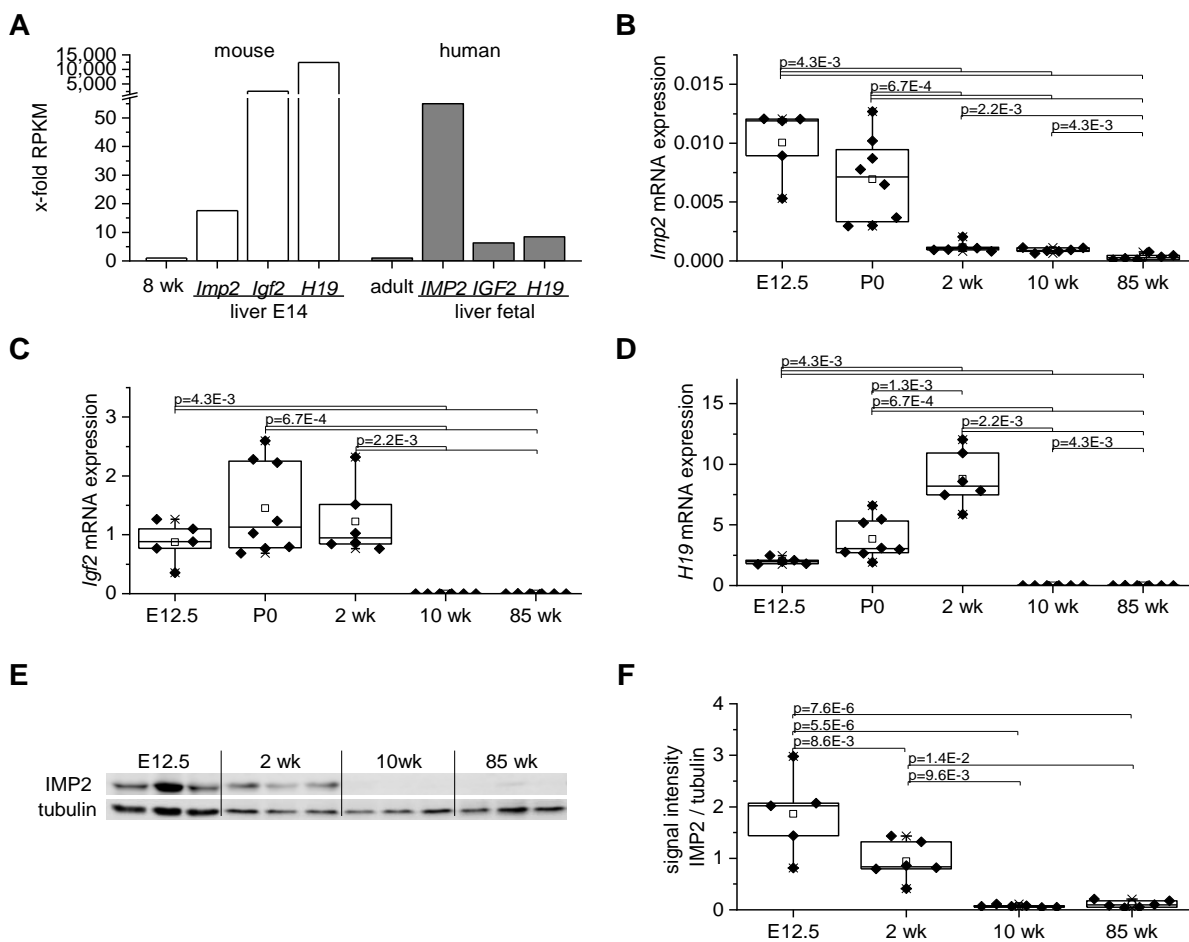
Figure 10: Expression of IMP2*,* IGF2*, and* H19 *in embryonic and adult livers. A:* IMP2*,* IGF2*, and* H19 *gene expression from available RNA sequencing data sets of murine (PRJNA66167) and human (PRJNA280600) fetal liver compared to adults. Data are expressed as x-fold from the adult liver. B, C, D: qPCR analysis of* Imp2 *(B),* Igf2 (C)*, and* H19 *(D) in livers of fetal (E12.5; n=5), newborn (P0, n=8), 2-, 10-, and 85-week-old (each n=6) mice. E, F: Western blot analysis of IMP2 protein expression in fetal, young, and adult mouse livers. Representative picture of Western blot (E) and quantification of IMP2 levels normalized to tubulin (F) are shown. Imp2 signal intensities were quantified and normalized to the loading control values of tubulin. B, C, and D: Data are shown as the ratio of mRNA expression of the gene of interest to the reference gene* Ppia*. Results are presented as means ± SEM or box plots with 25th/75th percentile boxes, geometric medians (line), means (square), and 10th/90th percentile as whiskers. P-values were calculated by Mann Whitney U test with Bonferroni correction. RPKM: Reads per kilobase transcript per million reads.*

A high fetal hepatic expression of IMP2 suggests a role of IMP2 in undifferentiated liver cells. Since the degree of liver progenitor cell activation and ductular reaction have been shown to correlate with the severity of human chronic liver disease, the expression of *IMP2* and common progenitor markers in gene expression data sets from human cirrhotic tissue (GSE14323) was first analyzed. Human cirrhotic and cirrhosis-associated HCC liver tissues showed an increased expression of *IMP2* in parallel with the human liver progenitor cell marker genes *SOX9*, *SPP1*/osteopontin, *CDH1*, *PROM1/CD133*, *BEX1*, and *EPCAM* (Figure 11).

Genes	cirrhosis without HCC		cirrhosis with HCC	
	x-fold change	p-value	x-fold change	p-value
IMP2	1.77	2.9E-08	1.58	1.5E-03
SOX9	4.67	1.9E-17	3.71	2.3E-10
SPP1	5.44	7.7E-11	4.40	6.8E-05
CDH1	1.63	4.0E-09	1.81	6.0E-05
AFP	0.91	6.0E-02	1.05	4.8E-01
PROM1	4.86	8.9E-13	2.95	4.7E-10
BEX1	1.47	3.7E-05	1.65	8.3E-07
EPCAM	14.71	6.8E-15	13.61	2.3E-10
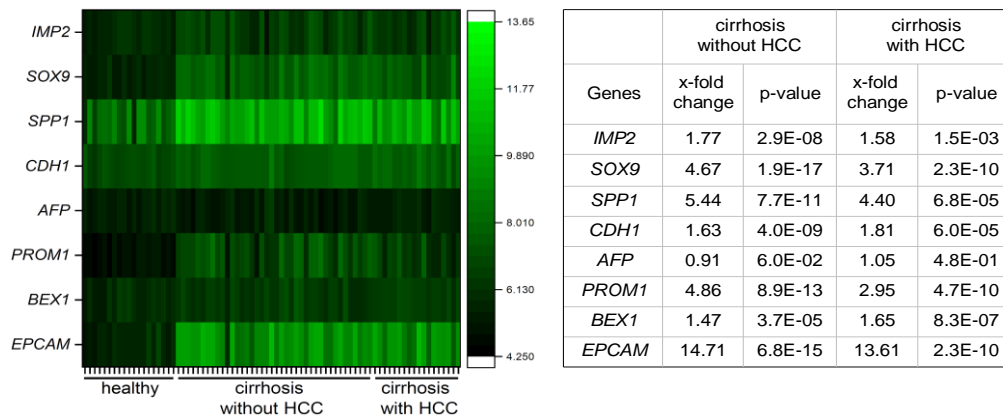
Figure 11*: Elevated stem cell marker expression in human cirrhotic and HCC/cirrhotic tissue. Analysis of GEO data set GSE14323 for* IMP2, SOX9, SPP1, CDH1, AFP, PROM1, BEX1*, and* EPCAM *gene expression in human cirrhotic (n=41) and cirrhosis-associated HCC (HCC/cirrhotic: n=17) liver samples. Values are shown as x-fold of healthy (n=19) liver samples and p-values were generated in comparison to healthy tissue (Mann-Whitney U test or Welch's t-test).*

The impact of *IMP2* overexpression in the liver on stem cell features was investigated in a mouse model with hepatic overexpression of *IMP2-2/p62*, a human splice variant of *IMP2*. qPCR analyses of these transgenic livers revealed an upregulation of the murine homologous liver progenitor cell marker genes *Spp1* and *Cdh1*, while *Krt19* and *Sox9* were not altered (Figure 12 A). To further study the impact of *IMP2-2/p62* expression on liver progenitor cell occurrence in the context of liver disease, livers of *IMP2-2/p62* transgenic mice challenged with a NASH-inducing MCD diet were analyzed. A strong ductular reaction in livers of *IMP2-2/p62* transgenic mice was observed in our group after 4 weeks of MCD feeding compared to wild-type animals, based on immunohistochemical Krt19 stainings (Simon, 2013). These livers were further analyzed for progenitor marker expression in this work. An induction of *Krt19* and *Sox9* mRNA expression was found and the expression of *Spp1* and *Afp* was induced to a greater extent in MCD-fed *IMP2-2/p62* transgenic mice compared to their wild-type littermates (Figure 12 B). Since liver progenitor cell occurrence is often described together with ECM remodeling, the expression of ECM components in the occurring ductular reaction of *IMP2-2/p62* transgenic livers was further investigated. The ductular reaction was accompanied by the deposition of ECM components, such as laminin and hyaluronic acid, determined by immunohistochemical stainings (experiments carried out by Dr. S. M. Kessler and Dr. Y. Simon, Figure 12 C).
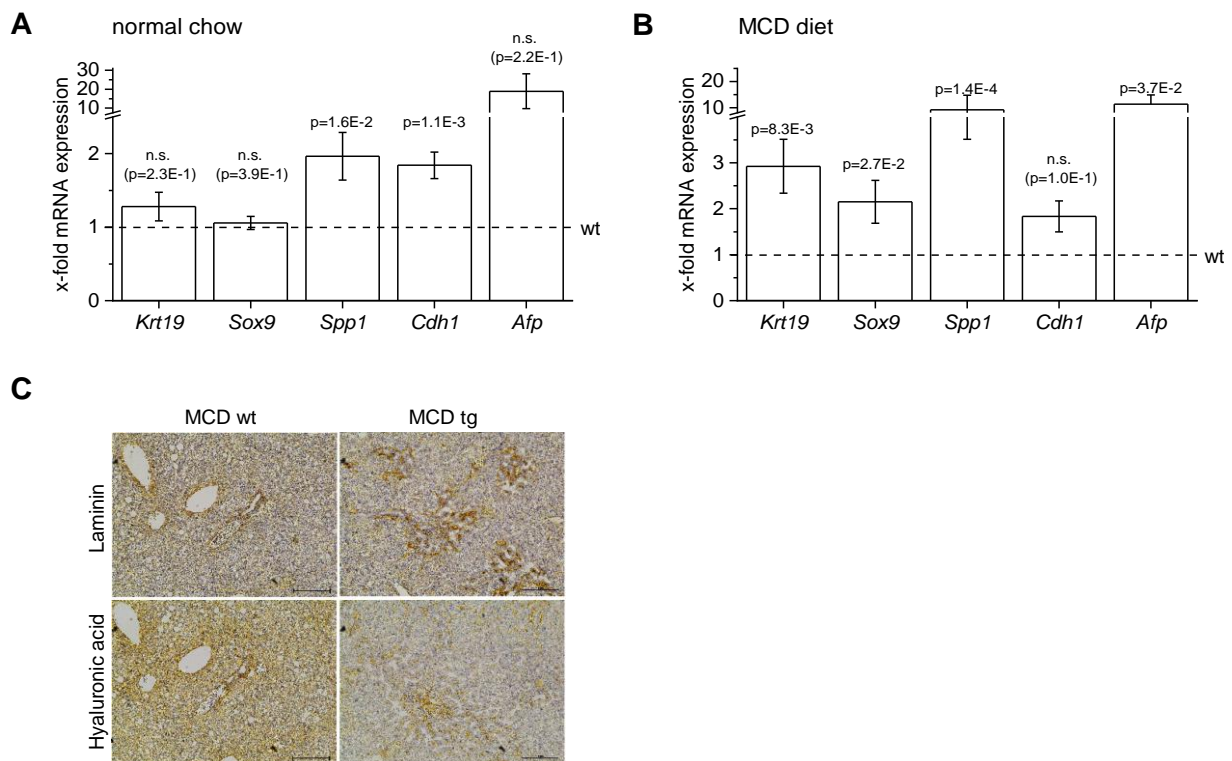
Figure 12: *Elevated stem cell marker and extracellular matrix component expression in* p62 *transgenic mice. A, B: Expression analysis of* Krt19, Sox9, Spp1, Cdh1*, and* Afp *in* p62 *transgenic (tg) mice (n=11-13) on normal chow (A) and on MCD diet (B), shown as x-fold of wild types (wt) (n=12-13). C: Representative immunohistochemical staining for laminin and hyaluronic acid in* p62 *transgenic animals fed an MCD diet. A, B: Results are shown as means ± SEM. Statistical significance compared to wild types was determined by Mann Whitney U test or Welch's t-test.* Rn18s *was used as the reference gene. n.s.: not significant.*

2.3 Discussion

In the present study, an age-dependent IMP2 expression pattern is shown and together with previous work an oncofetal character of IMP2 not only in human but also in murine liver is strongly supported. Furthermore, hepatic overexpression of *IMP2-2/p62*, a human splice variant of *IMP2*, promoted a ductular reaction accompanied by undifferentiated cells and ECM deposition in a murine MCD model of NASH.

The age-dependent pattern of IMP2 expression in murine liver with high embryonal and minimal adult expression was confirmed on mRNA as well as protein level in agreement with previous studies (Hammer *et al.*, 2005). As expected, the highest embryonal expression was found at embryonic day 12.5 (Nielsen 1999). In contrast to these results, IMP2 has been suggested to be ubiquitously expressed on mRNA and protein level in adult murine tissue, including the liver (Dai *et al.*, 2011; Bell *et al.*, 2013). However, these studies did not quantitatively compare expression levels in the embryonic state with the adult one. In addition, re-expression of *IMP2* and its splice variant *IMP2-2/p62* has been described in liver cancer (Kessler *et al.*, 2013, 2015) underlining its oncofetal expression pattern. Furthermore, *IMP2* has been described to promote an undifferentiated character of HCC (Kessler *et al.*, 2015). Thus, it was suggested that *IMP2* might promote undifferentiated liver cells and investigated the expression of liver progenitor cell markers.

Expression of *Cdh1*, which was elevated upon *IMP2-2/p62* transgene expression, was shown to increase with elevated numbers of progenitor cells (Van Hul *et al.*, 2009). In agreement with the literature (Furuyama *et al.*, 2011; Y. Chen *et al.*, 2015; Shimata *et al.*, 2018), an induction of *Krt19* and *Sox9* occurred during ductular reaction, which was induced by *IMP2-2/p62* expression upon MCD-feeding. Although *Spp1* and *Sox9* are usually expressed by liver progenitor cells (Syn *et al.*, 2011; Pritchett *et al.*, 2012), their expression was also found in de-differentiated mature hepatocytes in a liver-injury induced model (Tarlow *et al.*, 2014). Increased *Afp* expression further suggests dedifferentiation processes (Yanger *et al.*, 2013) induced by *IMP2-2/p62*. Thus, the here presented findings favor the hypothesis that *p62* promotes undifferentiated or dedifferentiated cells.

Sox9 was found to regulate ECM component expression and *Spp1* (osteopontin). *IMP2-2/p62* transgenic mice showed significantly elevated levels of *Spp1* and when fed an MCD diet ECM deposition was detected by immunological stainings for laminin and hyaluronic acid. *Spp1* functions as a pro-fibrogenic ECM protein and was reported to promote fibrogenesis in an MCD-induced model (Syn *et al.*, 2011, 2012). Neutralization of the protein resulted in abrogated liver progenitor cell responses and fibrogenesis (Coombes *et al.*, 2015), indicating a crucial role of *Spp1* in progression of NAFLD. Interestingly, the *IMP2-2/p62* transgenic mice were shown to have an elevated collagen deposition and increased fibrosis (Simon, 2013; Simon *et al.*, 2014), suggesting a promoted fibrogenesis due to *IMP2-2/p62*-induced liver progenitor cell appearance. By inhibition of ECM components, especially laminin, liver progenitor cell activation and expansion was shown to be

impaired (Kallis *et al.*, 2011). Laminin was reported to surround liver progenitor cells in rat and mouse liver injury models, as well as in human cirrhotic livers (Lorenzini *et al.*, 2010). Furthermore, ECM production and deposition were proposed to occur before liver progenitor cell expansion and around liver progenitor cells in a CDE-induced liver injury rat model (Van Hul *et al.*, 2009), underlining the importance of ECM with liver progenitor cell occurrence.

Taken together, hepatic *IMP2-2/p62* expression is accompanied by progenitor or dedifferentiated cell populations and enhances ductular reaction with ECM deposition, and thereby promoting fibrosis.

Parts of the results presented in this chapter have been used for a publication submitted to *Frontiers in medicine:* CZEPUKOJC B, BARGHASH A, TIERLING S, NAß N, SIMON Y, KÖRBEL C, CADENAS C, VAN HUL NKM, SACHINIDIS A, HENGSTLER JG, HELMS V, LASCHKE MW, WALTER J, HAYBAECK J, LECLERCQ I, KIEMER AK, and KESSLER SM IGF2 mRNA binding protein 2 transgenic mice are more prone to develop a ductular reaction and to progress towards cirrhosis.

3 CHAPTER II

Different models of steatosis in *p62* transgenic mice

3.1 Introduction

Various dietary regimens are used in murine models to elucidate the pathogenesis of NAFLD and AFLD (Bertola, 2018). The genetic mouse model with a liver-specific expression of the human *p62* was described as a model for simple steatosis with none to mild inflammation (Tybl *et al.*, 2011; Laggai *et al.*, 2014). To study the pathogenesis towards inflammation or fibrosis, a second hit for this model is needed. *p62* was found to amplify NASH in an MCD feeding model (Simon *et al.*, 2014). However, the diet results in a significant body weight loss and loss of liver mass (Anstee *et al.*, 2006). Additionally, the comparison between MCD diet-induced NASH and human NASH is difficult because of differences in etiology (Larter, 2007). Therefore, models mimicking overnutrition like high-fat diets provide a more accurate model and were shown to have similar lipid alterations and histological changes as human NAFLD patients (Gorden *et al.*, 2011). Furthermore, in NASH patients and murine NASH models endogenous ethanol was found to be elevated (Cope *et al.*, 2000; Nair *et al.*, 2001; Baker *et al.*, 2010; Zhu *et al.*, 2013). An ethanol diet or endogenous ethanol can lead to a leaky gut, from which lipopolysaccharides translocate to the liver and induce inflammation (Szabo *et al.*, 2015). Therefore, in the following chapter two feeding models, the high-fat diet and the administration of ethanol in drinking water, were investigated with the objective of inducing steatosis and inflammation. In these models, the impact of hepatic *p62* expression was examined. The best suitable feeding model was planned to be chosen for KC depletion and epigenetic analysis (see Chapter III).

3.2 Results

3.2.1 High-Fat Diet (HFD)

To induce steatosis and inflammation mice were fed an HFD based on milk fat for 12 weeks. Milk fat diets were reported to promote more severe steatosis than lard fat diets (Sutter *et al.*, 2012).

Macroscopic examination of the livers showed no abnormalities (Figure 13 A). Analysis of microscopic HE stainings of liver sections revealed lipid accumulation within *p62* tg livers, while it did not occur in any of the wild-type livers, on either diet (Figure 13 B).
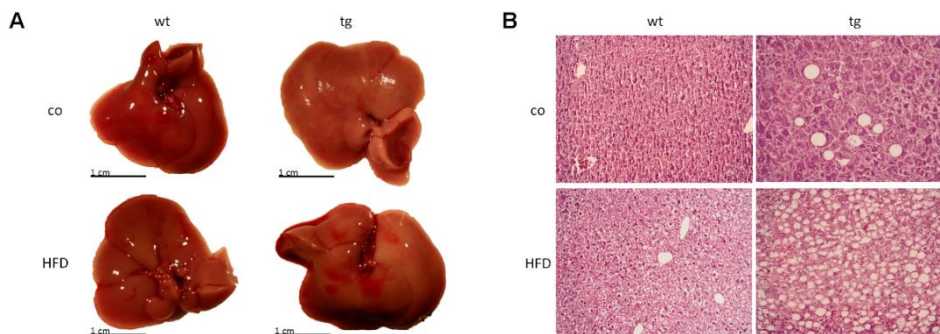
Figure 13*: Representative macroscopic pictures (A) and HE stainings (B) of livers and liver sections (original magnification: 200x) from wild-type (wt) and* p62 *transgenic (tg) animals fed a high-fat diet (HFD) or a control diet (co) for 12 weeks. n(co wt)=21; n(co tg)=19; n(HFD wt)=22; n(HFD tg)=18.*

Overall, HFD-fed mice had significantly increased body weight (Figure 14 A, B), while the liver to body ratio did not differ (Figure 14 C). Total lipid analysis revealed no differences, neither between genotypes nor between treatment groups (Figure 14 D).
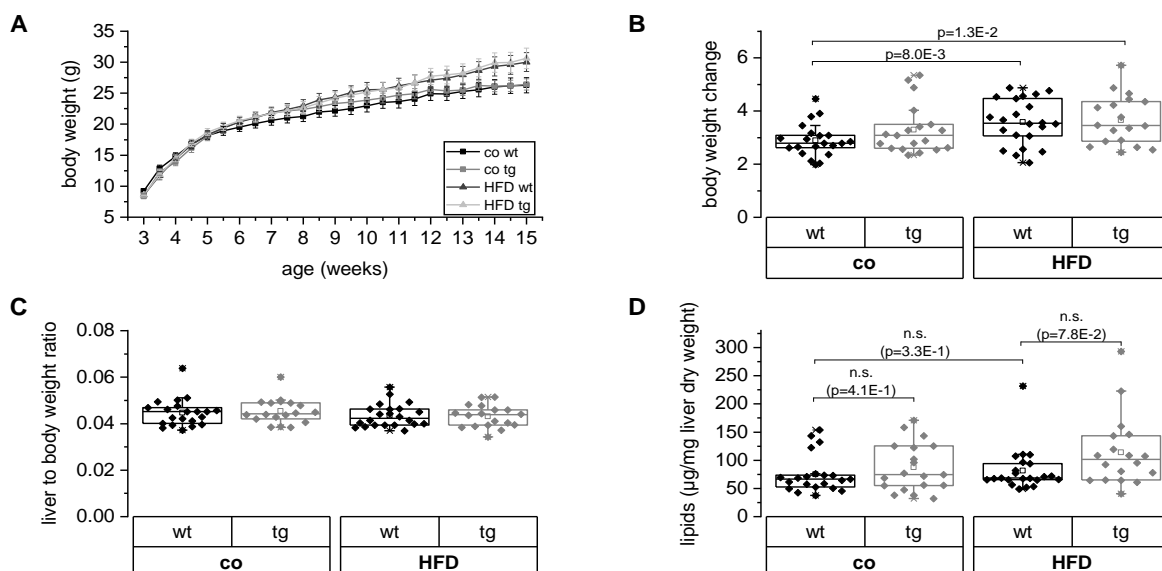
Figure 14*: Body weight, liver weight, and total lipids of wild-type (wt) and* p62 *transgenic (tg) animals on control (co) or high-fat diet (HFD) for 12 weeks. A: Body weight over time. B: Change of body weight at the age of 15 weeks compared to the weight at the beginning of the diet. C: Liver to body weight ratio. D: Total lipid analysis determined by the colorimetric sulfo-phospho-vanillin method. Results are shown as means ± SEM (A) or box plots with 25th/75th percentile boxes, geometric medians (line), means (square), and 10th/90th percentile as whiskers (B-D). P-values were calculated by Mann Whitney U test with Bonferroni correction (significance level set at p≤1.25E-2). n(co wt)=21; n(co tg)=19; n(HFD wt)=22; n(HFD tg)=18; n.s.=not significant.*

Determination of serum parameters to assess the health of the animals revealed decreased glucose levels in *p62* tg animals on control and high-fat diet compared to their wild-type littermates (Table 3). The lack of altered ALT and AST levels indicated the absence of inflammation.

Table 3: *Serum parameters of wild-type (wt) and* p62 *transgenic (tg) animals on control (co) or high-fat diet (HFD) for 12 weeks (n=18-22 each). Values are expressed as mean±SEM. P-values were calculated by Mann Whitney U test with Bonferroni correction (*$p<0.0125$ in comparison to co wt).*

	co		HFD	
	wt	**tg**	**wt**	**tg**
Number animals (n)	21	19	22	18
Serum ALT (U/l)	287.4 ± 74.1	321.4 ± 90.9	363.2 ± 75.5	375.9 ± 70.4
Serum AST (U/l)	2,517 ± 683	2,693 ± 870	3,357 ± 763	3,932 ± 843
Serum cholesterol (mg/dl)	125.0 ± 10.2	121.3 ± 7.03	140.7 ± 9.76	128.9 ± 6.81
Serum glucose (mg/dl)	330.3 ± 25.8	220.8 ± 20.3 *	237.8 ± 30.5	213.3 ± 28.5 *
Serum HDL (mg/dl)	100.6 ± 9.21	95.6 ± 7.63	112.6 ± 7.68	109.9 ± 7.22
Serum triglycerides (mg/dl)	247.8 ± 26.0	176.2 ± 15.8	295.6 ± 27.7	213.6 ± 21.4

In order to investigate possible inflammatory changes or changes in fatty acid and cholesterol metabolism, mRNA expression analysis was performed. No differences in expression of inflammatory markers F4/80/*Adgre1* and *Il1β*, or genes involved in fatty acid and cholesterol metabolism (liver X receptor and HMG-CoA reductase) was seen, neither between genotype nor between diets (Figure 15 A-D). These results underline the absence of inflammation.
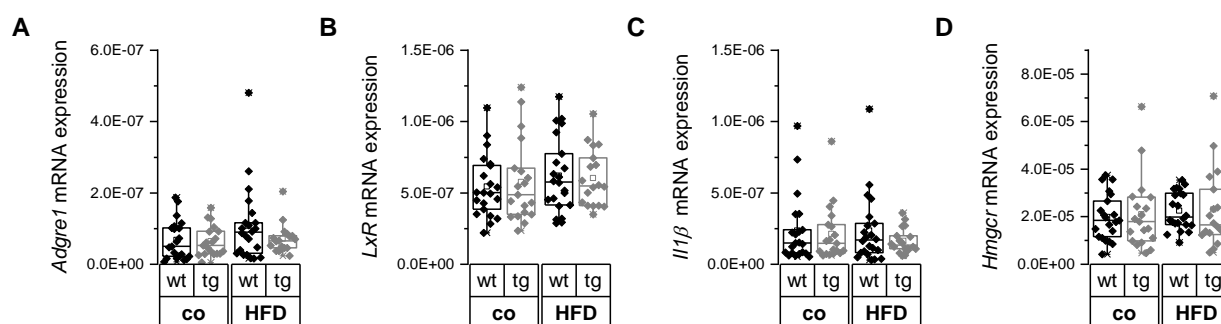
Figure 15: *Hepatic expression of genes involved in fatty acid and cholesterol metabolism and inflammatory markers. A-D: qPCR analysis of* Adgre1 *(F4/80) (A),* LxR *(B),* Il1β *(C), and* Hmgcr *(D) in livers of wild-type (wt) and* p62 *transgenic (tg) animals fed a high-fat (HFD: n(wt)=22; n(tg)=18) or control diet (co: n(wt)=21; n(tg)=19). Results are shown as box plots with 25th/75th percentile boxes, geometric medians (line), means (square), and 10th/90th percentile as whiskers. Data are presented as the ratio of mRNA expression of the gene of interest to the reference gene* Rn18s*.*

Since a tendency in total lipids within the liver was seen, a more detailed analysis by ESI-MS/MS was performed to reveal changes in the lipidome between genotypes and diets (Table 4, Supplemental figure 7-1 - Supplemental figure 7-3). The *p62* tg animals on the control diet had elevated levels of saturated cholesteryl ester, total species of ceramides, and polyunsaturated lysophosphatidylcholine when compared to the corresponding wild types (Table 4).

Livers of wild-type, as well as p62 tg animals on HFD, displayed mostly decreased levels of sphingolipids and glycerophospholipids compared to the corresponding genotype on control diet (Table 4).

Table 4: *Simplified table of significantly increased or decreased lipid classes in livers of high-fat diet-fed (HFD) wild-type (wt) or p62 transgenic mice (tg) compared to the control diet (co) (n=18-21 per group). Increased levels of lipid classes are highlighted in dark grey and decreased levels in light grey color. The lipidome was determined by ESI-MS/MS by. Corresponding figures are shown in Supplemental figure 7-1 - Supplemental figure 7-3. CE: cholesteryl ester, CER: ceramide, SM: sphingomyelin, PC: phosphatidylcholine, PE: phosphatidylethanolamine, PE P: PE based plasmalogens, PS: phosphatidylserine, PG: phosphatidylglycerol, PI: phosphatidylinositol, LPC: lysophosphatidylcholine, sat: saturated species, unsat: unsaturated species, total: all species.*

			HFD wt compared to co wt	HFD tg compared to co tg	co tg compared to co wt	HFD tg compared to HFD wt
Sterol lipids	CE	sat			↑	
		polyunsat	↑			
Sphingolipids	CER	sat		↓	↑	
		unsat	↓	↓	↑	
		total	↓	↓	↑	
	SM	monounsat	↓	↓		
		polyunsat		↑		
		unsat	↓	↓		
Glycero-phospholipids	PC	monounsat	↓	↓		
	PE	monounsat	↓	↓		
		polyunsat		↓		
		unsat		↓		
		total		↓		
	PE P	PE P-16:0				↑
		PE P-18:0	↑		↑	
	PS	monounsat	↓	↓		
	PG	total		↓		
	PI	monounsat	↓	↓		
	LPC	sat	↓	↓		
		monounsat	↓	↓		
		polyunsat	↓	↓	↑	
		unsat	↓	↓		
		total	↓	↓		

Due to the lack of steatosis and inflammation, the chosen HFD model was considered inadequate. Therefore, a new approach to induce inflammatory changes was used (c.f. 0).

3.2.2 Ethanol in drinking water

The second dietary approach to induce steatosis and inflammation in mice was the administration of ethanol in drinking water for 4 weeks (based on Zhou *et al.*, 2002). This model was shown to induce mild steatosis (Cook *et al.*, 2007).

After 4 weeks of ethanol intake, mice showed an increased liver to body weight ratio compared to the control diet, without changes between genotypes (Figure 16 C). The increase in the liver to body weight ratio in ethanol-treated animals in both genotypes was due to increased liver weights, while body weight did not change (m_{liver} (co wt) =1.09±0.05 g, m_{liver} (EtOH wt) =1.22±0.05 g, p=5.1E-2; m_{liver} (co tg) =1.08±0.05 g, m_{liver} (EtOH tg) =1.22±0.05 g, p=4.2E-2) (Figure 16 A, B). Total lipid content of the livers did not differ, neither between genotype nor between diets (Figure 16 D).
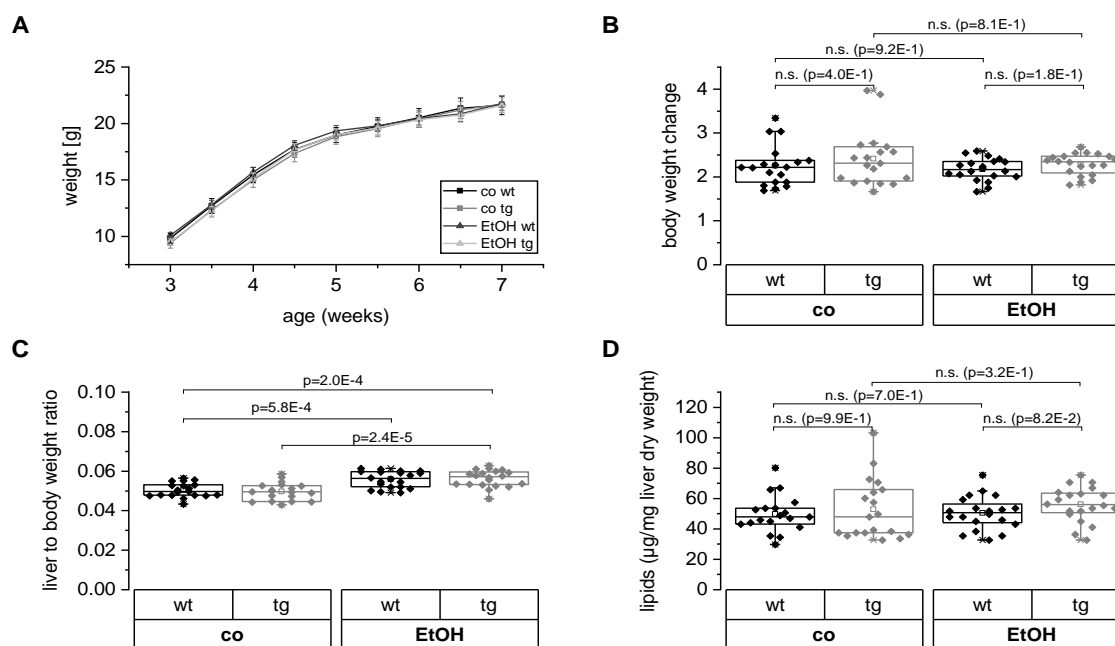
***Figure 16***: *Body, liver weight, and total lipids of wild-type (wt) and* p62 *transgenic (tg) animals on control (co) or ethanol in drinking water (EtOH) diet for 4 weeks. A: Body weight over time. B: Change of body weight at the age of 4 weeks compared to the weight at the beginning of the diet. C: Liver to body weight ratio. D: Total lipid analysis determined with the colorimetric sulfo-phospho-vanillin method. Results are shown as means ± SEM (A) or box plots with 25th/75th percentile boxes, geometric medians (line), means (square), and 10th/90th percentile as whiskers (B-D). P-values were calculated by one-way ANOVA in C and by Mann Whitney U test with Bonferroni correction in B and D (significance level set at p≤1.25E-2). n(co wt)=19; n(co tg)=19; n(EtOH wt)=20; n(EtOH tg)=20; n.s.=not significant.*

Histological analysis of HE and Sirius red stainings revealed no occurrence of steatosis and/or fibrosis, independent of genotype or diet. Nevertheless, a higher percentage of *p62* tg animals showed apoptosis compared to wild types, while less apoptosis occurred on the ethanol diet (Figure 17 A). The ethanol drinking led to less lobular lymphocytic inflammation in the wild-type and *p62* tg group, while there were no changes in infiltrates of neutrophilic granulocytes in *p62* tg animals (Figure 17 B, C).
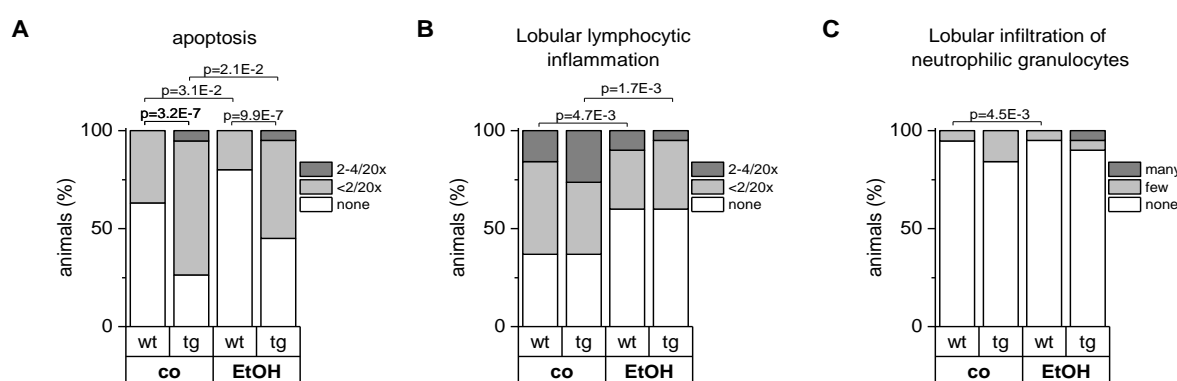
Figure 17: *Histological scoring of HE stainings for apoptosis (A), lobular lymphocytic inflammation (B), and lobular infiltration of neutrophilic granulocytes (C) of livers from wild-type (wt) and* p62 *transgenic (tg) mice treated with ethanol in drinking water (EtOH) for 4 weeks. P-values were determined with a chi-square test. co: control.*

The ethanol in drinking water administration was an insufficient feeding model to promote steatotic and inflammatory features. Therefore, the model for the Kupffer cell depletion and epigenetic analysis in Chapter III.1 and III.2 was changed to a Lieber-DeCarli (LDC) diet, which could be confirmed to induce steatosis and inflammation (see Chapter III) as previously reported (Pritchard *et al.*, 2007).

3.3 Discussion

The liver-specific expression of *p62* was shown to cause a simple steatosis (Tybl *et al.*, 2011). A second hit, such as an MCD diet, is required to amplify steatosis and inflammation (Simon, 2013; Simon *et al.*, 2014) for studying NASH. Still, the MCD diet has a big drawback: the effect of a significant loss of body weight and liver mass (Anstee *et al.*, 2006). Therefore, in this study the effect of *p62* on the pathogenesis of NAFLD/AFLD in a feeding model, mimicking over-nutrition, ethanol consumption or endogenous ethanol production, was elucidated. Two approaches were pursued, HFD feeding and ethanol in drinking water administration.

The HFD led to an increased body weight change but lacked steatosis and signs for inflammation after 12 weeks of feeding. Various dietary regiments exist and the development of steatosis and inflammation not only depends on the duration of feeding but also on different diet compositions, such as the fat content, cholesterol content, and lipid species. Dietary fatty acids may also play an important role in the promotion or inhibition of NAFLD (Ferramosca *et al.*, 2014; Juárez-Hernández *et al.*, 2016). Hepatic expression of *p62* did not promote amplification of steatosis or the induction of inflammation as expected, possibly due to the age. Characterization of the *p62* transgenic animals showed decreased hepatic *p62* expression in 10-week-old mice (Tybl *et al.*, 2011). Therefore, an earlier endpoint was chosen for further experiments and a change of diet, since the feeding of the HFD was not able to induce steatosis.

Given that elevated endogenous levels of ethanol are found in NASH patients and murine NASH models (Cope *et al.*, 2000; Nair *et al.*, 2001; Baker *et al.*, 2010; Zhu *et al.*, 2013), administration of ethanol was chosen as a new approach. The administration of ethanol led to increased liver weight, but histological analysis and total hepatic lipid content did not show steatosis. Further, liver sections lacked infiltration on neutrophils, which was described in alcohol-fed mice and supposed to promote progression of AFLD (Ramaiah *et al.*, 2007; Chang *et al.*, 2015). Probably, the chosen time point of 4 weeks feeding was too short to provoke steatosis, as developed steatosis was shown after 8 weeks of ethanol diet (Brandon-Warner *et al.*, 2012). Furthermore, the C57Bl/6J mouse strain is a rather alcohol-preferring strain, whereas DBA/2J mice have a higher aversion to alcohol (Lê *et al.*, 1994; Wahlsten *et al.*, 2006; Blizard, 2007; Yoneyama *et al.*, 2008; D'Souza El-Guindy *et al.*, 2010). DBA mice can resist eating or can be adversely affected by the diet, resulting in weight loss or increased mortality (Bertola *et al.*, 2013). Since we crossed these two stains, their amount of alcohol consumption is unknown and was not monitored. Thus, the intake of alcohol might have been not enough to cause significant steatosis in this short period of time. Regarding changes between genotypes, total hepatic lipid content tended to be increased in ethanol-fed *p62* transgenic mice, indicating a possible amplification of lipid storage.

The genetic background of mouse strains used for modeling NAFLD/AFLD is crucial. Some mouse strains are more prone to a steatosis-like phenotype and alcohol-induced fatty liver disease (D'Souza El-Guindy *et al.*, 2010; Tsuchiya *et al.*, 2012; Fengler *et al.*, 2016). The mice in this work had a mixed background, as C57Bl/6J crossed with DBA/2J mice were used. However, even in genetically identical

inbred C57Bl/6J mice, the response to high-fat feeding has been reported to be heterogeneous (Burcelin *et al.*, 2002; Koza *et al.*, 2006; Duval *et al.*, 2010): This mouse strain was proposed to divide into low- and high-metabolic responders, while high-metabolic responders showed inflammation and more severe lipid accumulation compared to low-metabolic responders upon high-fat diet feeding (Duval *et al.*, 2010).

Emerging data reveal a major role of the intestinal microbiome in the susceptibility of liver disease (Hartmann *et al.*, 2019). The absence of intestinal microbiota in germ-free mice resulted for instance in increased hepatic steatosis and ethanol metabolism (Chen *et al.*, 2015). Fecal microbiota transplantation from ALD-resistant to ALD-susceptible mice prevented alcohol-induced liver injury in mice (Ferrere *et al.*, 2017). Furthermore, mice receiving the microbiome from a patient with alcoholic hepatitis followed by alcohol treatment, developed more severe liver inflammation (Llopis *et al.*, 2016).

Taken together, HFD and ethanol in drinking water feeding were inadequate to induce steatosis.

4 CHAPTER III

The role of p62 and Kupffer cells in steatohepatitis

III-1   Differential gene expression associated with epigenetic changes and the role of Kupffer cells in steatohepatitis

III-2   Epigenomic profiling of hepatocytes overexpressing the lipogenic and tumor-promoting mRNA binding protein p62/IMP2-2

4.1 Introduction

For the understanding of the pathogenesis of AFLD and NAFLD, it is important to study the interaction and crosstalk between parenchymal and non-parenchymal cells, including immune cell populations within the liver. Kupffer cells (KCs) have been implicated in fatty liver disease. Still, their role in the progression of steatohepatitis and in inflammation is controversially discussed because of their pleiotropic functions (Dixon *et al.*, 2013; Gao *et al.*, 2016). Depletion of KCs was suggested to attenuate experimental AFLD and NAFLD (Adachi *et al.*, 1994; Lanthier *et al.*, 2011). Their activation trough translocated LPS deriving from a 'leaky gut' with consequent activation of the inflammatory cascade, is one proposed important mechanism (Rao, 2009; Harte *et al.*, 2010; Wong *et al.*, 2015). Additional aspects that have an influence on susceptibility or progression of steatohepatitis are epigenetic changes promoted by environmental factors including diet and alcohol (Mathers *et al.*, 2010). Different methylation patterns have been described in different stages of NAFLD (Murphy *et al.*, 2013; Zeybel *et al.*, 2015). Therefore, in the following chapter (III-1) the role of KCs and epigenetically regulated changes in gene expression in steatohepatitis were investigated.

In the liver, *p62* expression was shown to induce simple steatosis (Tybl *et al.*, 2011) and with an additional second hit, such as a diet, an amplification of inflammation was described (Simon *et al.*, 2014). Since the administration of ethanol in drinking water was inadequate to induce steatohepatitis (Chapter II) mice were fed a steatohepatitis-inducing liquid ethanol diet, as devised by Lieber and DeCarli (Lieber *et al.*, 1989). This *ad libitum* feeding was shown to induce steatosis and inflammation after 6 weeks (Pritchard *et al.*, 2007). Here (III-2), the impact of *p62* expression in this steatohepatitis model in the presence or absence of KCs was investigated and further characterization of the *p62* transgenic model was performed. Previous studies reported that the expression of the imprinted genes *IGF2* and *H19* is elevated by p62 (Tybl *et al.*, 2011). Thus, the aim of the following chapter (III-2) was to further characterize the animal model with regard to the epigenome of hepatocytes and hepatic non-parenchymal cells (NPCs).

4.2   Results

III-1   Differential gene expression associated with epigenetic changes and the role of Kupffer cells in steatohepatitis

III-1.1   Liver damage due to clodronate liposome treatment and augmented serum cholesterol due to LDC feeding

To address the role of KCs in steatohepatitis, we performed four different treatment groups (Table 5). Mice were fed for 5 weeks either a control diet (co) or a steatohepatitis-inducing Lieber-DeCarli diet (LDC) as shown by Pritchard *et al.* (Pritchard *et al.*, 2007). Additionally, KCs were depleted *via* clodronate liposome (clo) injections (Van Rooijen, 1989), while PBS was administered as a control.

Table 5: *Overview of the treatment groups for investigating the role of Kupffer cells in steatohepatitis. co: control diet; clo: clodronate liposomes; LDC: Lieber-DeCarli diet; KC: Kupffer cells. Created with elements from Servier Medical Art (https://smart.servier.com/), licensed under a Creative Commons Attribution 3.0 Unported License.*

co + PBS	co + clo	LDC + PBS	LDC + clo
Control	Control/KC-depleted	Ethanol-containing diet	Ethanol-containing diet/ KC-depleted

Macroscopic examinations of the livers did not exhibit distinct changes in size or color between the different treatment groups (Figure 18). Only one animal fed the LDC diet and receiving clodronate liposomes showed large necrotic areas in the liver (arrow Figure 18).
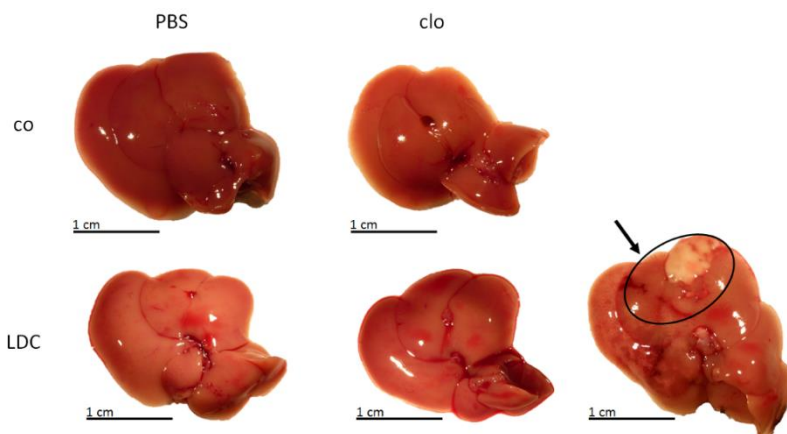
Figure 18: *Representative macroscopic pictures of livers from animals fed a Lieber-DeCarli (LDC) or a control (co) diet and treated with either PBS or clodronate liposomes (clo). The arrow indicates necrotic areas in the liver of one animal injected with clodronate liposomes and fed the LDC diet.*

In order to confirm the absence of KCs, the expression of the KC-specific marker *Clec4f* (Yang *et al.*, 2013; Lavin *et al.*, 2014) was determined by qPCR. *Clec4f* expression levels in clo-treated animals were diminished, indicating a successful depletion (Figure 19 A). With regard to the clo treatment, animals had decreased body weight (Figure 19 B, C), while liver weight did not differ (data not shown).

Concerning the effect of LDC feeding, PBS-treated animals showed a decreased liver to body weight ratio compared to the control diet (Figure 19 D); body weight was comparable, while liver weight tended to decrease in the LDC-fed PBS group.
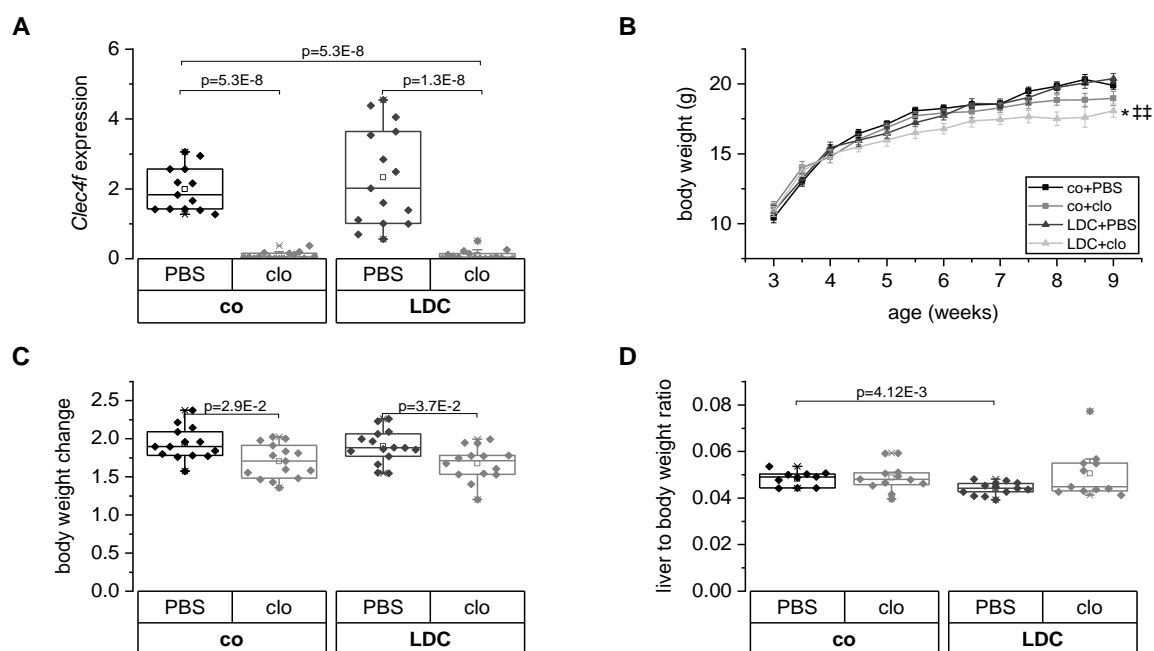
Figure 19: Confirmation of Kupffer cell depletion and body and liver weight analysis of animals fed a Lieber-DeCarli (LDC) diet, treated with PBS or clodronate liposomes (clo) for 5 weeks. A: Clec4f qPCR analysis. Data are shown as the ratio of mRNA expression of Clec4f to the reference gene Csnk2a2 (n=13-15 each). B: Body weight over time (*p<0.05 compared to co+PBS, ‡‡p≤0.01 compared to LDC+PBS). C: Body weight change at the age of 9 weeks compared to the weight at the beginning of the diet. D: Liver to body weight ratio after sacrificing. Results are shown as means ± SEM (B) or box plots with 25th/75th percentile boxes, geometric medians (line), means (square), and 10th/90th percentile as whiskers. P-values were calculated by Mann Whitney U test with Bonferroni correction in A and D and by One-way ANOVA in B and C.

Serum parameters were determined to obtain a first indication of alterations in inflammatory or metabolic changes. Clo-treated animals compared to the respective control had significantly elevated ALT levels indicating liver damage. Also, AST levels were higher in clo-treated LDC-fed mice (Table 6). Regarding metabolic alterations, the LDC diet led to increased serum levels of HDL in the PBS-treated group and increased cholesterol levels in both treatment groups compared to the respective control (Table 6). These results indicate a dysregulation in cholesterol metabolism due to LDC feeding.

Table 6: Serum levels of animals fed a normal chow (co) or an LDC diet in combination with PBS or clodronate liposome (clo) injections (n=10-13 per group). Data are shown as mean ± SEM. P-values of ALT and AST were determined by Mann Whitney U test with Bonferroni correction: **p<2.5E-3 compared to co+PBS, †††p<2.5E-4 compared to LDC+PBS. P-values of cholesterol and HDL were calculated by One-Way ANOVA: ***p<1E-3 compared to co+PBS, ‡‡‡p<1E-3 compared to co+clo.

	co		LDC	
	PBS	**clo**	**PBS**	**clo**
Number animals (n)	10	12	13	11
Serum ALT (U/l)	49.5 ± 5.60	102 ± 20.6 **	51.2 ± 3.31	529 ± 263 ** †††
Serum AST (U/l)	325 ± 42.3	555 ± 70.7	337 ± 44.9	1,290 ± 363 ** †††
Serum cholesterol (mg/dl)	70.0 ± 4.65	77.9 ± 4.98	104 ± 4.15 ***	106 ± 3.51 *** ‡‡‡
Serum glucose (mg/dl)	381 ± 30.9	328 ± 36.2	402 ± 26.2	309 ± 38.0
Serum HDL (mg/dl)	60.5 ± 4.04	64.2 ± 4.76	97.3 ± 4.59 ***	81.4 ± 8.06
Serum triglycerides (mg/dl)	131 ± 11.9	131 ± 13.7	177 ± 14.5	175 ± 16.1

Since liver damage occurred, inflammatory changes were also suggested. However, mRNA expression levels for *Tnfα*, *Il6*, and *Il1β* were below the detection limit in all treatment groups (data not shown). Reduced expression of the endogenous anti-inflammatory mediator glucocorticoid-induced leucine zipper (Gilz, gene name: *Tsc22d3*) was seen in LDC-fed mice, as determined by qPCR (Figure 20 A), suggesting inflammatory changes. In clo-treated animals, a downregulation could derive from the depletion of macrophages expressing *Gilz*.

An increased gut permeability can induce liver inflammation, as described in patients with alcoholic and non-alcoholic steatohepatitis (Szabo *et al.*, 2010; Wang *et al.*, 2010). In order to test the hypothesis of an ethanol-induced leaky gut, endotoxins were measured in the serum of LDC-fed mice. While mean and median LPS levels were elevated in mice fed the LDC diet compared to the control diet, the values did not have statistical significance (Figure 20 B).
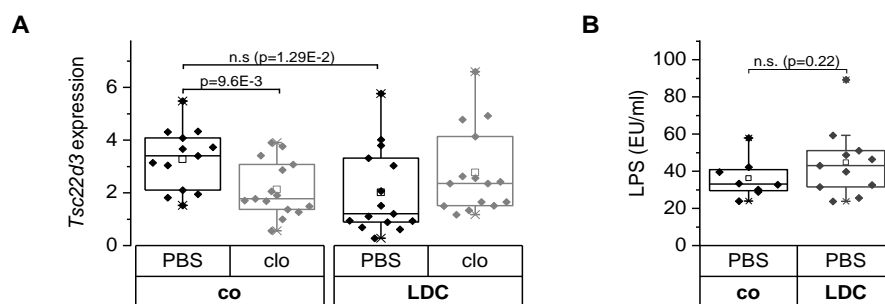
Figure 20*: Tsc22d3 mRNA expression in the liver and serum endotoxins levels. A: Tsc22d3 qPCR analysis of animals fed a control or Lieber-DeCarli (LDC) diet and treated with PBS or clodronate liposomes (clo). Data are shown as the ratio of mRNA expression of Tsc22d3 to the reference gene Csnk2a2 (n=13-15 per group). P-values were determined by Mann Whitney U test with Bonferroni correction (significance level set at p≤1.25E-2). B: Endotoxin in the serum of mice fed an LDC diet (n=11) compared to the control diet (n=8). The quantification was performed by an endpoint fluorescent assay EndoZyme® II Recombinant Factor C Assay (Hyglos GmbH). Results are shown as box plots with 25th/75th percentile boxes, geometric medians (line), means (square), and 10th/90th percentile as whiskers. LPS: lipopolysaccharide. n.s.: not significant.*

III-1.2 Hepatic accumulation of lipids due to LDC feeding and the impact of clodronate liposome treatment

Liver sections were microscopically analyzed by HE stainings but did not show steatosis in any of the treatment groups. Given that microvesicular lipid incorporations are difficult to evaluate microscopically by HE stainings, lipidomic analyses *via* ESI-MS/MS were performed in order to determine changes in hepatic lipids due to treatment and diet.

Accumulation of hepatic triglycerides (TG) as a hallmark of ALFD and NAFLD occurred in LDC-fed animals, compared to the respective control (Figure 21 A). Furthermore, all measured lipid classes were altered in the livers of LDC-fed animals. The analysis revealed an accumulation of sterol lipids (CE and FC), glycerophospholipids (PC, PE, PI), and sphingolipid species (saturated CER and total SM), assuming a general increased hepatic lipid incorporation (Figure 21 B - D, Supplemental table 7-2, Supplemental figure 7-4 -Supplemental figure 7-6). The elevated levels of cholesterol ester (CE) and free cholesterol (FC), confirm the previously suggested dysregulated cholesterol homeostasis. The only decreased species were unsaturated ceramides (CER) (Figure 21 E) and unsaturated sphingomyelins (SM) (Supplemental table 7-2, Supplemental figure 7-4 C, D).

When comparing clo-treated to PBS-treated mice on control diet, only CER were detected in a higher concentration and the SM to CER ratio was decreased (Figure 22 A, Supplemental figure 7-4 C).

The LDC diet-induced increase of the most abundant lipid classes, i.e. TG, phosphatidylcholine (PC), and phosphatidylinositol (PI), was completely abrogated in the livers of clo-treated animals (Figure 21 A-C), suggesting an impact of the clo treatment on the reduction of these lipids.

In contrast, hepatic levels of FC, unsaturated CER, and lysophosphatidylcholine (LPC) were increased in clo-treated animals (Figure 21 D-F), indicating a contribution to the accumulation of these lipids. Furthermore, the PC to LPC and the CE to FC ratio were decreased in clo-treated LDC-fed mice (Figure 22 B, C). No effect was seen on CE, SM, phosphatidylserine, PE-based plasmalogens, or phosphatidyl-glycerol (Supplemental table 7-2, Supplemental figure 7-4 - Supplemental figure 7-6).
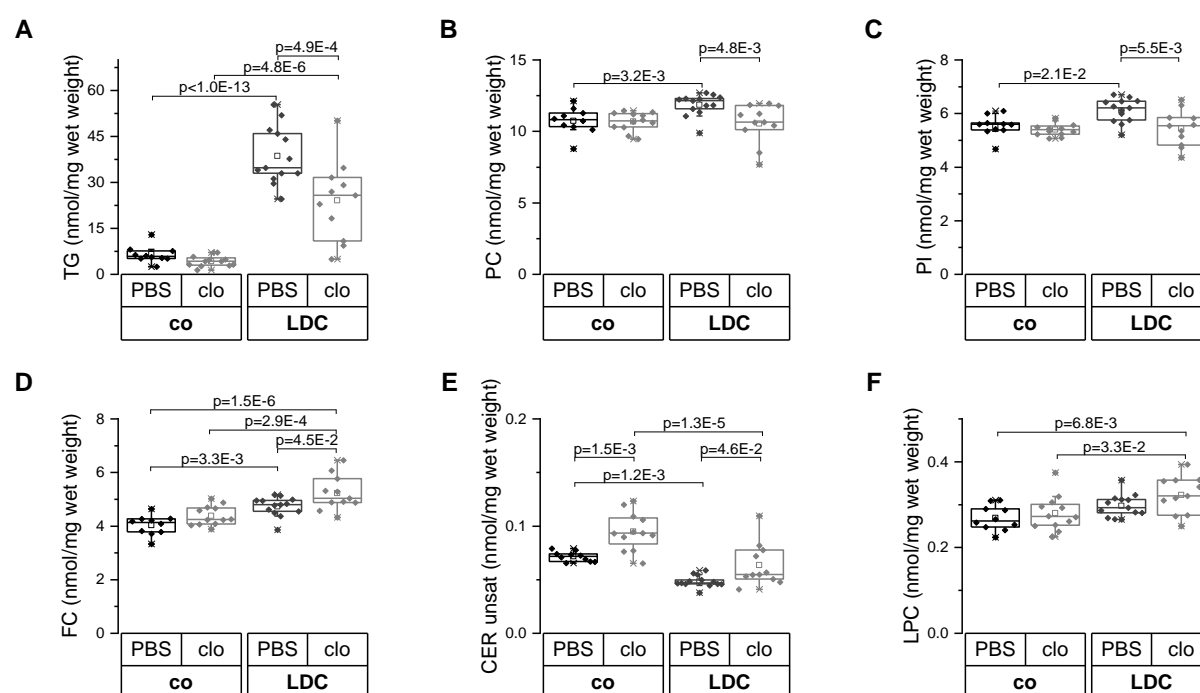
Figure 21: Impact of the LDC diet and Kupffer cells on selected lipid classes. Whole livers from animals fed a Lieber-DeCarli (LDC) or control (co) diet and treated with PBS as control or clodronate liposomes (clo) for 5 weeks (n=10-13 per group) were analyzed. A-G: Lipidomic analysis of triglycerides (TG) (A), phosphatidylcholine (PC) (B), phosphatidylinositol (PI) (C), free cholesterol (FC) (D), unsaturated ceramides (CER) (E), lysophosphatidylcholine (LPC) (F) via ESI-MS/MS. Results are shown as box plots with 25th/75th percentile boxes, geometric medians (line), means (square), and 10th/90th percentile as whiskers. P-values in A, B, D, and F were calculated by One-Way ANOVA and in C and E by Mann Whitney U test with Bonferroni correction.
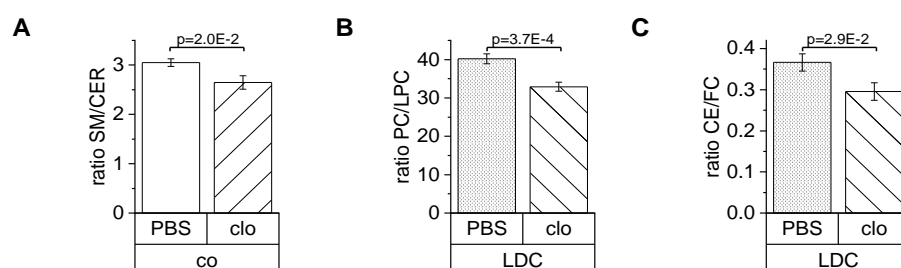
Figure 22: Ratios of hepatic lipids in clodronate liposome (clo)-treated mice on control or Lieber-DeCarli (LDC) diet. Data are shown as the mean±SEM. P-values were calculated with t-test.

III-1.3 Treatment-dependent differential gene expression and DEGs associated with epigenetic changes in hepatocytes and non-parenchymal cells

Hepatocytes and NPCs were isolated from animals of each treatment group and epigenomes were analyzed in two animals of each group. RNA sequencing was performed to reveal the transcriptome, reduced representative bisulfite sequencing (RRBS) to analyze the genome-wide methylation profile, and DNaseI-sequencing to identify open chromatin regions.

Analyzing the methylation profile of hepatocytes from LDC-fed mice compared to the control, 1,352 differentially methylated regions (DMRs) were found in total with a similar amount of hyper- and hypo-methylated regions (43.2%/56.8%). In addition, RNA-sequencing revealed 504 differentially expressed genes (DEGs) with 182 being associated with epigenetic changes, i.e. DMRs and/or differentially open chromatin regions (DOR) as determined by DNaseI-sequencing (Table 7).

In the NPC fraction isolated from mice receiving an LDC diet compared to the control, 5,422 mostly hypomethylated (71.1%) DMRs were found by RRBS.

Table 7: *Number of differentially expressed genes (DEG) and DEGs associated with epigenetic changes, i.e. differentially methylated regions (DMR) and/or differential open chromatin regions (DOR) of hepatocytes and non-parenchymal cells of animals receiving a control (co) or a Lieber-DeCarli (LDC) diet treated with PBS or clodronate liposomes (clo) for Kupffer cell depletion (n=2 each). DEGs were determined by RNA-sequencing, DMRs by reduced representative bisulfite sequencing and DORs by DNaseI-sequencing. Up: upregulated, down: downregulated*

	co+clo compared to co+PBS			LDC+PBS compared to co+PBS			LDC+clo compared to LDC+PBS			LDC+clo compared to co+clo		
Hepatocytes	**total**	up	down	**total**	up	down	**total**	up	down	**total**	up	down
DEG	**196**	85	111	**504**	245	259	**479**	192	287	**126**	47	79
DEG + DMR and/or DOR	**58**	19	39	**182**	74	108	**24**	9	15	**60**	22	38
Non-parenchymal cells	**total**	up	down	**total**	up	down	**total**	up	down	**total**	up	down
DEG	**1940**	812	1128	**839**	462	377	**678**	266	412	**9**	5	4
DEG + DMR and/or DOR	**924**	380	544	**337**	180	157	**125**	37	88	**5**	3	2

Venn diagrams (Figure 23) display slightly overlap of DEGs associated with DMRs and/or DORs between the different treatment comparisons in hepatocytes (A) and NPCs (B).
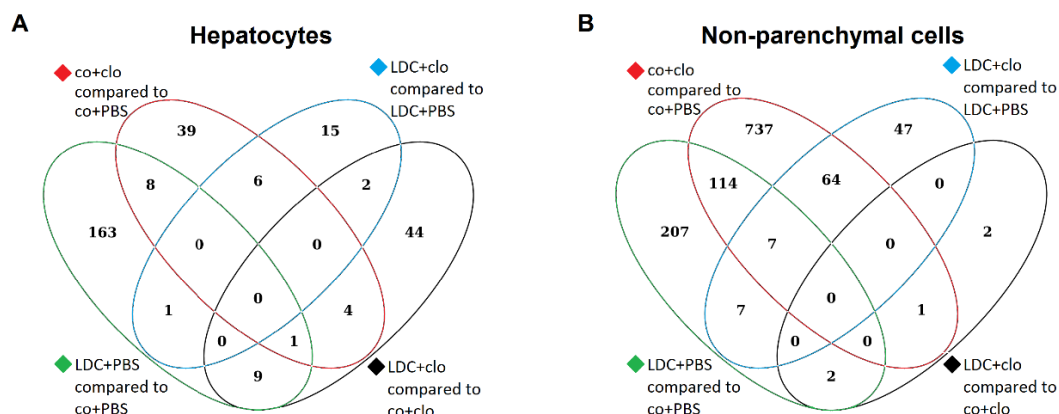
Figure 23: *Venn diagram displaying the overlap of differentially expressed genes associated with epigenetic changes (DMR and/or DOR) from different treatment comparisons of hepatocytes (A) and non-parenchymal cells (B). co: control diet; clo: clodronate liposomes; LDC: Lieber-DeCarli diet.*

III-1.3.1 Impact of LDC feeding on DEGs associated with epigenetic changes in hepatocytes and NPCs

a) Upregulation of lipid-associated pathways in hepatocytes isolated from LDC-fed mice

To identify altered biological processes of DEGs, Kyoto Encyclopedia of Genes and Genomes (KEGG) pathway and Gene Ontology (GO) term enrichment analyses were performed using the STRING database V10.5 (Szklarczyk *et al.*, 2015, 2017). To visualize significantly altered biological processes, semantic clustering was performed to identify similar GO terms and to generate multidimensional scaling scatter plots using the REVIGO tool (Supek *et al., 2011)*.

Comparing upregulated DEGs of hepatocytes between LDC-fed and control diet-fed animals, GO term enrichment analysis showed that several upregulated genes play a role in the 'response to lipopolysaccharide' (GO:0032496; FDR=2.1E-2; OGC=10; matching proteins: Alpl, Ccrn4l, Ednrb, F2r, Mrc1, Ptgfr, Raet1d, Sparc, Thbd, Vldlr; data not shown). Together with increased serum LPS levels, a leaky gut and subsequent translocation of LPS to the liver can be suggested.

Figure 24 shows a simplified heatmap of all DEGs associated with epigenetic changes (in total 182) in hepatocytes isolated from LDC-fed mice compared to the control diet.
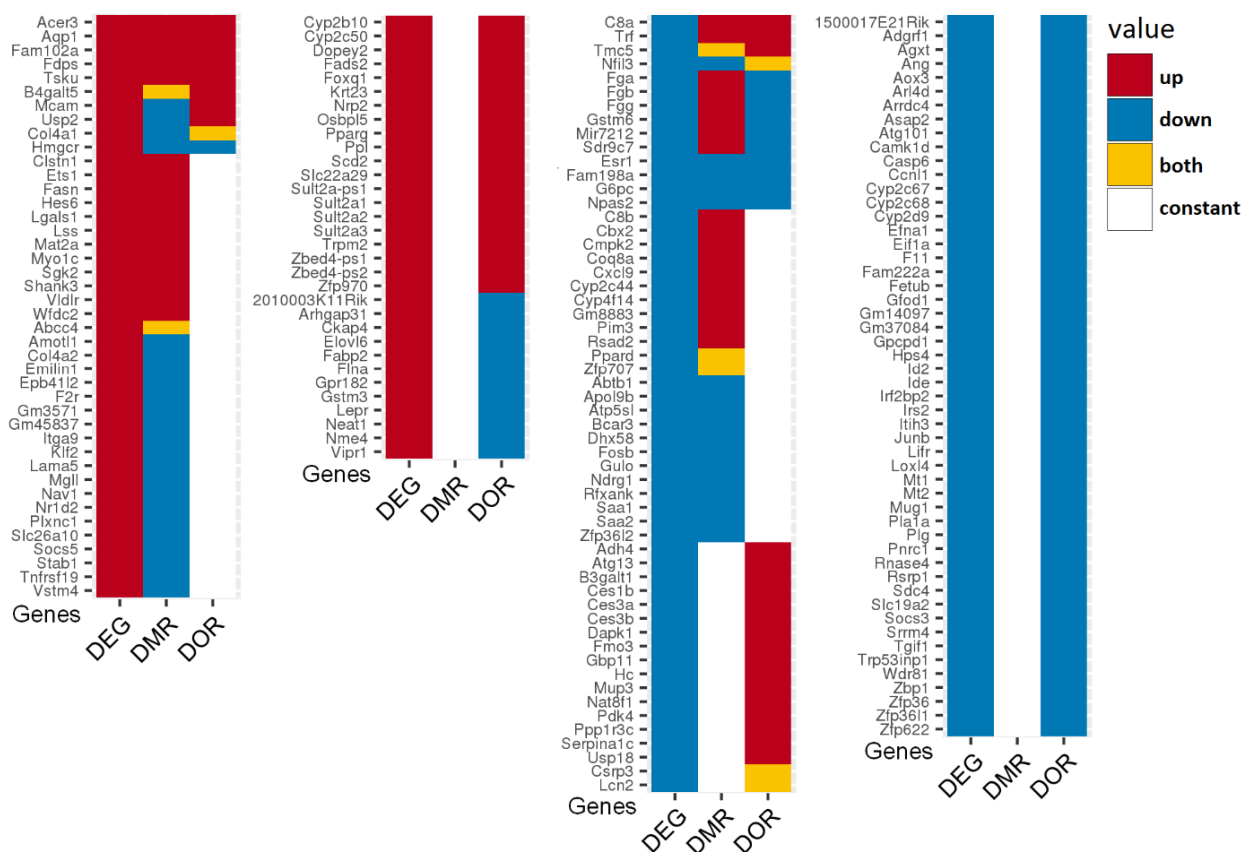
Figure 24*: Simplified heatmap of the 182 differentially expressed genes (DEGs) associated with differentially methylated regions (DMRs) and/or differentially open chromatin regions (DORs) for the comparison of hepatocytes isolated from animals fed an LDC diet to the control diet. DEGs were determined by RNA-sequencing, DMRs by reduced representative bisulfite sequencing, and DORs by DNaseI-sequencing.*

Induced genes associated with epigenetic changes upon LDC feeding were involved in 'lipid metabolism', 'fatty acid metabolism', and 'cholesterol metabolism' (Figure 25 A) in compliance with the performed lipidomic analyses and the suggested dysregulation of lipid and cholesterol metabolism.
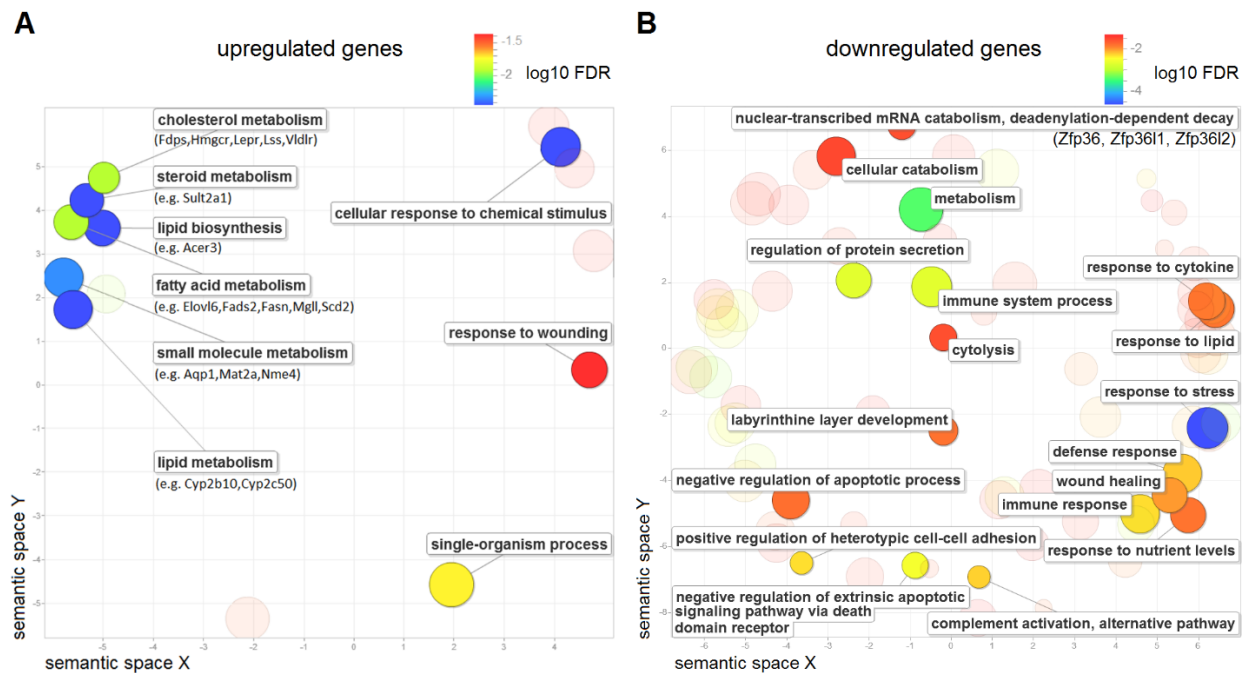
Figure 25*: GO enrichment analysis of upregulated (A) and downregulated (B) genes associated with epigenetic changes in hepatocytes isolated from animals fed an LDC diet compared to the control diet. GO terms for biological processes were categorized using semantic clustering and plotted by the REVIGO tool to identify similar GO terms among the enriched terms. Semantically similar GO terms remain closer together. Examples of genes included in the GO terms are shown in brackets. The circles represent individual GO terms or cluster of GO terms related to similar processes. Semantically similar GO terms remain closer together. The circle size corresponds to the percentage of genes annotated with the term in the reference database (UniProt for mus musculus) (larger means more general and smaller more specific GO term). The circle color illustrates the false discovery rate (in log10 FDR) of the GO enrichment analysis: red indicates the lowest and blue the highest significance.*

Notwithstanding the significant upregulation of *Hmgcr* (1.98 fold, p=1.2E-5; Figure 24) and *Elovl6* (1.79 fold, p=2.4E-4), the RNA sequencing result could not be verified by qPCR analysis of whole liver samples of animals fed the LDC diet compared to the control diet (Figure 26 A, B). Therefore, the epigenetic analyses have to be construed with caution, due to a small number of animals and individual variations.

Downregulated genes associated with epigenetic changes (Figure 24), in hepatocytes from LDC-fed mice compared to the control i.a. play a role in the 'complement and coagulation cascades' as determined by KEGG pathway analysis (KEGG 4610; FDR=1.66E-8; matching proteins: C8a, C8b, F11, Fga, Fgb, Fgg, Hc, Plg, Serpina1c; data not shown). GO term enrichment analysis revealed a contribution in biological processes such as 'negative regulation of apoptotic process', 'wound healing', 'defense response', and 'immune response' (Figure 25 B). Moreover, the downregulated genes were involved in 'nuclear-transcribed mRNA catabolic process, deadenylation-dependent decay' (Figure 25 B). Here, *Zfp36* plays a central role and its downregulation was confirmed by qPCR in whole liver tissue (Figure 26 C), suggesting an impaired degradation of nuclear-transcribed mRNAs.
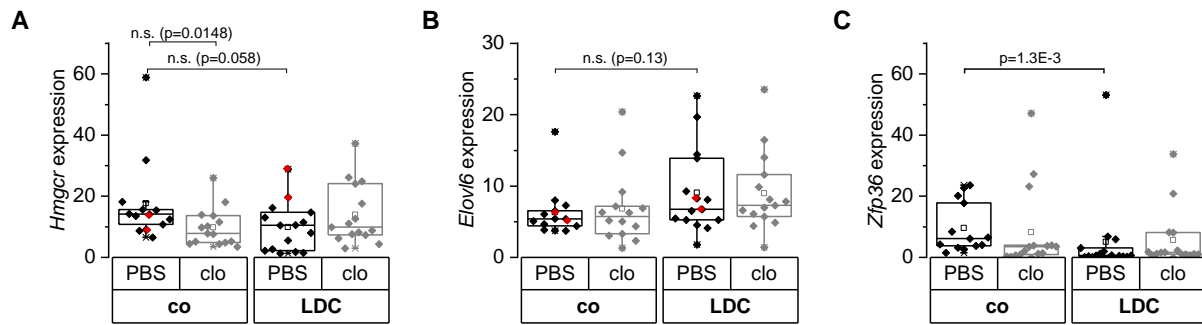
Figure 26*: Hmgcr, Elovl6, and Zfp36 expression in LDC-fed animals. mRNA expression analysis of* Hmgcr *(A),* Elovl6 *(B), and* Zfp36 *(C) determined by qPCR of animals fed a control (co) or Lieber-DeCarli (LDC) diet and treated with PBS or clodronate liposomes (clo). The measurements were performed on whole livers (n=13-15 per group). Marked in red are the expression levels of whole liver cell lysates of the animals used for RNA-sequencing. Data are shown as the ratio of mRNA expression of the gene of interest to the reference gene* Csnk2a2 *(n=13-15 per group). P-values were determined by Mann Whitney U test with Bonferroni correction (significance level set at p≤1.25E-2). Results are visualized as box plots with 25th/75th percentile boxes, geometric medians (line), means (square), and 10th/90th percentile as whiskers. n.s.: not significant.*

   b)   DEGs associated with epigenetic changes in NPCs of LDC-fed mice are involved in morphology and immune response

In order to characterize changes in NPCs during steatohepatitis, deregulated genes associated with epigenetic changes, i.e. DMR and/or DOR, were analyzed in NPCs isolated from mice fed an LDC diet compared to the control diet. A simplified heatmap is shown in Supplemental figure 7-13.

LDC-diet led to increased apoptosis (Figure 27 A) and induced genes associated with epigenetic changes playing a role in morphogenetic changes with ECM remodeling ('regulation of anatomical structure morphogenesis', 'extracellular matrix organization', 'regulation of cell migration', 'response to wounding'; Supplemental figure 7-14 A). Within these processes, the expression of genes encoding for collagen (*Col14a1*, *Col4a1*, *Col4a2*, *Col6a2*), laminin (*Lamb1*, *Lamc1*), matrix metalloproteinase (*Mmp2*, *Mmp17*), and extracellular matrix protein 1 (*Ecm1*) was increased. Furthermore, LDC-fed mice displayed lymphocytic inflammation and infiltrations of neutrophils (Figure 27 B and C).

Downregulated DEGs associated with epigenetic changes were enriched in immune response and 'regulation of endothelial cell apoptotic process' (Supplemental figure 7-14 B) and pathways, such as 'complement and coagulation cascades', 'chemokine signaling pathway' (data not shown).
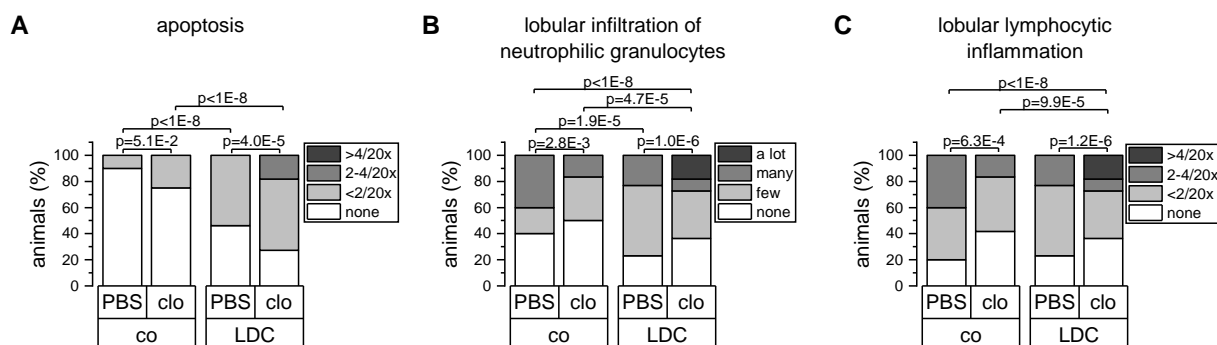
Figure 27*: Histological analysis of livers from control (co) or LDC-fed mice in the presence (PBS) or absence (clo) of Kupffer cells (n=10-13). A-C: Histological scoring of HE stainings for apoptosis (A), lobular infiltration of neutrophilic granulocytes (B), and lobular lymphocytic inflammation (C). P-values determined by Chi-square test.*

III-1.3.2   Impact of clodronate liposome treatment on gene expression in hepatocytes and NPCs

In the following section, several treatment groups were compared to identify the impact of clo treatment on the transcriptome. First, clo treatment on control diet was analyzed (co+clo vs. co+PBS a)). Second, the effect of macrophage depletion on LDC-fed mice was determined (LDC+clo vs. LDC+PBS b)). Third, the effect of the LDC-diet on clo-treated animals was investigated (LDC+clo vs. co+clo c)). For all comparisons downregulated genes in hepatocytes were involved in the complement system, partly associated with epigenetic changes (see supplement 7.3.1-7.3.3)

a)   Deregulated genes in hepatocytes of clo-treated mice play a role in the inflammatory response and the complement cascade

The comparison of clo-treated animals to the control revealed upregulated genes involved in e.g. 'leukocyte migration involved in inflammatory response', 'neutrophil aggregation', 'regulation of cell death', and 'inflammatory response'. As proposed by RNA sequencing, the mobilization of leukocytes was confirmed by histological analysis showing neutrophil infiltration (Figure 27 B). Furthermore, the expression of *Cxcl1*, a chemokine produced also in hepatocytes (Su *et al.*, 2018), was increased (3.1 fold, p=2.32E-9). As a consequence of clo treatment, lymphocytic inflammation and apoptosis occurred (Figure 27 A, C), consistent with elevated serum ALT suggesting liver damage (cf. Table 6).

Among the downregulated genes, enriched GO terms were involved in 'innate immune response' and 'apoptotic cell clearance' (Supplemental figure 7-7 B). Further, biological processes correlating to lipid metabolism and gluconeogenesis were changed (Supplemental figure 7-7 B). Beside *Elovl3* downregulation, only genes encoding for the major urinary proteins (*Mup3*, *Mup5*, *Mup10*, *Mup11*, *Mup16*, and *Mup19*) were altered in these processes.

b)   Clodronate liposome treatment during LDC feeding alters the expression of genes involved in cell division and DNA replication, and shows infiltrates of immune cells in the NPC fraction

The impact of clo treatment in LDC-fed mice on differential gene expression was analyzed in order to investigate the role of Kupffer cells in steatohepatitis. Increased *Apoa4* expression was found and confirmed by qPCR (p=2.7E-3, LDC+clo compared to LDC+PBS, Figure 34). Cell proliferation was suggested by induced genes in hepatocytes enriched in 'DNA replication', 'cell cycle', and 'cell division', including an upregulation of lipocalin-2 (*Lcn2;* 1.75 fold, p=3.5E-2) (Supplemental figure 7-9 A). Furthermore, NPCs had deregulated genes associated with epigenetic changes (A) also playing also a role in 'cell cycle', 'cell division' (Supplemental figure 7-15 A, B).

An upregulation of immunoglobulin genes not associated with epigenetic changes was found in the hepatic NPC fraction comparing clo-treated to PBS-treated LDC-fed animals (Supplemental figure 7-16 B). Moreover, histological analysis of liver sections revealed infiltration of neutrophilic granulocytes and apoptosis (Figure 27 A, B). Thus, clo treatment during LDC diet-induced infiltrates of immune cells resulting in a different cell type composition in the NPC fractions, possibly contributing to a stronger lobular lymphocytic inflammation (Figure 27 C).
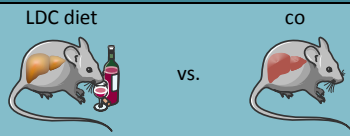
Clo treatment led to the downregulation of genes involved in 'granulocyte chemotaxis' and 'regulation of cytokine production', as expected due to macrophage depletion.

c) LDC feeding in clodronate liposome-treated mice did not alter DEGs involved in lipid, cholesterol, or fatty acid metabolism

LDC feeding in clo-treated mice revealed only downregulated genes in hepatocytes being enriched in e.g. 'immune response' (Supplemental figure 7-11). Moreover, downregulated genes were involved in lipid biosynthesis and gluconeogenesis. Here, no other genes involved in lipid metabolism were altered, except for major urinary proteins (*Mup10, Mup16, Mup3;* data not shown), indicating an impact of macrophages on lipid- and cholesterol-associated differential gene expression.

III-1.4   Overview of results for LDC feeding and clodronate liposome treatment

Table 8:   *Overview of the most important results for investigating the impact of LDC-feeding and clodronate liposome (clo) treatment. Different treatment groups were compared to each other. vs.: versus/compared to; KC: Kupffer cells; co: control; LDC: Lieber-DeCarli; CE: cholesteryl ester; CER: ceramide; FC: free cholesterol; LPC: lysophosphatidylcholine; PC: phosphatidylcholine, PE: phosphatidylethanolamine; PI: phosphatidylinositol; SM: sphingomyelin; TG: triglycerides; ↑: increased; ↓: decreased; = no changes. Created with elements from Servier Medical Art (https://smart.servier.com/), licensed under a Creative Commons Attribution 3.0 Unported License.*

Effect of LDC-diet	
LDC diet co	
↑ serum cholesterol ↑ HDL = ALT, AST ↑ TG, SM, PC, PE, PI, CE, FC, saturated CER	Infiltration of neutrophils, lymphocytic inflammation ↑ apoptosis ↓ *Gilz*
DEGs associated with epigenetic changes	
↑ Upregulated genes in **hepatocytes** enriched in lipid, fatty acid, and cholesterol metabolism = *Hmgcr* and *Elovl6* expression ↑ Upregulated genes in **NPCs** enriched in processes of physiology and morphology, including ECM remodeling ↑ genes encoding for collagen, laminin, and MMPs	↓ Downregulated genes enriched in the complement system, 'negative regulation of apoptotic process' ↓ *Zfp36* expression

Effect of KC depletion (a)	Effect of KC depletion in LDC diet (b)	Effect of LDC diet in KC-depleted mice (c)
KC-depleted co co	KC-depleted LDC diet LDC diet	KC-depleted LDC diet KC-depleted co
↑ ALT ↓ body weight change	↑ ALT and AST ↓ body weight change	↑ serum cholesterol = ALT and AST
Infiltration of neutrophils, lymphocytic inflammation ↑ apoptosis	↑ apoptosis, ↑ infiltration neutrophils, ↑ lymphocytic inflammation	↑ apoptosis, ↑ infiltration neutrophils, ↑ lymphocytic inflammation
↑ CER ↓ SM/CER ratio	↓ TG, PC, PI ↑ FC, CER unsat ↓ PC/LPC, CE/FC	↑ LPC
deregulated genes in the immune system and a downregulation of genes involved in the complement system		
↑ **Upregulated genes** enriched in		
'leukocyte migration involved in inflammatory response', 'neutrophil aggregation' ↑ *Cxcl1*	'cell cycle, 'cell division', 'DNA replication' 'response to reactive oxygen species' ↑ *Lcn2* ↑ *Apoa4*	No changes in lipid, cholesterol, or fatty acid metabolism
↓ **Downregulated genes** were enriched in		
'apoptotic cell clearance', lipid biosynthesis and gluconeogenesis: ↓ *Mup*	'granulocyte chemotaxis', 'regulation of cytokine production'	lipid biosynthesis and gluconeogenesis: only ↓ *Mup*

III-2 Epigenomic profiling of hepatocytes overexpressing the lipogenic and tumor-promoting mRNA binding protein p62/IMP2-2

III-2.1 *p62* expression is treatment dependent and abrogates LDC-induced elevated serum levels of cholesterol, HDL, and triglycerides

A potential role of *p62* overexpression was investigated on the epigenome of hepatocytes and on a potential paracrine effect on the epigenome of hepatic NPCs. In order to investigate how *p62* expression impacts steatohepatitis dependent on KC presence or absence, wild-type and *p62* transgenic mice (tg) were fed an LDC diet and treated with PBS as a control or clo (Table 9).

Table 9: *Overview of the treatment groups for investigating the impact of* p62 *expression in an LDC-feeding model treated with PBS or clodronate liposomes (clo). co: control diet; LDC: Lieber-DeCarli diet; KC: Kupffer cells; p62↑: p62 transgenic mice expressing* p62 *exclusively in the liver. Created with elements from Servier Medical Art (https://smart.servier.com/), licensed under a Creative Commons Attribution 3.0 Unported License.*

wild-type (wt) mice			p62 transgenic (tg) mice			
co + PBS	co + clo	LDC + PBS	co + PBS	co + clo	LDC + PBS	LDC + clo
control	control/ KC-depleted	Ethanol-containing diet	control	control/ KC-depleted	Ethanol-containing diet	Ethanol-containing diet/ KC-depleted

Macroscopic examinations of livers did not reveal changes in size or color in any of the treatment groups. In the liver of one *p62* tg mice on control and two *p62* tg mice on LDC diet, receiving clo, histological analysis revealed large necrotic areas and macroscopical abnormalities (arrows Figure 28).
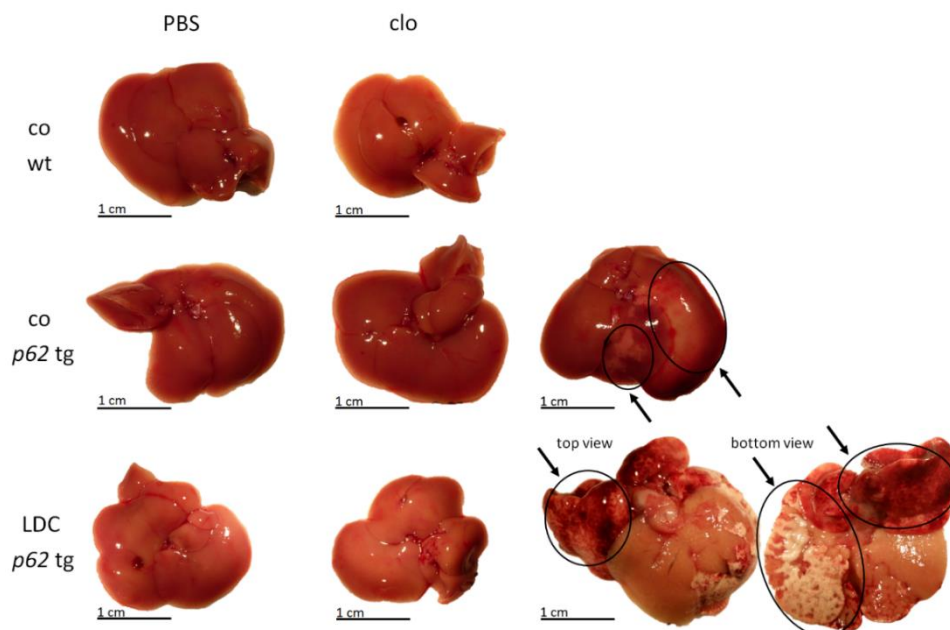
Figure 28: *Macroscopic pictures of livers from wild-type (wt) and* p62 *transgenic (tg) animals fed a Lieber-DeCarli (LDC) or a control (co) diet and treated with either PBS or clodronate liposomes (clo). Arrows indicate necrotic areas in the liver of* p62 *transgenic animals injected with clodronate liposomes fed a control or an LDC diet.*

In order to confirm KC depletion, *Clec4f* mRNA expression levels were determined by qPCR. In the clo-treated groups, expression was almost completely abrogated, indicating a successful depletion (Figure 29 A). Furthermore, *p62* expression was determined showing variable expression levels in tg animals (Figure 29 B). LDC diet and clo treatment significantly decreased hepatic *p62* expression (Figure 29 B), so that these mice cannot be referred to as tg animals.
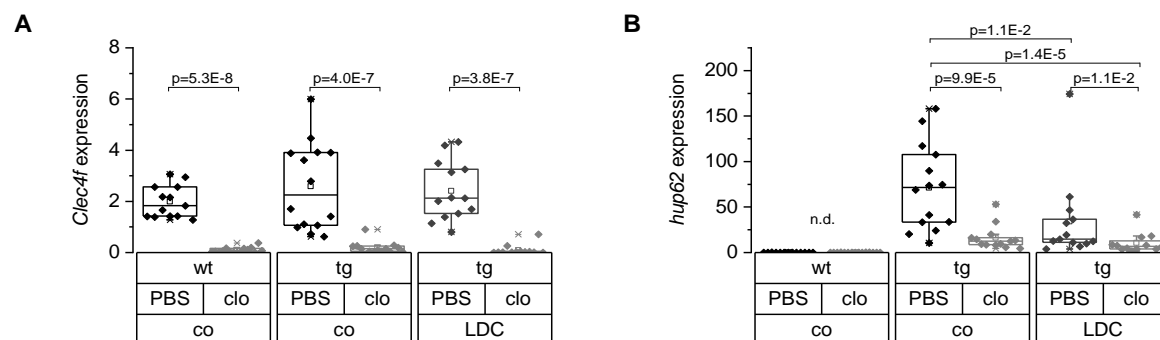
Figure 29: *Confirmation of Kupffer cell depletion and p62 expression. A-B: qPCR analysis of* Clec4f *(A) and p62 (B) mRNA expression of wild-type (wt) and p62 transgenic (tg) animals fed a control (co) or Lieber-DeCarli (LDC) diet and treated with PBS or clodronate liposomes (clo) for 5 weeks (n=12-15 per group). Data are shown as the ratio of mRNA expression of the gene of interest to the reference gene* Csnk2a2*. Results are shown as box plots with 25th/75th percentile boxes, geometric medians (line), means (square), and 10th/90th percentile as whiskers. P-values were calculated by Mann Whitney U test with Bonferroni correction. n.d.: not determined*

With regard to the impact of *p62* expression, no changes in weight gain, liver weight or in the liver to body weight ratio were seen compared to wild-type mice (Figure 30 A-D). Treatments had similar effects in both genotypes: decreased body weight change due to clo treatment (Figure 30 B) and decreased liver to body weight ratios in LDC-fed mice due to decreased liver weight (Figure 30 C, D).
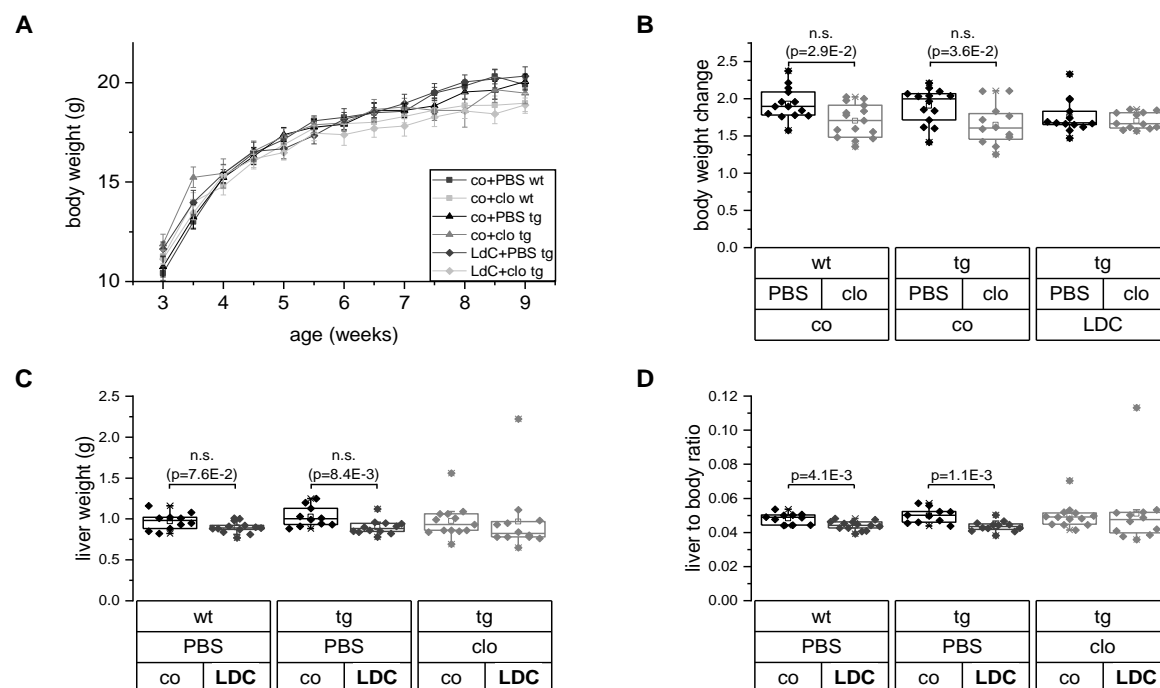
Figure 30: *Body and liver weight analysis of wild-type (wt) and p62 transgenic (tg) animals fed a control (co) or a Lieber-DeCarli (LDC) diet and treated with PBS or clodronate liposomes (clo) (n=12-15 each). A: Weight over time. B: Change of body weight at the age of 9 weeks compared to the weight at the onset of diet. C, D: Liver weight (C) and liver to body weight ratio (D) after sacrificing. Results are shown as means ± SEM (A) or box plots with 25th/75th percentile boxes, geometric medians (line), means (square), and 10th/90th percentile as whiskers. P-values were calculated by Mann Whitney U test with Bonferroni correction (significance level set at p≤8.33E-3). n.s.: not significant.*

Serum parameters were determined to reveal metabolic alterations. Also, the hepatic lipidome was determined by ESI-MS/MS since microsteatosis as it occurs in *p62* transgenic animals is complicated to detect by analysis of microscopic HE stainings of liver sections.

Even though the LDC diet significantly diminished *p62* expression, mice exhibited differences in serum and hepatic lipids. The determination of serum parameters revealed that hepatic expression of *p62* abrogated increased serum levels of cholesterol, HDL, and triglycerides during LDC feeding (Figure 31 A-C). As hepatic triglycerides (Figure 31 D), CE, and FC (Supplemental figure 7-3) were accumulated to the same extent in both, wild-type and *p62* tg animals on LDC diet, an impaired lipid export out of the liver in tg animals can be suggested.

Comparing to wild-type animals, the expression of *p62* did not increase hepatic levels of triglycerides, neither on control nor on LDC diet. An impact of *p62* expression was only observed on ceramide levels; hepatic *p62* expression on control diet increased ceramide levels (Figure 31 E). Further changes in lipid storage between genotypes were not detected (Supplemental figure 7-17 - Supplemental figure 7-20).
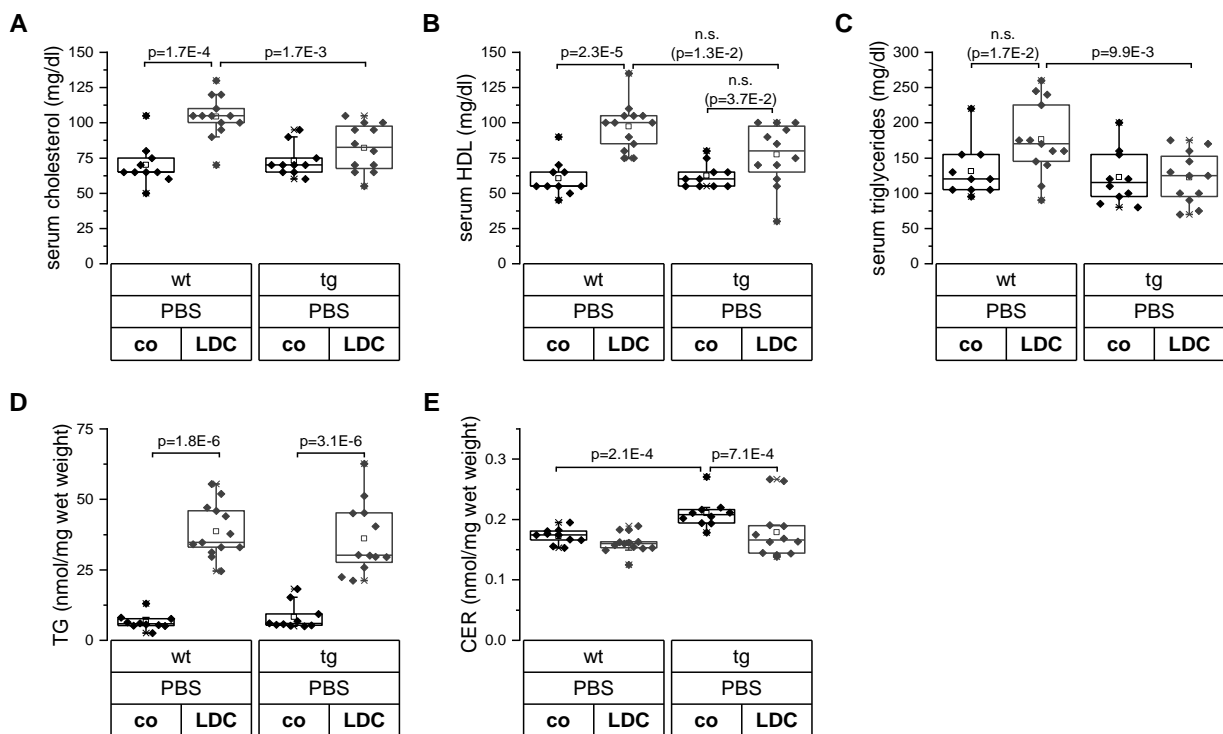
Figure 31*: Impact of p62 expression on serum and hepatic lipids. A-C: Serum levels of cholesterol (A), HDL (B), triglycerides (C), and hepatic levels of triglycerides (TG) (D), ceramides (CER) (E) of wild-type (wt) and* p62 *transgenic (tg) animals fed a normal chow (co) or a Lieber-DeCarli (LDC) diet. Liver tissue lipidomes (D, E) were determined by ESI-MS/MS. Results are shown as box plots with 25th/75th percentile boxes, geometric medians (line), means (square), and 10th/90th percentile as whiskers. P-values were determined by Mann Whitney U test with Bonferroni correction (significance level set at p≤1.25E-2). n.s.: not significant.*

Histological analysis of liver tissues revealed increased apoptosis in *p62* tg animals compared to wild types in all treatment groups (Figure 32 C). Furthermore, *p62* tg livers showed less lymphocytic inflammation and lobular infiltration of neutrophilic granulocytes compared to wild types except for the combination of LDC diet and clo treatment, where both were increased (Figure 32 A, B).
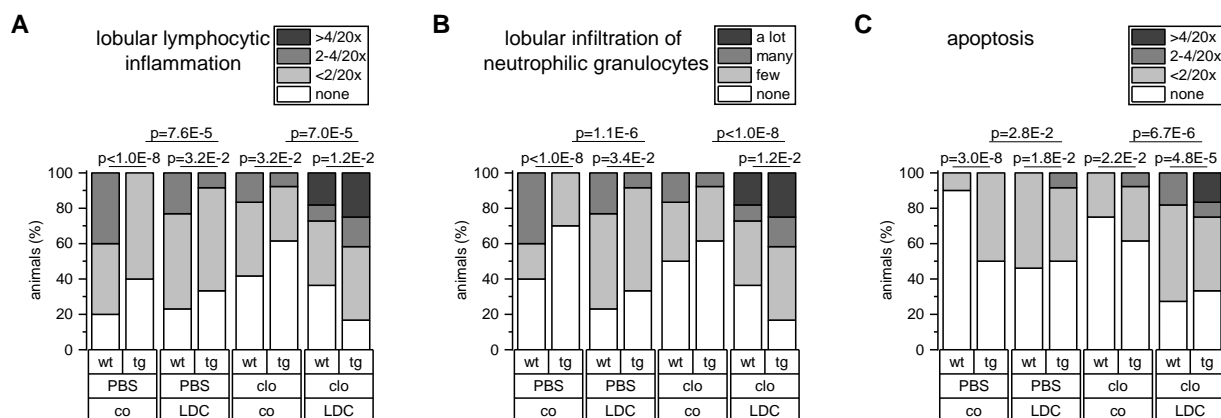
***Figure 32**: Histological scoring of HE stainings for lobular lymphocytic inflammation, lobular infiltration of neutrophilic granulocytes, and apoptosis of livers from control (co) or LDC diet-fed wild-type (wt) or p62 transgenic (tg) mice treated with PBS or clodronate liposomes (clo) (n=10-13 per group). P-values were calculated with the chi-square test.*

III-2.2 Differentially expressed genes associated with epigenetic changes in hepatocytes of *p62* transgenic mice are involved in lipid metabolism

Previous studies in our group reported elevated expression of imprinted genes, *H19* and *IGF2*, in *p62* tg mice (Tybl *et al.*, 2011). Therefore, a further characterization of the *p62* tg mouse was performed with regard to a potential role on the epigenome of hepatocytes and a potential paracrine action on the epigenome of hepatic NPCs. Thus, hepatocytes and NPCs from wild-type and *p62* tg animals receiving the control diet were isolated and epigenomes were analyzed by RRBS, RNA sequencing, and DNaseI sequencing.

RBBS revealed 674 DMRs for hepatocytes of *p62* tg mice, compared to wild types. There were similar amounts of hyper- and hypomethylated regions (55.5% / 44.5%). In NPCs isolated from *p62* tg mice 1,888 mostly hypomethylated DMRs were found (85.4%). However, NPCs of *p62* tg animals had only 42 DEGs compared to wild types, among which only 5 genes were associated with epigenetic changes, i.e. DMRs and/or DORs (Table 10, Figure 33). This indicates a rather minor paracrine effect on NPCs.

***Table 10**: Amount of differentially expressed genes (DEGs) and DEGs associated with epigenetic changes, i.e. differentially methylated regions (DMRs) and/or differentially open chromatin regions (DOR) of hepatocytes and non-parenchymal cells from* p62 *transgenic (n=2) animals compared to wild types (n=2). DEGs were determined by RNA-sequencing, DMRs by reduced representative bisulfite sequencing and DORs by DNaseI-sequencing.*

	p62 transgenic vs wild-type					
	co+PBS tg compared to co+PBS wt					
	Hepatocytes			Non-parenchymal cells		
	total	up	down	total	up	down
DEG	**237**	136	101	42	8	34
DEG + DMR and/or DOR	**61**	20	41	5	2	3

With regard to the impact of *p62* expression on hepatocytes, 237 genes were differentially expressed in comparison to wild types (Table 10). The 136 upregulated genes play a role in e.g. "ECM-receptor interaction" as determined by KEGG pathway analysis (FDR=3.73E-02; matching proteins: *Cd44*, *Hspg2*, *Lama5*, *Spp1;* data not shown), confirming an increased expression of the liver progenitor cell marker *Spp1* (cf. Chapter I). Previous studies reported that especially the expression of the imprinted genes *Igf2* and *H19* is elevated by *p62* (Tybl *et al.*, 2011; Kessler *et al.*, 2015). In this study, the expression levels *Igf2* and *H19* were significantly increased, but not associated with epigenetic changes in hepatocytes (*Igf2*: 1.65 fold change, p=3.3E-3; *H19*: 1.48 fold change, p=2.6E-2), indicating a regulation of the expression independent of epigenetic changes. *H19* and *Igf2* were both upregulated in NPCs and associated with a hypomethylation (Figure 33), suggesting a possible contamination with hepatocytes.

In hepatocytes, epigenetic changes were associated with 61 DEGs (Table 10), listed in the following simplified heatmap (Figure 33).
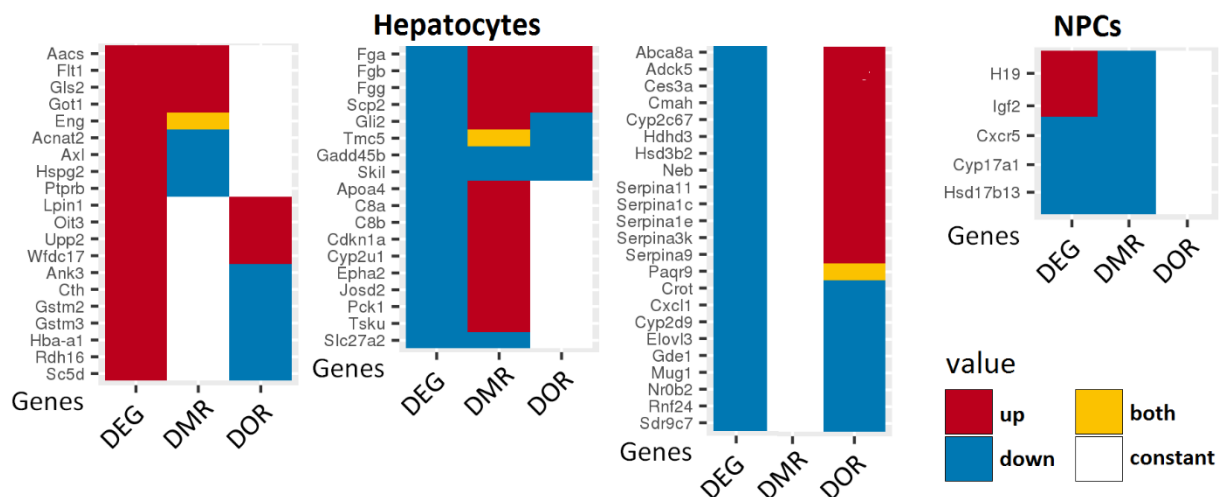
***Figure 33**: Simplified heatmap of the differentially expressed genes (DEGs) associated with differentially methylated regions (DMRs) and/or differentially open chromatin regions (DORs) of hepatocytes and non-parenchymal cells (NPCs) isolated from* p62 *transgenic animals in comparison to wild types.*

Among the 61 DEGs associated with epigenetic changes in *p62* transgenic hepatocytes, 41 genes were downregulated and 20 upregulated (Figure 33). Within these downregulated genes, *Elovl3* (0.54 fold, p=4.5E-4) was associated with less accessible chromatin and *Apoa4* (0.37 fold, p=5.8E-30) with a hypermethylation. Both genes play a role in "lipid metabolic process", and "fatty acid metabolic process" as determined by GO Term enrichment analysis (Figure 34).

The downregulation of *Apoa4* in *p62* transgenic mice was confirmed on mRNA level by qPCR (Figure 35) and was also observed in all other treatment groups except for the control treatment with LDC diet, suggesting a reversed effect due to LDC feeding.
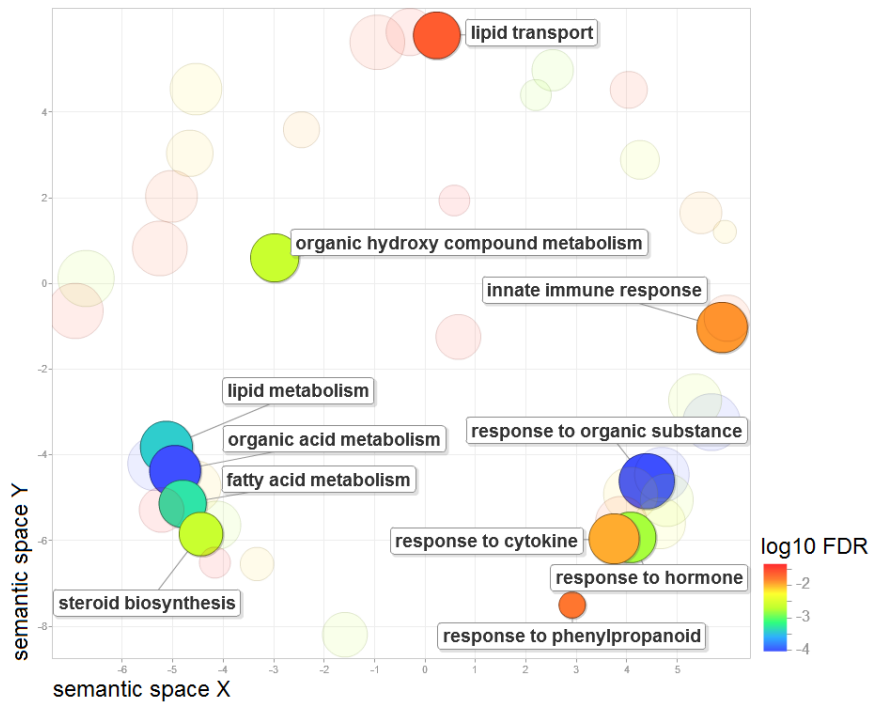
Figure 34: *GO biological process enrichment analysis of differentially expressed genes associated with epigenetic changes (DMR and/or DOR) of hepatocytes isolated from* p62 *transgenic (n=2) animals compared to wild types (n=2). GO terms were categorized using semantic clustering and plotted by the REVIGO tool to identify similar GO terms among the enriched terms. Semantically similar GO terms remain closer together. Examples of genes included in the GO terms are shown in brackets. The circles represent individual GO terms or cluster of GO terms related to similar processes. The circle size corresponds to the percentage of genes annotated with the term in the reference database (UniProt for mus musculus) (larger means more general and smaller more specific GO term). The circle color illustrates the false discovery rate (in log10 FDR) of the GO enrichment analysis: red indicates the lowest and blue the highest significance.*

Figure 35: *:* Apoa4 *mRNA expression analysis for the comparison of* p62 *transgenic to wild-type animals.* Apoa4 *mRNA expression in whole liver samples of wild-type (wt; n=13) and* p62 *transgenic (tg; n=14) animals with control (co) or LDC diet and treated with PBS od clodronate liposomes (clo), determined by qPCR analysis. Data are shown as the ratio of mRNA expression of* Apoa4 *to the reference gene* Csnk2a2. *The fold changes are shown on top of the graph corresponding to the comparisons between genotypes within the same treatment groups. Results are shown as box plots with 25th/75th percentile boxes, geometric medians (line), means (square), and 10th/90th percentile as whiskers. P-values were calculated by Mann Whitney U test and with t-test for LDC+clo.*

4.3 Discussion

4.3.1 LDC-fed mice showed features of a steatohepatitis

To induce steatohepatitis, the administration of an ethanol-containing diet was chosen. Ethanol not only plays an important role in the development of AFLD, but also in NAFLD, as endogenous levels of ethanol are found in NASH patients and murine NASH models (Cope *et al.*, 2000; Nair *et al.*, 2001; Baker *et al.*, 2010; Zhu *et al.*, 2013). As ethanol metabolism takes place in the liver, the liver is prone to ethanol toxicity, lipotoxicity through alterations in the hepatic metabolism of lipids, and the development of steatosis (Cook *et al.*, 2007). An initial step in the current project was to verify steatohepatitis due to the LDC diet.

Here it is shown that LDC feeding induced apoptosis, neutrophilia, hepatic lipid accumulation, and altered gene expression involved in lipid metabolism in hepatocytes. In NPCs, deregulated genes were associated with morphogenic changes and ECM remodeling.

4.3.1.1 LDC feeding dysregulated lipid and cholesterol homeostasis

In this study, LDC-fed mice exhibited an increased hepatic lipid incorporation, especially of CE and FC, and upregulated genes associated with epigenetic changes in lipid- and cholesterol-associated pathways, pointing towards a steatohepatitis. The pathogenic relevance of hepatic cholesterol has been emphasized in the context of liver injury and inflammation (Ioannou, 2016). In human patients, increased hepatic FC was shown to be elevated in NASH, but not in steatosis (Puri *et al.*, 2007; Caballero *et al.*, 2009; Min *et al.*, 2012). Furthermore, FC was shown to mediate hepatic lipotoxicity (Mota *et al.*, 2016). The lack of an upregulation of *Hmgcr* gene expression, encoding the HMG-CoA-reductase and catalyzing a necessary step in the biosynthesis of cholesterol, suggests increased hepatic cholesterol levels independent of gene expression. The HMG-CoA reductase was shown to be stronger regulated on protein, than on mRNA level (Jiang *et al.*, 2018). Thus, a regulation on protein level is more likely. A decreased cholesterol excretion is rather unlikely since serum cholesterol and HDL were elevated.

LDC feeding induced hepatic expression of genes associated with epigenetic changes playing a role in lipid-associated pathways, i.e. fatty acid and cholesterol metabolism. Previous studies reported altered expression and methylation of CpG islands of genes involved in lipid metabolism in LDC-fed mice (Kutay *et al.*, 2012). Additionally, Kutay *et al.* found reduced DNA methyltransferase (Dnmt) activity. Interestingly, though, loss of one copy of *Dnmt1* was shown to protect from alcoholic steatosis and to downregulate lipid-associated genes.

4.3.1.2 LDC feeding-induced hepatic apoptosis and inflammatory changes

Susceptibility to alcohol-induced liver injury is dependent on the microbiome (cf. 3.3). Ethanol intake can lead to changes in the intestinal microbiome composition and subsequent gut barrier dysfunction

in animal models as well as humans (Bajaj, 2019), accentuating the relevance of the gut-liver interactions in liver disease (Schnabl *et al.*, 2014; Tripathi *et al.*, 2018). Gut permeability permits LPS translocation to the liver, activating KCs and other immune cells *via* TLR signaling and, ultimately, inducing a downstream pro-inflammatory cascade (Seki *et al.*, 2012). In contrast to published data (Szabo *et al.*, 2010), serum LPS only tended to increase in LDC-fed mice. These differences can have several reasons. Only small changes, such as different maintenance chow or two distinct animal facilities can make mice more or less susceptible to experimentally-induced alcoholic liver injury (Ferrere *et al.*, 2017; McClain *et al.*, 2017). This reason should rather be ruled out since upregulated genes in hepatocytes showed an impact on 'response to lipopolysaccharide', supporting the actual presence of LPS in the liver. Rather a problem in the detection of LPS is assumed. In contrast to the classical LPS assay utilizing the Limulus Amebocyte Lysate (LAL) test, a recombinant Factor C (rFC) assay with higher specificity and sensitivity (0.001 EU/ml) was used (Ding *et al.*, 2001). Manufacturers do not recommend classical LAL or rFC assays for LPS detection in sera due to the presence of assay inhibitors, making endotoxin detection challenging (Gnauck *et al.*, 2015). However, these assays are still used for LPS detection in sera. Heating and diluting the samples was performed here, as recommended for patient sera (Huang *et al.*, 2016). Still, not sufficient sample dilution or inadequate measurement parameters cannot be ruled out, resulting in the lack of LPS detection.

In contradiction to the literature (Bykov *et al.*, 2006; Pritchard *et al.*, 2007), ethanol feeding in the here used setting decreased gene expression of the complement system (i.a. for C3, C6, C8, C9). Concordantly, data from the literature describe that inflammatory cytokine expression and serum ALT were increased after long-term feeding in C1q- or C3-deficient mice (Roychowdhury *et al.*, 2009; Cohen *et al.*, 2010), suggesting additional pathways involved in mediating chronic liver disease. An increase in transaminases, which usually indicates liver damage, was not detected in animals. Still, liver damage can also occur without elevated ALT serum levels, as it was shown in NAFLD (Papandreou *et al.*, 2007; Fracanzani *et al.*, 2008) as well as in alcoholic hepatitis (Diehl *et al.*, 1984; Malakouti *et al.*, 2017). Furthermore, the ethanol feeding-induced apoptosis and hepatic neutrophil infiltration in this study are thought to promote hepatocyte injury (Ramaiah *et al.*, 2007). This is supported by experiments in a mouse model of steatohepatitis, where deletion of neutrophils ameliorated alcoholic liver injury (Chang *et al.*, 2015). Unexpectedly, PBS-treated control mice exhibited infiltrations of neutrophils, which might be explained by repeated intraperitoneal (i.p.) injections (6-8 injections within 5 weeks), making comparisons to the control more difficult. Still, apoptosis, hepatic neutrophilia, and lymphocytic inflammation point towards inflammatory changes in the LDC-fed mice.

The LDC feeding suppressed the hepatic expression of *Gilz*, which has been previously reported to be downregulated under inflammatory conditions (Berrebi *et al.*, 2003; Zhang *et al.*, 2009; Hahn *et al.*, 2014; Hoppstädter *et al.*, 2015) and in livers of patients with alcoholic hepatitis (Hamdi *et al.*, 2007). In HFD obesity-induced mice, *Gilz* expression was shown to be reduced in the whole liver, particularly in KCs; this downregulation promoted liver inflammation (Robert *et al.*, 2016). Interestingly, two subsets of macrophages were shown to infiltrate upon the LDC diet, showing either anti- or pro-inflammatory phenotypes (Wang *et al.*, 2014). This might explain also downregulated genes involved in immune response in the LDC-fed mice.

Another factor pointing towards an onset of steatohepatitis is a downregulation of *Zfp36*, also known as tristetraprolin (TTP). *Zfp36* encodes for a zinc-finger RNA-binding protein which was found to target cytokine and chemokine mRNAs including *Tnf-α*, *Ifn-γ*, or *Il-6* (Lai *et al.*, 1999; Sauer *et al.*, 2006; Ogilvie *et al.*, 2009; Van Tubergen *et al.*, 2011; Zhao *et al.*, 2011). Reduced hepatic TTP levels were also found in murine models of obesity and in human diabetic livers (Sawicki *et al.*, 2018). *Zfp36*-deficient mice suffer from severe chronic inflammation (Taylor *et al.*, 1996; Carballo *et al.*, 1998), demonstrating the importance of *Zfp36* in anti-inflammatory responses (Sanduja *et al.*, 2012).

Taking together, altered immune activation, increased apoptosis, and inflammatory changes are pointing towards an onset of steatohepatitis in LDC-fed mice. However, the inflammatory phenotype was not very pronounced. Several factors can affect the severity of the ethanol-induced steatohepatitis, particularly with regard to the microbiome (cf. 3.3), the ethanol concentration of the diet, age, and strain of mice (Fengler *et al.*, 2016).

The originally developed LDC diet with a maximal intake of 36% of calories as ethanol, equivalent to 6.4% (v/v) ethanol, was diminished in this study to 5% (v/v) ethanol according to published concentrations (Bertola *et al.*, 2013). Nevertheless, the concentration had to be further decreased to 4% (v/v) ethanol because of unexpected spontaneous death events. A reason for the high mortality can be the age of the mice since ethanol feeding in younger and lighter mice can develop weight loss or hypothermia (Bertola *et al.*, 2013). In contrast to the recommended 8- to 11-week-old mice with body weight over 20 g, an early onset of the diet was chosen (4-week old with a weight around 15 g) due to the drop of *p62* expression in older mice (Tybl *et al.*, 2011). Additionally, an increased infection due to numerous injections cannot be excluded. The control mice already showed a high lobular lymphocytic inflammation with infiltration of neutrophils. Increased mortality of younger LDC-fed mice (6- to 8-week-old) was reported with an additional infection with *Mycobacterium tuberculosis* in comparison with older mice (17- to 22-month-old) (Tripathi *et al.*, 2018). Accordingly, the age and beginning of ethanol feeding is an important factor.

Varlinskaya and Spear suggested a greater ethanol tolerance of adolescent rats compared to their adult counterparts (Varlinskaya *et al.*, 2006). Adolescent C56Bl/6 mice were shown to consume more alcohol and also to increase their intake in adulthood compared to their adult counterparts (Moore *et al.*, 2010). However, this behavior is dependent on the genotype since it was not seen in DBA mice (Moore *et al.*, 2010). Thus, the genetic background of mice used for modeling ALD is crucial, as heterogeneous metabolic responses and severity of ethanol-induced steatohepatitis might differ between strains (cf.3.3). Little is known about the alcohol preference or genetic/epigenetic susceptibility to alcohol-induced liver damage in the herein used crossing between C57BL/6J and DBA/2J mice.

4.3.1.3   DNA methylation changes and ECM remodeling-associated morphogenic changes in NPCs

Epigenetic modifications are emerging as an important mechanism contributing to the regulation of stable as well as transient gene expression. Epigenetic changes in the germline even determine susceptibility to diet-induced obesity and insulin resistance in the next generation (Huypens *et al.*, 2016), making it an interesting research topic for metabolic diseases. In this study, altered gene

expression associated with differential DNA methylation and DNase1 footprint was analyzed. Further epigenetic analyses, including histone modifications and miRNA expression, are presently being performed and not available yet.

The DNA methylation profile from LDC-fed mice compared with the control diet, revealed a similar amount of hyper- and hypomethylated regions in hepatocytes, with a slight tendency towards hypomethylation. In the NPC fraction mostly hypomethylated DMRs were found by RRBS. Published data reported ethanol-induced global DNA hypomethylation due to the reduction of the principal methyl donor SAM in experimental animals and humans with AFLD (Lu *et al.*, 2000, 2006). A decrease in SAM or feeding of methyl donor nutrition deficient diets has been associated with hepatic steatosis (Mato *et al.*, 2007; da Silva *et al.*, 2014; Lee *et al.*, 2014). Also, a global hypomethylation of differentially methylated CpG sites was suggested to distinguish advanced NASH from simple steatosis in patients (Murphy *et al.*, 2013). In contrast to these previously published data, the here presented results distinguish between parenchymal and non-parenchymal cells, showing clear hypomethylation in NPCs, suggesting an important role of the presence of NPCs in the examined epigenetic changes. Nevertheless, recruitment of inflammatory cells, including neutrophils (as seen above), monocytes, and macrophages upon ALD or chronic ethanol ingestion (Szabo *et al.*, 2009) changes the cell composition of the NPC population. As different types or analyzed the infiltrates were not distinguished, the influence on epigenetic changes probably arises also from infiltrated cells. Furthermore, contaminations of the NPC fractions with hepatocytes during isolation and separation of the cells are also possible. RNA sequencing analysis of NPCs from LDC-fed mice further suggests increased morphogenic changes with ECM remodeling, possibly pointing towards tissue repair after injury and/or apoptosis. One possible reason can be an ethanol-induced activation of HSCs. LDC-feeding was shown to directly stimulate epigenetic modifications in HSCs and to increase the expression of ECM proteins (Page *et al.*, 2015).

In conclusion, induced hepatic lipid accumulation, altered lipid metabolism and immune activation, increased apoptosis, and inflammatory changes are pointing towards an onset of steatohepatitis in LDC-fed mice with an important role of NPCs in morphogenic changes and ECM remodeling.

4.3.2 Macrophages influence the development of ethanol-induced steatohepatitis

A role of Kupffer cells, the liver resident macrophages, within the process of fatty liver disease has been controversially discussed due to their pleiotropic functions (Dixon *et al.*, 2013; Gao *et al.*, 2016). In the herein study, clodronate liposome injections in combination with different diets to investigate differences regarding inflammatory events or steatohepatitis ware used.

The "liposome-mediated macrophage 'suicide' technique" with clodronate liposomes (clo) is frequently used in studies investigating macrophage function (Van Rooijen, 1989; van Rooijen *et al.*, 1996; Feng *et al.*, 2011; Lanthier *et al.*, 2015). In agreement with the literature (Rooijen *et al.*, 1994; Clementi *et al.*, 2009), Kupffer cells were successfully reduced in clo-treated mice. However, a limitation of this study is that the intraperitoneal (i.p.) administration route of clo is a nonspecific way of depleting macrophages (Lanthier *et al.*, 2010). It not only affects KCs but i.a. also abdominal adipose

tissue macrophages (ATMs) (Biewenga *et al.*, 1995; Leendertse *et al.*, 2009; Lanthier *et al.*, 2010; Bu *et al.*, 2013).

Herein, an increased hepatic injury, inflammation, and accumulation of toxic lipids in steatohepatitis-induced macrophage-depleted mice is reported. Hence, the data suggest a rather protective role of macrophages in the progression of ALD.

4.3.2.1 Macrophage depletion influences the immune response, leads to neutrophil infiltration, and metabolic changes

Macrophage depletion caused distinct effects on metabolic changes as decreased body weight changes and infiltrations of neutrophils. Both were reported in studies using clo or a macrophage Fas-induced apoptosis transgenic mice to deplete macrophages (Wu *et al.*, 2017; Bader *et al.*, 2019), showing that macrophages regulate neutrophil homeostasis (Gordy *et al.*, 2011). Lee *et al.* using a lysozyme M promoter-directed Cre (LysM[Cre]) diphtheria toxin model for macrophage depletion strongly indicated decreased energy intake as the main cause for body weight loss in macrophage-depleted animals (B. Lee *et al.*, 2014). In contrast, Bu *et al.* showed suppressed weight gain, while food intake did not alter in mice chronically administered with clo (Bu *et al.*, 2013). In fact, less energy intake cannot be ruled out. Food intake during the control diet using normal chow was not monitored. For LDC-fed animals, the amount of eaten diet was monitored and a reduced caloric intake could be observed when injected with clo (p=0.03; LDC+PBS: 9.83±0.27 kcal/mouse/day and LDC+clo: 8.95±0.23 kcal/mouse/day; each n=14 animals, 2 mice housed in one cage). Another factor affecting the variance in weight gain and food intake might be the influence of a social hierarchy among cage-mates (Ellacott *et al.*, 2010) since the animals were group-housed due to limited space. Thus, neutrophilia and weight loss might be the result of macrophage depletion and not the clo treatment itself, as it was also reported in other macrophage depletion models, possibly leading to less energy intake.

Macrophage depletion increased hepatic expression of *Cxcl1* in control animals and enhanced infiltrations of neutrophils in mice on the LDC diet. It is not surprising that the lack of macrophages provoked a deregulation of the immune system, recruitment of inflammatory cells, and consequently a changed cell composition in the NPC fraction. Neutrophils are supposed to promote progression of steatohepatitis by inducing hepatocyte injury *via* the release of ROS and pro-inflammatory mediators (Ramaiah *et al.*, 2007; Chang *et al.*, 2015). Blockade or deletion of important chemokines for neutrophil recruitment (*Cxl1, E-selectin*) was shown to prevent neutrophil infiltration and alleviate liver injury (Bertola *et al.*, 2013; Chang *et al.*, 2015; Wieser *et al.*, 2017), confirming an injury-promoting function of neutrophils. However, more neutrophilic infiltration in patients with ASH was shown to cause a better outcome of the disease (Altamirano *et al.*, 2014). Neutrophils not only have detrimental effects but can also function against bacterial infections and stimulate liver regeneration (Gao *et al.*, 2016). This might explain the increased gene expression correlating with 'cell cycle' and 'cell division'. Thus, feeding of the steatohepatitis-inducing diet in the absence of macrophages led to hepatocyte proliferation and possible liver regeneration in response to injury.

An increased *Lcn2* expression, as detected here in macrophage-depleted mice during LCD feeding, was also found to promote liver regeneration (Xu *et al.*, 2015) and to be protective against acute liver injury induced by hepatotoxins (Borkham-Kamphorst *et al.*, 2013). Nevertheless, *Lcn2* is also proposed to drive hepatic neutrophil infiltration, steatosis, and liver injury (Cai *et al.*, 2016; Wieser *et al.*, 2016). Furthermore, hepatic *Lcn2* expression is highly elevated under inflammatory conditions and in ALD (Asimakopoulou *et al.*, 2016; Xiao *et al.*, 2017), confirming the suggested inflammatory changes due to macrophage depletion during LDC diet.

In contrast to the literature reporting KC depletion to alleviate liver-injury and inflammation (Adachi *et al.*, 1994; Tosello-Trampont *et al.*, 2012), the data clearly show increased ALT and AST levels in clodronate-treated LDC-fed mice. Thus, the results point rather towards increased liver injury and hepatocyte proliferation in response to clo treatment in steatohepatitis. As macrophages are effector cells of the innate immune system, their depletion might represent a potential infection risk caused by microbial contamination. Absence of macrophages may increase bacteria and/or virus titers for instance. Even though it was paid attention to perform injections under clean conditions, an infection by frequent injections to maintain depletion over a long period of time cannot be completely excluded.

The absence of macrophages led to increased apoptosis pointing towards increased injury. The results are supported by investigations of Teratani *et al.* demonstrating an aggravated CCl_4-induced liver fibrosis in KC-depleted mice fed a high-cholesterol diet (Teratani *et al.*, 2012).

Taken together, the data suggest aggravated hepatic injury with inflammation as a result of macrophage depletion in steatohepatitis-induced mice.

4.3.2.2 Livers of clodronate-treated and LDC-fed mice had decreased triglycerides, but accumulated lipids known to induce lipotoxicity

LDC feeding in the absence of macrophages revealed deregulated genes encoding for major urinary proteins (Mups) without altering genes relating to lipid, cholesterol or fatty acid metabolism. Mups are produced in the liver and found to participate in the regulation of lipid and glucose metabolism (Charkoftaki *et al.*, 2019). However, their mechanism of physiological function is not well understood. Decreased levels of *Mup1* were found in genetic (db/db) or HFD-induced obesity in mice (Hui *et al.*, 2009; Zhou *et al.*, 2009). Replenishment of recombinant *Mup1* in these mice was found to ameliorate glucose intolerance, reduce hepatic triglycerides, and decrease the expression of glucogenic and lipogenic genes. In clodronate-treated mice, decreased TGs were found, but also decreased *Mup1* expression, suggesting the involvement of other mechanisms. Interestingly, downregulation of *Mup1*, *Mup4*, and *Mup5* was detected in mice with dietary restriction (Miller *et al.*, 2002; Dhahbi *et al.*, 2004; Giller *et al.*, 2013). As discussed above, a reduced caloric intake due to macrophage depletion is possible and could lead to decreased *Mup* expression.

Depletion of KCs and/or ATMs with clo or gadolinium chloride ($GdCl_3$), a selective toxicant for KCs, has been described to be associated with the protection of mice from developing hepatic steatosis (Rivera *et al.*, 2007; Neyrinck *et al.*, 2009; Huang *et al.*, 2010). In agreement, decreased hepatic TGs in LDC-fed macrophage-depleted mice was also shown, but contrary to Bu *et al.* changed expression of genes

involved in lipogenesis could not be confirmed (Bu *et al.*, 2013). Furthermore, the results contradict previous publications showing unchanged levels of hepatic CER and cholesterol in macrophage-depleted livers (Huang *et al.*, 2010; Stienstra *et al.*, 2010).

The lipidomic analysis showed only altered ceramide levels in macrophage-depleted mice on the control diet, suggesting an important impact of macrophages in ceramide homeostasis. As one aspect of the underlying mechanism, an elevated SM to CER ratio (Figure 22) can be an indicator for increased turnover as a result of sphingomyelinase activity (Hannun *et al.*, 2008). Increased hepatic CER are thought to play an important role during inflammation and apoptosis due to relevant signaling properties (Clugston *et al.*, 2011; Pagadala *et al.*, 2012). This might explain the increased apoptosis of macrophage-depleted mice, showing that macrophage depletion on control diet already increases hepatotoxic ceramide.

The reduction of hepatic TG in LDC-fed macrophage-depleted mice might be explained by an increased hepatic *Apoa4* expression. Apolipoprotein A-IV has a wide variety of functions in lipid metabolism and metabolic regulation and is found on the surface of newly synthesized chylomicrons. Hepatic expression of *Apoa4* was proposed to enhance TG secretion from the liver (VerHague *et al.*, 2013). However, serum triglycerides were not changed. Further, PC was proposed to be a source for TGs in the liver (van der Veen *et al.*, 2012), which in part might explain diminished TG levels by reduced PC. A decrease of PC while LPC is accumulated, as shown by the decreased PC to LPC ratio (Figure 22), might be explained by an increased conversion of PC to LPC *via* phospholipase A2, which can, in turn, be activated by increased ceramide (Huwiler *et al.*, 2001).

Increased LPCs are clinically associated with atherosclerosis, acute and chronic inflammation (Schmitz *et al.*, 2010), and have been implicated to induce hepatocyte lipoapoptosis (Han *et al.*, 2008; Hirsova *et al.*, 2016). Together with FC, both are shown to mediate hepatic lipotoxicity (Mota *et al.*, 2016). Increased hepatic FC is multifactorial in origin, including e.g. increased synthesis related to increased Hmgcr expression or activity, increased hydrolysis of CE to FC, impaired CE synthesis, increased uptake from circulation, or decreased excretion (Min *et al.*, 2012). Although only limited inferences can be drawn about mechanistic aspects from lipidomic approaches, a decreased CE to FC ratio could suggest increased hydrolysis of CE. Elevated synthesis due to increased Hmgcr activity, but not expression, is another possibility since *Hmgcr* mRNA expression did not alter.

KCs and ATMs were shown to accumulate toxic lipids in HFD-fed mice, including cholesterol and ceramides, and to exhibit a pro-inflammatory phenotype when fat-laden (Leroux 2012). Macrophage depletion in LCD-fed mice diminished 'protective' hepatic lipids such as TG, PC, PI, and led to an accumulation of toxic lipids, such as CER, LPC, and FC and thereby increasing the risk for liver damage and/or fibrosis. Thus, a crucial role of macrophages in maintaining lipid homeostasis and protection of the liver from lipotoxicity-induced damage is suggested.

4.3.3 Lack of lipid accumulation in *p62* tg mice, but decreased *Apoa4* expression

Hepatic *p62* expression was shown in our group to induce simple steatosis (Tybl *et al.*, 2011). Here, a further characterization of the *p62* mouse model on the epigenome was performed and addressed the role of *p62* in a steatohepatitis model of LDC feeding dependent on the presence or absence of macrophages.

A diminished *p62* expression due to clo treatment and LDC diet was shown. Increased incorporation of lipids within hepatocytes could lead to changed expression pattern. However, steatosis in 2- and 4-week-old mice on MCD-diet did not alter *p62* mRNA expression (Simon, 2013). Furthermore, clo treatment induced liver damage and apoptosis. The therefore increased loss of cells could explain the deficit in *p62* expression. Newly generated hepatocytes by liver regeneration or repair could lack expression of *p62*, as *p62* was shown to be expressed in a heterocellular pattern (Simon, 2013) and shown to have high interindividual variability (Tybl *et al.*, 2011), possibly due to reduced promoter activity.

In accordance with a previous publication (Laggai *et al.*, 2013), CER were increased in *p62* tg mice on control diet. But, in contrast, they were the only altered lipid class. As discussed before and also detected in clo treated animals on control diet, increased CER levels could derive from increased sphingomyelinase activity since the SM to CER ratio was significantly decreased in *p62* tg animals (0.82 fold change; p=7.6E-5). As seen before, increased hepatic CER play an important role during inflammation and apoptosis (Clugston *et al.*, 2011; Pagadala *et al.*, 2012).

The age of *p62* expressing mice is crucial in experimental settings. The herein mice were sacrificed at the age of 9 weeks. The lack of differences between genotypes could derive from the deficit of *p62* expression levels, as it was shown to be strongly decreased at the age of 10 weeks (Tybl *et al.*, 2011). However, mRNA expression was still upregulated. *p62* tg mice with a normal histology were shown to not reveal significantly increased fatty acid content in the liver (Laggai *et al.*, 2014), explaining the consistency between genotypes in this work.

Analysis of DEGs associated with epigenetic changes revealed altered lipid and metabolic pathways with a downregulation of *Apo4*. As seen before, hepatic *Apoa4* expression was described to enhance TG secretion from the liver (VerHague *et al.*, 2013). Thus, a hepatic downregulation in *p62* tg mice could reduce lipid export from the liver and explain hepatic lipid accumulation, while serum cholesterol and TG were decreased, compared to wild types. The downregulation was seen in all treatment groups, emphasizing an important role of *Apoa4* in *p62* tg animals.

Taken together, the *p62* expression did not alter hepatic lipid accumulation in control or LDC feeding probably due to diminished *p62* expression due to age. Nevertheless, *p62* expression increased CER in the control treatment and strongly decreased *Apoa4* expression in all treatment groups underlining its role in *p62* tg animals.

5 SUMMARY

NAFLD and AFLD range among the most prevalent liver diseases in developing as well as in developed countries. It is therefore important to understand the mechanism of disease pathogenesis and the progression from steatosis toward steatohepatitis, cirrhosis, and HCC.

In the present work, the role of p62/IMP2-2 was investigated in steatohepatitis and in the progression towards malignancy and the role of macrophages in steatohepatitis was examined.

The insulin-like growth factor 2 (IGF2) mRNA binding protein (IMPs) family members IMP1 and IMP3 have been classified as oncofetal proteins. IMP2 expression in the adult liver is controversially discussed, not least due to the lack of quantitative data in IMP2 expression. The human splice variant p62/IMP2 2 was found to promote steatohepatitis and to be upregulated in HCC. Therefore, it was aimed to clarify the expression of IMP2 in the adult liver and to characterize the influence of p62 on the progression toward fibrosis. A high fetal IMP2 expression with only minimal levels in adult livers of human and mice, confirming an oncofetal appearance, was demonstrated. Employing transgenic mice, p62/IMP2-2 induced the expression of liver progenitor cell markers, such as Spp1 and Cdh1. When challenged an MCD diet, p62 transgenic mice additionally upregulated progenitor marker expression (Krt19, Sox9) and were more susceptible to a ductular reaction and the development of fibrosis. Human gene expression data further supported increased expression of IMP2 in parallel with liver progenitor cell marker genes in liver disease.

As the expression of the imprinted genes Igf2 and H19 were found to be elevated by p62, it was aimed to further characterize the p62 transgenic mouse model with regard to a potential role on the epigenome. Differentially expressed genes (DEGs) associated with epigenetic changes, i.e. differentially methylated regions (DMRs) and/or differentially open chromatin regions (DOR) were mostly found in hepatocytes of p62 transgenic mice. These genes particularly play a role in lipid metabolism and fatty acid metabolism. To further characterize the impact of p62 on lipid accumulation, lipidomic analysis revealed only an elevated accumulation of ceramides. When challenged with a steatohepatitis-inducing Lieber-DeCarli (LDC) diet, no changes in hepatic lipid accumulation were found compared to wild-type animals. However, hepatic p62 expression abrogated the LDC-induced increase in serum levels of cholesterol, HDL, and triglycerides. Further, it induced a downregulation of Apoa4, suggesting an impaired lipid export from the liver. Interestingly, the p62-induced Apoa4 downregulation was observed in all treatment groups, including macrophage-depleted

mice. The impact of p62 expression on macrophage-depleted steatohepatic mice was not further analyzed since clodronate liposome treatment strongly diminished hepatic p62 expression.

Susceptibility to steatohepatitis can be promoted by epigenetic changes. Furthermore, interaction and crosstalk between parenchymal and non-parenchymal cells (NPCs), including Kupffer cells, has emerged as a critical mechanism in the pathogenesis of steatohepatitis. Still, the role of Kupffer cells in the progression of liver disease is controversially discussed. Therefore, the role of macrophages, i.e. Kupffer cells and adipose tissue macrophages, and epigenetically regulated changes in gene expression in a murine model using a steatohepatitis-inducing LDC diet were analyzed. The ethanol containing LDC diet-induced neutrophilia, lymphocytic inflammation, and apoptosis. Furthermore, LDC feeding dysregulated lipid and cholesterol homeostasis. Lipidomic analysis showed increased hepatic lipid incorporation. Additionally, upregulation of genes involved in lipid and cholesterol pathways was associated with epigenetic changes in hepatocytes. In NPCs, upregulated genes associated with epigenetic changes were shown to play a role in morphogenic changes and ECM remodeling. In order to investigate the role of macrophages in steatohepatitis, i.p. injections of clodronate liposomes were performed to deplete macrophages. In this steatohepatitis model, the absence of macrophages led to increased neutrophilia, lymphocytic inflammation, and apoptosis. Liver damage was detected by increased serum levels of AST and ALT. Furthermore, hepatic cell proliferation was suggested by upregulated genes in hepatocytes as well as in NPCs. Also, hepatocytes expressed Lcn2, known to be highly elevated under inflammatory conditions and in ALD. Interestingly, lipidomic analysis revealed abrogated hepatic levels of triglycerides, phosphatidylcholine, and phosphatidylinositol in the absence of macrophages, possibly due to induced hepatic export, as indicated by increased Apoa4 expression. Concurrently, lipids knowing to induce lipotoxicity were accumulated, i.e. free cholesterol, and lysophosphatidylcholine. Thus, macrophages appear to be rather protective in the presented steatohepatitis model.

Taken together, this work provides insight into epigenetic changes and macrophages in steatohepatitis and the role of p62/IMP2 in dedifferentiation and contributes to a better understanding of processes involved in the pathogenesis of liver diseases.

6 EXPERIMENTAL PROCEDURES

6.1 Materials

PCR, qPCR primers, and dual-labeled probes were obtained from Eurofins MWG Operon (Ebersberg, Germany). *Taq*-Polymerase (5 U/µl), 10 x *Taq* buffer and the dNTP mix (containing dATP, dCTP, dGTP and dTTP at a concentration of 10 mM, each) were from Genscript (Piscataway, NJ, USA). LE Agarose was purchased from Biozym Scientific GmbH (Oldendorf, Germany) and ethidium bromide (#E1510) from Sigma-Aldrich (St. Louis, MO, USA).

Anti-Krt19 antibody (#52625) and anti-Afp antibody (#46799) for histological stainings were obtained from Abcam (Cambridge, United Kingdom), and the anti-laminin antibody (#L9393) from Sigma-Aldrich (St. Louis, MO, USA).

Mouse anti-tubulin (#T9026, LOT#024M4767V) antibody was from Sigma-Aldrich (St. Louis, MO, USA). Antibodies used for Western Blot detection were obtained from LI-COR Biosciences (Lincoln, NE, USA): IRDye® 680RD goat anti-rabbit (#926-68071, LOT# C60329-15), and IRDye® 800 CW goat anti-mouse (#926-32210, Lot# C50909-01).

All other chemicals were purchased either from Sigma-Aldrich (St. Louis, MO, USA; Steinheim, Germany), Carl Roth (Karlsruhe, Germany), and Grüssing (Filsum, Germany).

6.2 Mice and treatments

6.2.1 Animal welfare

Animal handling was conducted in compliance with the guidelines of the local animal welfare committee (permission number: 38/2013, 34/2010, 11/2013). Mice were housed in a 12/12h light/dark cycle under constant conditions (temperature: 22℃±2℃; relative humidity: 55%±10%) with food and water ad libitum, if not stated otherwise (cf. 6.2.4.2, 6.2.4.3).

6.2.2 Generation of *p62* transgenic animals

p62 transgenic mice were generated as previously described (Tybl *et al.*, 2011). In brief, DBA/2J *p62* mice containing the human *p62* gene under the control of the minimal cytomegaly virus promoter with

a tetracycline-resistance operon regulatory element (tetO) upstream of the promoter, do not express the p62 protein. They were crossed with C57BL/6J *LT2* transgenic mice, which carry a liver-enriched activator protein (LAP) promoter controlling the expression of the tetracycline transactivator (tTA) protein. In the double-positive *p62⁺/LT2⁺* transgenic offspring, the LAP promotor is activated *via* LAP, which is highly enriched in the liver, and tTA is expressed. It subsequently binds the tetO sequences resulting in an expression of the *p62* gene downstream of the promoter (Figure 36). *p62⁺/LT2⁺* mice are referred to as *p62* transgenic animals (tg) in this work and were compared to *p62⁻*/wild-type (wt) mice in the experiments. C57BL/6J and DBA/2J wild-type animals were purchased from Janvier Labs (Saint-Berthevin Cedex, France).
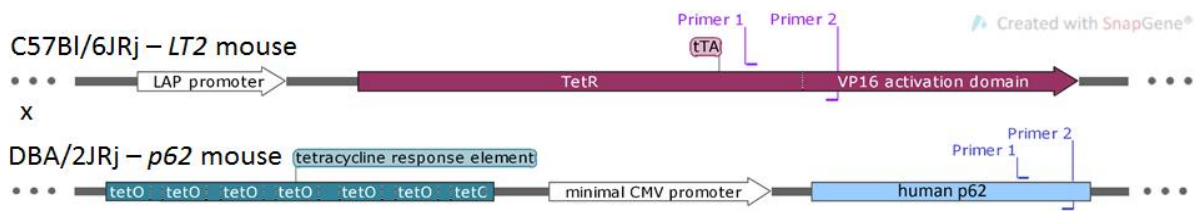
Figure 36: Generation of p62 transgenic mice. Liver-specific expression of p62 mRNA in double-positive p62⁺/LT2⁺ mice. Primer 1 and 2 indicate the binding region of primers used for genotyping. LAP: liver-enriched activator protein; tTA: tetracycline-controlled transactivator composed of TetR: tetracyclin Repressor fused to VP16 (positive-acting transcription factor); tetO: tetracycline-resistance operon regulatory element;-CMV: cytomegalovirus.

6.2.3   Genotyping

For genotyping, ear biopsies were taken from mice and digested in 100 µl of a solution containing 20 µg Proteinase K and 10 µl 10 x *Taq* buffer (in water) at 55°C while shaking (1500 U/min) for 1 hour or until the tissue was fully digested. Proteinase K (#03115879001, Roche Diagnostics GmbH, Mannheim, Germany) was heat-inactivated at 95°C for 15 min and 1 µl of the supernatant was used as template in the following PCR reaction with primers shown in Table 11.

Table 11: Primer sequences used for genotyping PCRs with amplicon sizes and gene bank accession numbers.

Gene	Forward primer sequence 5´-3´	Reverse primer sequence 5´-3´	Amplicon size	Gene bank accession number
tTA	GTGCAGAGCCAGCCTTCTTA	CCTCGATGGTAGACCCGTAA	129 bp	U89929
p62	CATCAAACAGCTGGCGAGAT	GTGCCCGATAATTCTGACGA	346 bp	AF057352

Reaction mixture:

Taq-Polymerase (5 U/µl)	2.5	U	
dNTPs (10 mM)	125	µM	
10 x *Taq*-buffer	2	µl	
primers (10 µM, each)	0.5	µM	
template	1	µl	
H₂O	ad 20	µl	

Conditions:

denaturation	95°C	5 min	
denaturation	95°C	30 s	35 cycles
annealing	57°C	30 s	
elongation	72°C	30 s	
final elongation	72°C	5 min	

The PCR products were separated by an agarose gel electrophoresis (cf. 6.4) for amplicon detection.

6.2.4   Diets and treatments

6.2.4.1   High-fat diet (HFD)

Mice (n=80 in total, Table 12) were randomly divided according to genotype (wt or tg) and sex into the experimental groups at the age of 3 weeks and received either the control (co; D12489B) or high-fat diet (HFD; D12266B, Table 13), based on milk fat (Sutter *et al.*, 2012), purchased from Research Diets (New Brunswick, NJ, USA), for 12 weeks.

Table 12: *Number of animals for each genotype and sex used in the high-fat diet (HFD) and control diet (co). wt: wild types; tg: p62 transgenic mice.*

Diet	Co				HFD			
Genotype	wt		tg		wt		tg	
Sex	f	m	f	m	f	m	f	m
Number of animals	11	10	9	10	10	12	10	8
Total/genotype	21		19		22		18	

Table 13: *Composition of the control and high-fat diet according to Research Diets.*

	Co D12489B	HFD D12266B
	kcal%	kcal%
Protein	16.8	16.8
Carbohydrate	72.6	51.4
Fat	10.6	31.8
kcal/g	**3.9**	**4.41**
Fatty acid composition	**g/kg**	**g/kg**
total	**44.7**	**151.8**
Saturated	11.9	40.3
Monounsaturated	11.9	40.5
Polyunsaturated	21	71.2
Ingredient	**g/kg**	**g/kg**
Casein, 30 Mesh	161.3	182.2
DL-Methionine	2.5	2.9
Corn Starch	423.1	206.2
Maltodextrin 10	29.7	71.9
Sucrose	246.2	278.1
Cellulose, BW200	25.5	28.8
Butter Fat, Anhydrous	12.5	42.4
Corn Oil	33.4	113.2
Mineral Mix S10001	34.0	38.4
Calcium Carbonate	4.7	5.3
Sodium Chloride	4.7	5.3
Potassium Citrate, 1 H_2O	11.5	12.9
Vitamin Mix V10001	9.3	10.5
Choline Bitartrate	1.7	1.9
FD&C Yellow Dye #5	0.1	0
FD&C Red Dye #40	0	0.1

Mice were sacrificed at the age of 15 weeks. Whole blood and livers were removed and processed as described in 6.2.5 and 6.2.6.

6.2.4.2   Ethanol in drinking water

At the age of 3 weeks, mice (total n=76, Table 14) were randomly divided according to genotype (wt or tg) and sex into the experimental groups.

Table 14: Number of animals for each genotype and sex used in the experiment with the application of ethanol (EtOH) in drinking water. wt: wild types; tg: p62 transgenic mice; co: control

Diet	Co				EtOH			
Genotype	wt		tg		wt		tg	
Sex	f	m	f	m	f	m	f	m
Amount	11	8	9	10	10	10	10	10
Total/genotype	19		19		20		20	

All mice received normal chow (#1320, Altromin, Lage, Germany). The ethanol-fed mice received an increasing concentration of ethanol (EtOH: 7 kcal/g, #32205-M, CAS Number: 64-17-5, Sigma-Aldrich, Steinheim, Germany) in drinking water (1st week: 2.5%, 2nd week: 5%, 3rd week: 10%, 4th week: 15% (v/v) EtOH) as the only drinking source. Control mice received an isocaloric solution of maltodextrin from maize starch (Lamperts Maltodextrin 12, PZN 8605783, Berco Arzneimittel, Kleve, Germany) in drinking water with a metabolic energy of 3.84 kcal/g. The amount of calories had to be adjusted to the intake of maltodextrin solution since mice that received this solution tended to drink more. Mice were sacrificed at the age of 7 weeks and whole blood and livers were removed and processed as described in 6.2.5 and 6.2.6.

6.2.4.3   Lieber-DeCarli diet and treatment with clodronate liposomes

Female wild-type (wt) and *p62* transgenic (tg) mice (n=111) were randomly divided into the experimental groups at the age of 3 weeks. The control group (co) received normal chow (#1320, Altromin, Lage, Germany). The other group was fed the Lieber-DeCarli (LDC, #F1258SP, BioServ, Flemington, NJ, USA) diet as the only food source. The composition of the diets is shown in Table 15.

Table 15: Metabolic energy, carbohydrate, and fatty acid composition of the control (co, #1320, Altromin) and Lieber-DeCarli (LDC, #F1258SP, BioServ) diet.

Metabolic energy	Co		LDC	
kcal from protein	24	%	17.2	%
kcal from fat	12	%	40.9	%
kcal from carbohydrate	64	%	15.4	%
kcal from ethanol (4%)			26.5	%
Total	3,188	kcal/kg	877.5	kcal/l
Carbohydrates				
Monosaccharides	0		1.3	g/l
Disaccharides	49.5	g/kg	4.8	g/l
Polysaccharides	358.9	g/kg	26.1	g/l
Fatty acids				
Total saturated	n.a.		5.2	g/l
Total monounsaturated	n.a.		23.5	g/l
Total polyunsaturated	n.a.		9.7	g/l

The diet was prepared as shown in Table 16 based on the manufacturer's instructions and Bertola *et al.*, 2013 with a magnetic stirrer and a magnetic stir bar. To one-third of the dry mix one-third of warm

water was added, and mixed until the product dispersed. This step was repeated, ethanol was added and the product was dispensed into liquid diet feeding tubes (#13260, BioServ, Flemington, NJ, USA).

Table 16: Directions for preparing 0% - 5% (v/v) ethanol liquid diet (#13260, BioServ). ρ (ethanol)=0.789 g/ml; energy density (ethanol)=7 kcal/g

Ethanol % in diet (v/v)	Finale volume (ml)	Diet dry mix (g)	Water [a] (ml)	95% ethanol (ml)	Calories from ethanol (kcal/l)	Calories from ethanol (%)
0%	100	14.1	95.4	-	-	-
1%	250	33.3	236.6	2.6	58.0	8.2
2%	250	33.3	234.0	5.3	116.5	15.3
4%	250	33.3	228.7	10.5	232.5	26.5
5%	250	33.3	226.1	13.2	290.5	31.1

Mice received the LDC diet for one week without ethanol, followed by one week of increasing ethanol concentrations: 2 days 1%, 2 days 2%, 3 days 4%. Due to unexpected spontaneous death events, the ethanol concentration was decreased to 4% during the feeding period. 9 animals (Table 17) were fed 5% (v/v) LDC diet for 22/12/6 days before lowering the concentration to 4% (v/v) ethanol and feeding was maintained for 7/17/23 days. The remaining 23 animals in each group remained on 4% LDC diet for 4 weeks. Additional to the diet, animals were injected with either PBS or clodronate liposomes (i.p. 10 µl per mg body weight). PBS-1x with pH7.2 (#9872, Cell Signaling, Danvers, MA, USA) contained 10 mM Na_2HPO_4, 10 mM NaH_2PO_4, 150 mM NaCl. Clodronate liposomes were purchased from Liposoma B.V. (Amsterdam, Netherlands). The concentration of clodronate in the suspension was 5 mg/ml and liposomes were suspended in sterile PBS (10 mM Na_2HPO_4, 10 mM NaH_2PO_4, >140 mM NaCl). 2 to 3 days before the onset of the control or LDC diet, injections were started and repeated every 5 to 7 days until mice were sacrificed at the age of 9 weeks. Total numbers of animals in the different diet and treatment groups are shown in Table 17. Animals (3-4) from selected treatment groups (wt: co+PBS, co+clodro, LDC+PBS, LDC+clodro; tg: co+PBS) were sent to the IfADo in Dortmund, where the isolation of hepatocytes and non-parenchymal cells (NPCs) was performed (see 6.13). Epigenetic profiling was performed with samples from 2 animals of each group (c.f. 6.14).

Table 17: Number of female animals for each genotype and treatment (i.p. injection of PBS or clodronate liposomes) fed either normal chow (co, #1320, Altromin) or the liquid ethanol Lieber-DeCarli (LDC, #F1258SP, BioServ) diet. wt: wild types; tg: p62 transgenic mice; PBS: Phosphate Buffered Saline (#9872, Cell Signaling); clodro: clodronate liposomes (Liposoma B.V.)

Treatment	Co				LDC			
Injections every 5-7 days	PBS		clodro		PBS		clodro	
Genotype	wt	tg	wt	tg	wt	tg	wt	tg
+ normal chow	14	14	15	13				
+ 22 days 5% + 7 days 4% EtOH					1	-	1	-
+ 12 days 5% + 17 days 4% EtOH					1	1	-	-
+ 6 days 5% + 23 days 4% EtOH					2	-	2	1
+ 29 days 4% EtOH					11	12	12	11
Total each treatment and genotype	14	14	15	13	15	13	15	12
Total number of animals	111							

6.2.4.4   Untreated animals

Liver tissues from C57BL/6J mice at the embryonic day E12.5 (n=5), newborns (P0, n=8), and at the age of 2, 10 and 85 weeks (each n=6) were obtained.

Wild-type (wt) and *p62* transgenic (tg) mice were generated and livers were examined by qPCR (wt: n=13, tg: n=13) and microarray analysis (n=10 each) at the age of 5 weeks (performed by Dr. S. M. Kessler).

In order to induce NASH, wild-type and *p62* tg mice were randomly divided into experimental groups at the age of 3 weeks and were fed either a methionine-choline-deficient diet (MCD, #960439, MP Biomedicals, Eschwege, Germany) (wt or tg: n=10) or a methionine choline supplemented control diet (co, #960441, MP Biomedicals, Eschwege, Germany) (wt or tg: n=12) for 4 weeks (performed by Dr. Y. Simon). For tumor induction, 3-week old wt (n=28) and *p62* tg (n=24) mice received an MCD diet; 4 weeks after the onset of MCD feeding animals obtained one injection of diethylnitrosamine (DEN, 5 mg/kg BW i.p.). Mice were sacrificed at the age of 15 weeks (performed by Dr. S. M. Kessler).

6.2.5   Serum Parameters

Whole blood was collected in 1.1 ml Z-Gel microtubes (#41.1500.005, Sarstedt, Nümbrecht, Germany) incubated for one hour at room temperature and centrifuged for 10 min at 6,000 x *g* and 4°C. The supernatant was transferred into a fresh tube and stored at -80°C until measurement. Serum levels of alanine aminotransferase (ALT), aspartate aminotransferase (AST), cholesterol, glucose, high-density lipoprotein (HDL), and triglycerides (TG) were determined by the cobas®8000 modular analyzers using Roche® reagents. The serum was diluted with 0.9% NaCl before measurements were performed at the "Zentrallabor des Universitätsklinikums des Saarlandes" (Homburg, Germany).

6.2.6   Preparation of Liver Tissue

Livers were removed and weighed. Half of the left lateral lobe, the left medial lobe with gallbladder, and one-third of the right lateral lobe were fixed in biopsy embedding cassettes (#17990, Engelbrecht Medizin- und Labortechnik GmbH, Germering, Germany) for 24 hours in 4% (w/v) formalin (#41-5313-00, Medite GmbH, Burgdorf, Germany) before paraffin embedding (6.12.1). The remaining liver tissue was snap frozen in liquid nitrogen and stored at - 80°C for further experiments (6.5, 6.7, 6.8, 6.11).

6.3 qPCR standard plasmid generation

PCR products of the gene of interest were generated and agarose gel electrophoresis (6.4) was performed. The product was cut out of the gel, cleaned up with the NucleoSpin® Gel and PCR Clean-up Kit (#740609, Macherey-Nagel, Düren, Germany), and the DNA concentration was measured. The amount of PCR product needed for ligation was calculated by the following equation:

$$ng\ of\ insert\ =\ \frac{ng\ vector\ \times kb\ size\ of\ insert}{kb\ size\ of\ vector}\ \times \frac{3}{1}\ (insert\ to\ vector\ molar\ ratio)$$

The PCR product was ligated into the pGEM®-T-Easy Vector (3015 bp, #A137A, Promega, Madison, WI, USA) according to the manufacturer's guidelines.

6.3.1 Bacterial culture

The *Escherichia coli (E. coli)* strain TOP10 (Invitrogen, Carlsbad, CA, USA) was used as a host organism for plasmid amplification. Bacteria were grown in lysogeny broth (LB) medium (Luria/Miller) supplemented with ampicillin (100 µg/ml). For the selection of single clones, LB$_{amp}$ agar plates (15 g per 1 l LB medium, 100 µg/ml ampicillin) were used.

6.3.2 Transformation

The transformation was performed according to the guidelines of the manufacturer. In brief, 50 µl competent *E. coli* cells were added to 2 µl of the solution of the ligated vector obtained as described above. After 20 min incubation on ice, bacteria were heat-shock transformed for 45-50 sec at 42°C and incubated on ice for 2 min. 950 µl SOC medium (0.5% yeast extract, 2% tryptone, 10 mM NaCl, 2.5 mM KCl, 10mM MgCl$_2$, 10 mM MgSO$_4$, 20 mM glucose in water) were added to the bacteria and the mixture was incubated at 37°C and 150 rpm for 1.5 h. 50 µl and 100 µl of the suspension were plated on LB$_{amp}$ plates and incubated overnight at 37°C and 5% CO$_2$. Colonies were picked and grown overnight in 7 ml LB with ampicillin at 37°C and 150 rpm.

6.3.3 Plasmid purification

Plasmid DNA was isolated from overnight cultures using High Pure Plasmid Isolation Kit (Version 9, Roche, Mannheim, Germany) according to the manufacturer's instructions. The DNA concentrations were determined by measuring the extinction of the DNA at 260 nm, and purity was checked by absorption measurement at 280 nm. Measurements were performed with a BioMate UV-Vis spectrophotometer (Thermo Electron Corporation, Schwerte, Germany) or with the Thermo Scientific™ NanoDrop Lite Spectrophotometer (Wilmington, DE, USA).

6.3.4 Sequencing of the qPCR standard plasmids

Sequencing reactions were performed by Eurofins MWG (Ebersberg, Germany) with 75 ng/µl plasmid DNA in 15 µl molecular water.

6.4 Agarose gel electrophoresis

For the detection of DNA, 1.5% (w/v) agarose gels (in 1 x TBE: 89.2 mM Tris, 89 mM boric acid, 2 mM EDTA in H$_2$O) containing 5 µg/ml ethidium bromide were used. Samples were loaded with a suitable volume of 10 x loading buffer (70% (v/v) glycerol, 40 mM EDTA, 0.02% bromphenol blue, 0.02% xylene cyanol, H$_2$0 ad 50 ml) and separated at 100 V. A 50 bp ladder (#SM0371, Thermo Fisher Scientific, Carlsbad, CA, USA) was used to determine the size of the DNA. Detections were carried out using a UV transilluminator (Biostep Dark Hood DH-40/50) and the software ArgusX1 (Biostep, Jahnsdorf, Germany).

6.5 RNA isolation and reverse transcription

6.5.1 RNA isolation

Total RNA was extracted in 600 µl Qiazol® lysis reagent (#79306, Qiagen, Hilden, Germany) using a high-performance dispenser (T25 digital IKA® ULTRA-TURRAX® dispersers) for the homogenization of snap-frozen liver tissue samples. After disruption and incubation for 5 min at room temperature, 175 µl of chloroform was added. The mixture was vortexed (15 s), incubated for 3 min at room temperature, and centrifuged at 13,523 x g at 4°C for 15 min. The supernatant was collected in a new reaction tube and RNA was precipitated by addition of ice-cold isopropanol 100% (1 volume) at -20°C overnight. The precipitate was centrifuged at 13,523 x g at 4°C for 10 min and the resulting pellet was washed with ice-cold ethanol 75% (v/v). The RNA was dried at 37°C and dissolved in DEPC-H_2O (#T143.2, Roth, Karlsruhe, Germany).

6.5.2 DNase digestion

RNA samples were digested with DNase I using the Ambion DNA-free™ kit (#AM1906, Invitrogen by Thermo Fisher Scientific, Vilnius, Lithuania) to remove residual DNA according to the manufacturer's instructions.

6.5.3 RNA concentration measurement

The RNA concentration was determined by measuring the extinction at 260 nm using the Thermo Scientific™ NanoDrop Lite Spectrophotometer (Wilmington, DE, USA).

6.5.4 SINE PCR

To confirm the absence of DNA in the isolated RNA samples, a PCR for Short Interspersed Nuclear Elements (SINEs) was performed using the following primers:

Forward: 5'-3' CTTCTGGAGTGTTTGAAGAC

Reverse: 5'-3' CTGGAACTCACTCTGAAGAC

5 ng DNA isolated from mouse liver, served as a positive control. The PCR was carried out in a Thermal Cycler (T100™, Bio-Rad, Richmond, CA, USA) using the following reaction mixture and conditions:

Reaction mixture:		Conditions:			
Taq-Polymerase (5 U/µl)	2.5 U	denaturation	94°C	8 min	
dNTPs (10 mM)	200 µM	denaturation	94°C	1 min	31
10 x *Taq*-buffer	2,5 µl	annealing	59°C	1 min	cycles
primers (10 µM, each)	0,2 µM	elongation	72°C	1 min	
template	1 µl	final elongation	72°C	10 min	
H_2O	ad 25 µl				

The PCR products were separated by an agarose gel electrophoresis (6.4) and were free of DNA when no smear was visible.

6.5.5 Reverse transcription

500 – 1,000 ng of RNA was reverse transcribed into cDNA using the high-capacity cDNA reverse transcription kit (#4368814, Applied Biosystems by Thermo Fisher Scientific, Vilnius, Lithuania) with an RNase inhibitor (RNaseOUT™, #10777-019, Invitrogen by Life Technologies, Carlsbad, CA, USA) according to the manufacturer's protocol. TE buffer (pH 8.0, #A0386,1000, AppliChem, Darmstadt, Germany) was added to the resulting cDNA to a final volume of 100 – 300 µl.

6.6 qPCR

6.6.1 Primer and probe sequences

Table 18: Primer sequences with concentrations and annealing temperatures as used for qPCR.

Gene	Forward primer sequence, 5'-3'	Reverse primer sequence, 5'-3'	Concentration each Primer	Annealing temp.
Csnk2a2	GTAAAGGACCCTGTGTCAAAGA	GTCAGGATCTGGTAGAGTTGCT	400 nM	60°C
Ppia	GGCCGATGACGAGCCC	TGTCTTTGGAACTTTGTCTGC	250 nM	58°C
Rn18S	AGGTCTGTGATGCCCTTAGA	GAATGGGGTTCAACGGGTTA	250 nM	61°C
Afp	CCAGGAAGTCTGTTTCACAGAAG	CAAAAGGCTCACACCAAAGAG	250 nM	60°C
Apoa4	TACGTATGCTGATGGGGTGC	ATCATGCGGTCACGTAGGTC	200 nM	60°C
Cd44	CAATGGGACGGTGGAAGACA	CAGATTCCGGGTCTCGTCAG	200 nM	60°C
Cdh1	CTTTTCGGAAGACTCCCGATT	GCTTTAGATGCCGCTTCACTGT	200 nM	60°C
Clec4f	CTTCGGGGAAGCAACAACTC	CAAGCAACTGCACCAGAGAAC	200 nM	57°C
Elovl6	ACA ATG GAC CTG TCA GCA AA	GTACCAGTGCAGGAAGATCAGT	100 nM	60°C
F4/80	CTTTGGCTATGGGCTTCCAGTC	GCAAGGAGGACAGAGTTTATCGTG	150 nM	60°C
H19	CAGAGGTGGATGTGCCTGCC	CGGACCATGTCATGTCTTTCTGTC	250 nM	60°C
Hmgcr	ATCCAGGAGCGAACCAAGAGAG	CAGAAGCCCCAAGCACAAAC	250 nM	60°C
Igf2	GGAAGTCGATGTTGGTGCTTCTC	CGAACAGACAAACTGAAGCGTGT	250 nM	60°C
Il1ß	GAGAGCCTGTGTTTTCCTCC	GAGTGCTGCCTAATGTCCC	250 nM	60°C
Imp2	CTGATCCCAGGGCTAAACCTC	AAGGGGTGATAGGGAGGACTG	200 nM	61°C
Krt19	AGCGTGATCAGCGGTTTTG	CCTGGTTCTGGCGCTCTATG	200 nM	60°C
Lamc1	TTTGATAGACGCGTGAACGATAA	TGGCGGGAATTCTCCTTAGA	200 nM	58°C
LxR	CCGACAGAGCTTCGTCC	CCCACAGACACTGCACAG	200 nM	60°C
Sox9	CCAGCAAGAACAAGCCACAC	CTTGCCCAGAGTCTTGCTGA	150 nM	60°C
Spp1	CCGAGGTGATAGCTTGGCTTAT	GACTCCTTAGACTCACCGCTC	200 nM	60°C
Zfp36	CTTCATCCACAACCCCACC	CAGGGAAGGGCCAGAAAAG	250 nM	59°C

Table 19: Primer and probe sequences as used for qPCR.

Gene	Forward primer sequence, 5'-3'	Reverse primer sequence, 5'-3'	Probe sequence (5'FAM-->3'BHQ)
hup62	GTT CCC GCA TCA TCA CTC TTA T	GAA TCT CGC CAG CTG TTT GA	TGT GAA TCT CTT CAT CCC AAC CCA GGC T

6.6.2   Standard plasmid dilution series

The isolated plasmid DNA (6.3.3) was diluted in TE buffer to the required amount of standard plasmid DNA used for qPCR standards with the following equation:

$$c_{end}\ (Plasmid\text{-}DNA) = \frac{c\ (plasmid)\,(^{ug}\!/_{ml})}{molecular\ weight\ (approx.\ 600\ ^{g}\!/_{mol}) \times length\ of\ plasmid\ with\ insert\ (bp)}$$

A plasmid standard dilution was run alongside the samples to confirm qPCR efficiency and to quantify target mRNAs in the cDNA samples. The standard concentration curve was generated with 60 to 6 E-5 attomole of standard when using 3 µl of the template, 80 – 8 x 10^{-5} attomole when using 4 µl of the template, or 100 – 1 x 10^{-4} when using 5 µl of the template.

6.6.3   Experimental procedure

The template cDNA and plasmid solutions were mixed with the corresponding reaction mixture in 96 wells plates and measured in a Real-Time PCR Detection System (C1000 Touch™ Thermal cycler with a CFX96™ Optics Module, Bio-Rad, Richmond, CA, USA). For the measurement with the dual-labeled probe, the conditions in the cycler were set to "emulation mode iCycler".

6.6.3.1   qPCR using SYBR® Green

The added amount of template cDNA and standard plasmid solution was 3 or 4 µl in a final volume of 20 µl. qPCR was performed using gene-specific primers (conditions see Table 18) and 5 x HOT FIREPol® EvaGreen® qPCR Mix Plus (Solis BioDyne, Tartu, Estonia) according to the manufacturer's instructions. All samples and standards were analyzed in triplicates using the following PCR conditions:

Conditions:

	95°C	15 min	
	94°C	15 sec	
temperature see Table 18		20 sec	39 cycles
	72°C	20 sec	
	95°C	10 sec	
Melting curve: 65.0°C to 95.0°C	Increment	0.5°C 0:05	

The relative expression was normalized to mRNA levels of the murine housekeeping genes *Rn18s*, *Ppia* or *Csnk2a2*, respectively. For Figure 10 B, E, F, Chapter III, two independent tests to determine the best suitable housekeeping gene for normalization were performed: using NormFinder (Andersen *et al.*, 2004) and geNorm (Vandesompele *et al.*, 2002). For both analyses, the same result was obtained, and the mRNA expression data of gene of interest were normalized to the most suitable housekeeping gene as stated in the figure legends.

6.6.3.2   qPCR using dual-labeled probes

Primer and probe sequences are given in **Table 19**. 5 µl of the template cDNA and the standard plasmid solution were mixed with the following reaction mixture and analyzed in triplicates using the following PCR conditions:

Reaction mixture:

		Conditions:			
Taq-Polymerase (5 U/µl)	2.5 U	denaturation	95°C	8 min	
dNTPs (10 mM)	125 µM	denaturation	95°C	15 sec	45
10 x *Taq*-buffer	2,5 µl	annealing	60°C	15 sec	cycles
primers (10 µM, each)	400 nM	elongation	72°C	15 sec	
Dual –labeled probe	60 nM	final elongation	25°C	25 sec	
MgCl$_2$	5 mM				
template	5 µl				
H$_2$O	ad 25 µl				

The relative expression was normalized to mRNA levels of the murine housekeeping genes *Csnk2a2*.

6.7 Western Blot analysis

6.7.1 Preparation of protein samples

Livers of mice were homogenized in lysis buffer (150 mM NaCl; 50 mM Tris-HCl, pH8.0; 1% Triton X-100; 0.1% SDS; 0.5% Natriumdesoxycholate; 5 mM EDTA) supplemented with 5 mM NaF, 2 mM Natriumorthovanate, and a protease inhibitor mixture (Complete® mini, #04 693 124 001, Roche Diagnostics GmbH, Mannheim, Germany). Samples were rotated for 30 min at 4°C, sonicated and centrifugated at 16,000 x *g* for 20 min at 4°C. The protein concentration of the supernatant was determined by Pierce™ BCA Protein Assay Kit (#23225, Thermo Fisher Scientific, Rockford, IL, USA) according to the manufacturer's protocol. The supernatant was aliquoted and stored at -80°C.

6.7.2 SDS-polyacrylamide gel electrophoresis (PAGE)

The samples were thawed on ice, loaded with Roti®-Load1 (4x–concentrated, #K929.1, Roth, Karlsruhe, Germany), and denatured at 95°C for 5 min. A prestained protein marker (10 to 180 kDa, #26616, Thermo Scientific, Carlsbad, CA, USA) was used to estimate the molecular masses of the samples. Equal protein amounts and a suitable marker volume were loaded onto the gel and separated in electrophoresis buffer (24.8 mM Tris, 192 mM glycine, 0.1% SDS) for 30 min at 80 V, followed by 2 h at 120 V. Preparation of the polyacrylamide gels (see below) and the electrophoresis was carried out using the Mini-PROTEAN® system (Bio-Rad, Richmond, CA, USA).

Composition:	resolving gel	stacking gel
Rotiphorese® Gel 30 (#3029.1, Roth, Karlsruhe, Germany)	12%	5%
Tris 1.5 M (pH 8.8)	375 mM	-
Tris 1 M (pH 6.8)	-	125.5 mM
SDS (10%)	0.1%	
APS (10%)	0.1%	
TEMED (#1.10732, Merck, Darmstadt, Germany)	0.1%	
H$_2$0 added for the desired volume		

6.7.3 Blotting

The separated proteins were transferred onto a polyvinylidene fluoride (PVDF) membrane, Immobilon®-FL, Merck Millipore Ltd., Tullagreen, Carrigtwohill, Co. Cork, Ireland) using a Mini Trans-Blot® Cell (Bio-Rad, Richmond, CA, USA). Prior to blotting, the membrane was activated for 30 sec in methanol. Sponges, blotting papers, gel, and membrane were equilibrated in transfer buffer (24.8 mM Tris, 192 mM glycine, 0.05% SDS, 20% methanol), followed by gel sandwich preparation. Blotting was carried out at 80 mA overnight. Unspecific binding sites were blocked by incubating the membrane in Rockland blocking buffer (#MB-070, obtained from Rockland, Gilbertsville, PA, USA) for 1.5 h.

6.7.4 Immunodetection

Antibodies were either diluted in PBST (0.1% (v/v) Tween20 in 1x PBS (136.89 mM NaCl, 2.68 mM KCl, 10.14 mM Na_2HPO_4, 1.76 mM KH_2PO_4, pH 7.4)) with 5% (m/v) dried milk pouder or Rockland blocking buffer (RBB) according to Table 20.

Table 20: *Antibody dilutions used for immunodetection.*

antibody	dilution
anti-human p62, rabbit IgG	1:1,000 in RBB
anti-α-tubulin, mouse IgG	1:1,000 in PBST + 5% [w/v] dried milk
IRDye® 800CW conjugated goat anti-mouse IgG	1:10,000 in RBB
IRDye® 680RD conjugated mouse anti-rabbit IgG	1:5,000 in RBB

The membranes were incubated with the primary antibody (anti-human p62) at 4°C overnight, followed by 4x washing for 5 min with PBST and incubation with IRDye® 680RD conjugated secondary antibody for 1.5 h at room temperature. The membrane was washed twice in PBST (5 min), followed by two washing steps in PBS (5 min) and incubation for 1.5 h at room temperature with the anti-α-tubulin primary antibody. After 4x washing the membrane with PBST, the incubation with IRDye®800 conjugated secondary antibody followed for 1.5 h. Prior to detection, the membrane was washed again in PBST (5 min, 2x) and then in PBS (5 min, 2x). Signals were detected using an Odyssey imager (Model 9120, LI-COR Biosciences, Lincoln, NE, USA). p62/IMP2 signal intensities were quantified using the Image Studio Software application (Ver 5.2, LI-COR®) and normalized to tubulin as a loading control.

6.8 Lipid extraction

Lipids were extracted from lyophilized liver tissue (adapted from Hara and Radin, 1978a; Laggai *et al.*, 2013), which was minced in liquid nitrogen with a mortar and a pestle. Freeze-dried liver tissue (15 mg) was dispersed with 18 volumes of hexane/2-propanol (3:2 (v/v)) for 10 min and centrifuged for 10 min at 4°C and 10,000 x *g*. The supernatant was transferred into a 1.5 ml glass vial (#60500-1109, DURATEC Analyzentechnik GmbH, Hockenheim, Germany), dried under nitrogen stream, re-dissolved in 200 µl chloroform-methanol (2:1 (v/v)), and stored at -20°C.

6.9 Colorimetric Sulfo-Phospho-Vanillin

The colorimetric Sulfo-Phospho-Vanillin assay used to quantify total lipids was adapted from Cheng *et al.* (Cheng *et al.*, 2011). As a standard solution olive oil was diluted in chloroform-methanol (2:1 (v/v)). 100 µg, 75 µg, 50 µg, 25 µg, 12.5 µg and 6.25 µg olive oil were used as a standard and handled like the samples. 5 µl of the lipid extracts were transferred into a 1.5 ml glass vial and the solvent was evaporated by incubation for 2 to 5 min at 90°C in a drying closet. Samples were cooled to room temperature, 100 µl of sulfuric acid (95-97%, #100731.1000, Merck, Darmstadt, Germany) was added and the mixture incubated for an additional 20 min at 90°C. After cooling the vials down to room temperature, 50 µl vanillin-phosphoric acid (0.2 mg vanillin per ml 17% orthophosphoric acid (85%, #20624, VWR, Darmstadt, Germany) was added, followed by 10 min incubation at room temperature. 100 µl of the colored solution was transferred to a 96 well plate and the absorption was measured at 550 mm using the Sunrise™ absorbance microplate reader (Tecan Austria GmbH, Grödig, Austria). The standard curve was created using Microsoft® Excel® 2013 and the OriginPro 2015 software (OriginLab Corporation, Northampton, MA, USA).

6.10 Measurement of Endotoxins

Serum endotoxins were measured using the EndoZyme® II Recombinant Factor C (rFC) Assay (#890030, Lot# 18238, Hyglos GmbH, Bernried am Starnberger See, Germany). The serum of the mice was diluted 1:500 in endotoxin-free water from the manufacturer and preheated for 15 min at 75°C, as recommended. For spike recovery, exogenous LPS (0.1 EU/ml) was added to the serum. The assay was performed according to the manufacturer's protocol. Samples with a recovery rate lower than 50% were excluded from the analysis.

6.11 Lipidomic analysis

Lipidomic data were generated within the German epigenome program 'DEEP' with the project number [O1KU1216F] (A.K.K.) in the Lipidomics Lab Regensburg at the Institute of Clinical Chemistry and Laboratory Medicine at the University Hospital of Regensburg in the group of Dr. G. Liebisch. Lipid quantification of liver homogenates was performed using electrospray-ionization mass spectrometry with a hybrid quadrupole-orbitrap QExactive mass spectrometer (Thermo Fisher Scientific, Bremen, Germany). Detailed methods for phosphatidylcholine (PC), sphingomyelin (SM), and lysophosphatidylcholine (LPC) are described in Liebisch *et al.* (2002, 2004). Phosphatidylethanolamine (PE), phosphatidylserine (PS), phosphatidylglycerol (PG), and phosphatidylinositol (PI) were measured as published in Binder *et al.* (2006) and Matyash *et al.* (2008) and PE-based plasmalogens (PE P) were quantified according to the principles described by Berry and Murphy (2004). The method for the analysis of ceramides (CER) is described in Liebisch *et al.* (1999) and for cholesteryl ester (CE) and free cholesterol in Liebisch *et al.* (2006). For the detection of triglycerides, the same method was used as for the CE.

6.12 Histologic staining of paraffin-embedded tissue

6.12.1 Fixation and paraffin embedding of tissue

The dehydration and paraffin infiltration was performed using the robust carousel tissue processor MTP (SLEE medical GmbH, Mainz, Germany). The fixed liver tissue was first dehydrated through an ethanol gradient, incubated in xylol, and infiltrated with paraffin (Roti®-Plast, #6642.6, Roth, Karlsruhe, Germany). The detailed sequence is shown in Table 21.

Table 21: *Programme for paraffin infiltration of tissue.*

step	solution	time (min)
1	formalin	1
2	70% isopropanol	90
3	70% isopropanol	90
4	80% isopropanol	90
5	90% isopropanol	90
6	100% isopropanol	90
7	100% isopropanol	90
8	xylol	90
9	xylol	90
10	xylol	90
11	paraffin	120
12	paraffin	120

After this process, the liver lobes were embedded in paraffin with the prewarming module MPS/W and the dispensing module MPS/P. The paraffin-embedded liver tissue from 3.2.2 and Chapter III was sent to Prof. Dr, Dr. J. Haybäck to the Department of Pathology at the Medical Faculty of the Otto-von-Guericke University Magdeburg for the generation of tissue sections, HE and Sirius red stainings, and the histological analysis and scoring.

6.12.2 Stainings and evaluation

Stainings for Chapter I were performed by Dr. S. M. Kessler. Paraffin-embedded liver sections were stained with hematoxylin-eosin (HE). Immunohistochemical (IHC) Krt19 detection was achieved using Dako EnVision+ System- HRP Labelled Polymer Anti Rabbit (#K4003, Dako, Carpinteria, CA, USA) with the anti-Krt19 antibody (1:1000). Epitopes were demasked with citrate buffer (10 mM, pH 6.0) in a water bath at 95°C for 45 minutes. For Laminin detection epitopes were demasked by proteinase K (20 µg/ml in TE buffer) incubation for 15 min at 37°C in a water bath. Anti-laminin antibody (1:200) was incubated for 1 h at room temperature followed by incubation with anti-rabbit Envision (Dako, Carpinteria, CA, USA) for 20 min at room temperature and DAB staining. Hyaluronic acid was detected by staining with a biotin-labeled hyaluronic acid binding protein (1:100, #AMS.HKD-BC41, Amsbio, Abingdon, United Kingdom) for 1 h at room temperature and detection by Streptavidin-HRP (#K3954, Dako, Carpinteria, CA, USA) for 20 min at room temperature and DAB staining.

Stainings were evaluated for ductular reaction, and hepatic collagen deposition by two independent, blinded investigators. P-values were determined by Chi-square test.

6.13 Isolation of hepatocytes and non-parenchymal cells

Isolation of primary hepatocytes and non-parenchymal cells (NPCs) from mouse livers was performed at the Systems Toxicology at the Leibniz research center for working environment and human factors (IfADo) at the TU Dortmund by Dr. K. Gianmoena, K. Rochlitz and Dr. C. Cadenas Garcia in the research group of Prof. Dr. med. J. G. Hengstler as described in Godoy *et al.* (Godoy *et al.*, 2013). In brief, the liver was perfused through the vena cava with an EGTA-containing buffer to remove blood and Ca^{2+}-dependent adhesion factors, followed by a perfusion with collagenase buffer to digest the extracellular matrix and to disperse the liver cells. After the digestion, the liver was excised and the liver capsule was opened under sterile conditions, and the cells were released into a suspension buffer. The cell suspension was filtered through a 100 µm gauze to remove tissue debris and centrifuged for 5 min at 4°C and 50 x *g*. After centrifugation of the cell suspension for 5 min at 4°C and 50 x *g*, NPCs were in the supernatant. The hepatocyte pellet was washed and the centrifugation step was repeated for greater purity. Aliquots of NPCs and hepatocytes were shipped to the genetic/epigenetic research group of Prof. Dr. J. Walter at Saarland University.

6.14 Epigenetic profiling

Sequencing data were generated within the German epigenome program 'DEEP' with the project number [O1KU1216F] (A.K.K.).

6.14.1 RNA sequencing

RNA sequencing was performed at the Institute of Clinical Molecular Biology (IKMB) at Kiel University in the group of Prof. Dr. P. Rosenstiel, statistical analysis of the results was performed by Dr. A. Sinha.

6.14.2 Reduced representation bisulfite sequencing (RRBS) and DNaseI sequencing

RRBS, DNaseI sequencing, and visualization by heatmaps were performed in the genetic/epigenetic research group of Prof. Dr. J. Walter at Saarland University by Dr. G. Gasparoni, Dr. N. Gasparoni, and Dr. K. Nordstöm.

6.15 GO term and KEGG pathway analysis

The Kyoto Encyclopedia of Genes and Genomes (KEGG) pathways and Gene Ontology (GO) enrichment analyses were performed using the STRING database V10.5 (http://string-db.org) (Szklarczyk *et al.*, 2015, 2017). For the statistics, the STRING database uses a Fisher's exact test, followed by a correction for multiple testing, the Benjamini-Hochberg False Discovery Rate (FDR) (Benjamini *et al.*, 1995; Rivals *et al.*, 2007). GO terms were categorized using semantic clustering to identify similar GO terms among the enriched terms with the web server REVIGO (http://revigo.irb.hr/.) (Supek *et al.*, 2011).

6.16 Cirrhotic HCC (human)

GEO dataset (GSE14323) was analyzed for differential gene expression between human cirrhotic (n=41), HCC-cirrhotic (n=17), and healthy (n=19) liver samples. The analysis was done by Dr. A. Barghash (School for Computer Engineering and Information Technology, German Jordanian University, Amman, Jordan).

6.17 Statistics

For illustration and statistical analyses the OriginPro 2015G software (OriginLab Corporation, Northampton, MA, USA) was used. Results are shown as means ± SEM or box plots with 25th/75th percentile boxes, geometric medians (line), means (square), and 10th/90th percentile as whiskers. Statistical significance was determined by t-test, one-way ANOVA or Mann-Whitney U test (with Bonferroni correction when comparing more than two groups) depending on normal distribution.
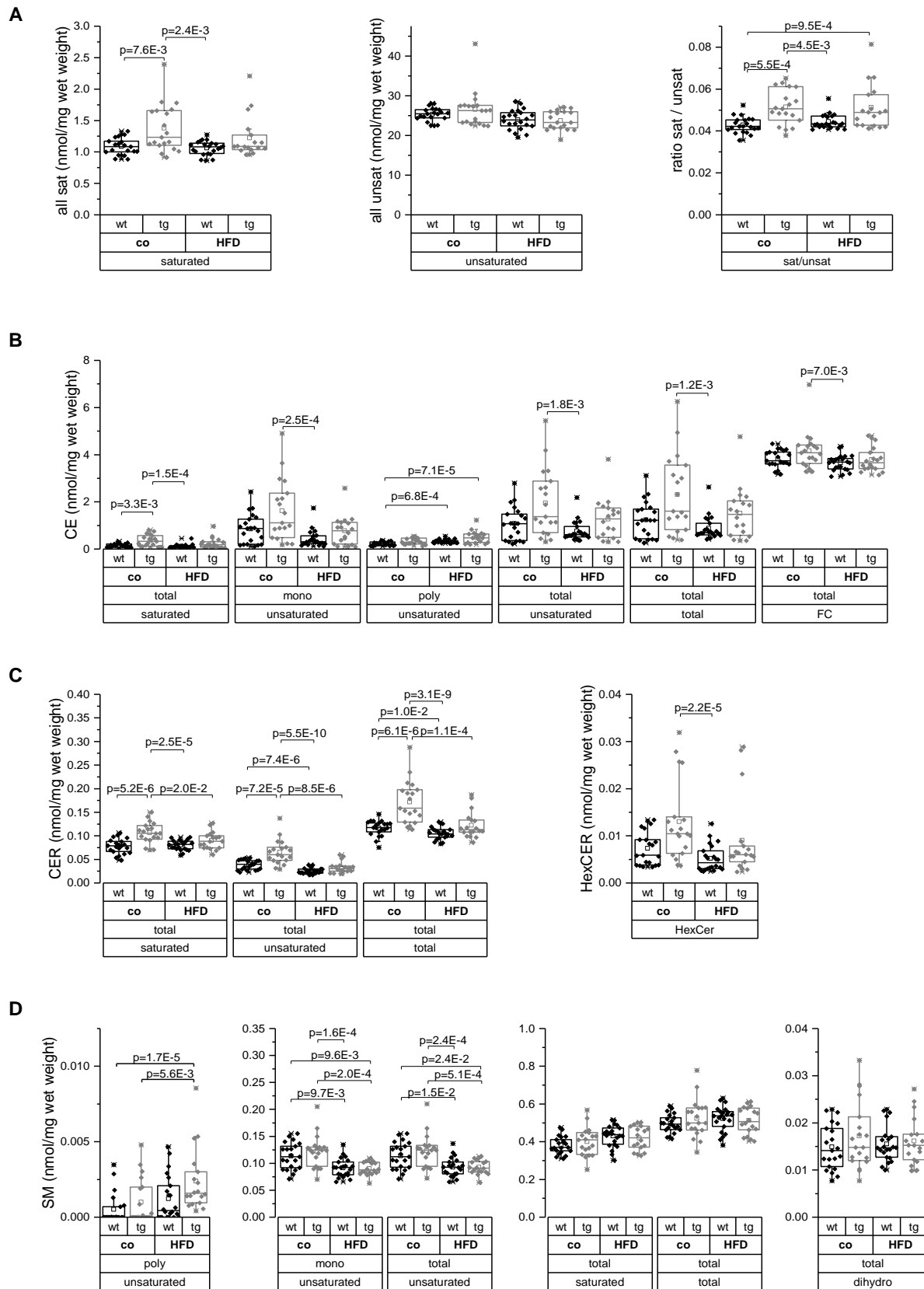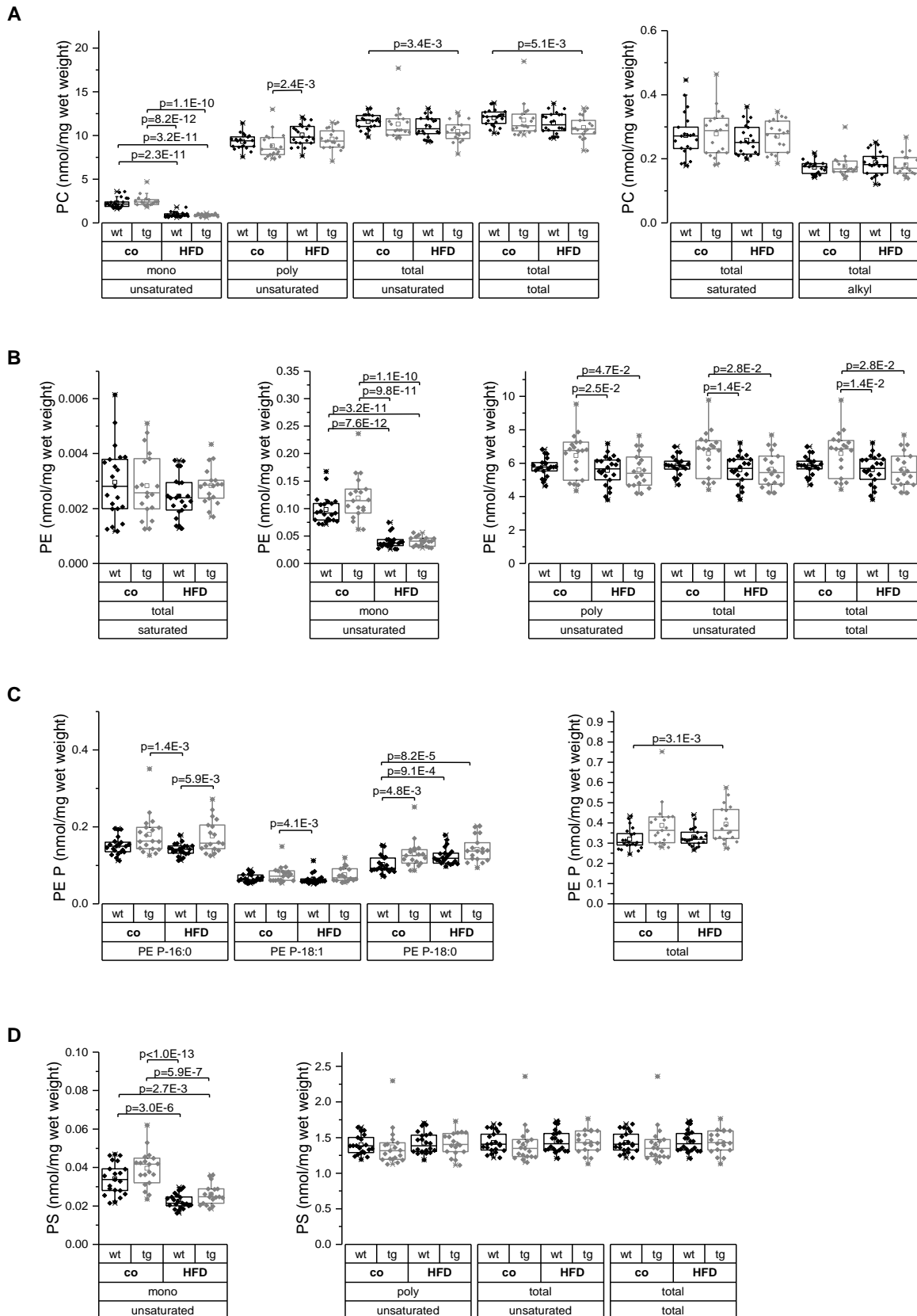
7 SUPPLEMENT

7.1 Lipidomic analysis: wild-type and *p62* transgenic high-fat diet-fed animals (3.2.1)

Supplemental table 7-1: Simplified table of significantly increased or decreased lipid classes in livers of high-fat diet (HFD) fed wild-type (wt) or p62 transgenic mice (tg) compared to the control diet (co) (n=18-21 per group). Increased levels of lipid classes are highlighted in dark grey and decreased levels in light grey color. Corresponding figures are shown in Supplemental figure 7-1 Supplemental figure 7-3. CE: cholesteryl ester, CER: ceramide, SM: sphingomyelin, PC: phosphatidylcholine, PE: phosphatidylethanolamine, PE P: PE based plasmalogens, PS: phosphatidylserine, PG: phosphatidylglycerol, PI: phosphatidylinositol, LPC: lysophosphatidylcholine, sat: saturated species, mono: monounsaturated species, poly: polyunsaturated species, total: all species.

			HFD wt compared to **co wt**	HFD tg compared to **co tg**	co tg compared to **co wt**	HFD tg compared to **HFD wt**
Sterol lipids	**CE**	sat			↑	
		poly	↑			
Sphingolipids	**CER**	sat		↓	↑	
		unsat	↓	↓	↑	
		total	↓	↓	↑	
	SM	mono	↓	↓		
		poly		↑		
		unsat	↓	↓		
Glycero-phospholipids	**PC**	mono	↓	↓		
	PE	mono	↓	↓		
		poly		↓		
		unsat		↓		
		total		↓		
	PE P	PE P-16:0				↑
		PE P-18:0	↑		↑	
	PS	mono	↓	↓		
	PG	total		↓		
	PI	mono	↓	↓		
	LPC	sat	↓	↓		
		mono	↓	↓		
		poly	↓	↓	↑	
		unsat	↓	↓		
		total	↓	↓		
All		sat			↑	
		unsat		↓		
		sat/unsat			↑	

Supplemental figure 7-1: Lipidomic analysis via ESI-MS/MS of wild-type (wt) and p62 transgenic (tg) animals fed a control (co) or high-fat diet (HFD) (n=18-21 each). A: All saturated, unsaturated species and the saturated to unsaturated ratio. B: Cholesteryl ester (CE) and free cholesterol (FC). C: Ceramide (CER) and hexosyl ceramide (HexCER). D: Sphingomyelin (SM) and dihydrosphingomyelin. P-values were calculated by Mann Whitney U test with Bonferroni correction (significance level set at p≤1.25E-2). One-way ANOVA for determination of statistical significance was used for the following species: CER saturated; SM saturated, monounsaturated, unsaturated, total. Results are shown as box plots with 25th/75th percentile boxes, geometric medians (line), means (square), and 10th/90th percentile as whiskers.

Supplemental figure 7-2: Lipidomic analysis via ESI-MS/MS of wild-type (wt) and p62 transgenic (tg) animals fed a control (co) or high-fat diet (HFD) (n=18-21). A: Phosphatidylcholine (PC). B: Phosphatidylethanolamine (PE). C: PE based plasmalogens (PE P). D: Phosphatidylserine (PS). P-values were calculated by Mann Whitney U test with Bonferroni correction (significance level set at p≤1.25E-2). One-way ANOVA for determination of statistical significance was used for the following species: PC saturated; PE saturated, polyunsaturated, total unsaturated, total; PS monounsaturated. Results are shown as box plots with 25th/75th percentile boxes, geometric medians (line), means (square), and 10th/90th percentile as whiskers.
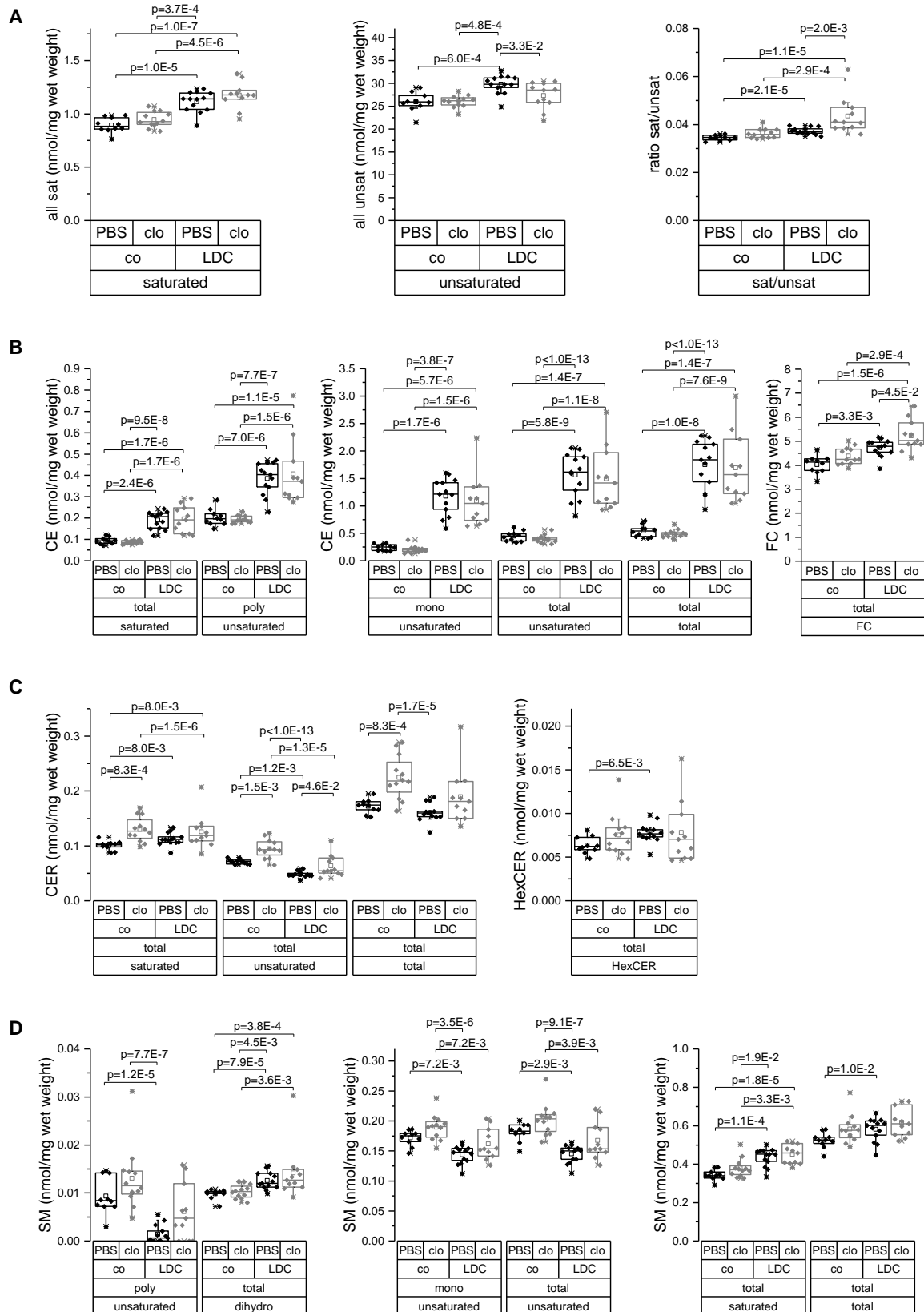
A

B

C
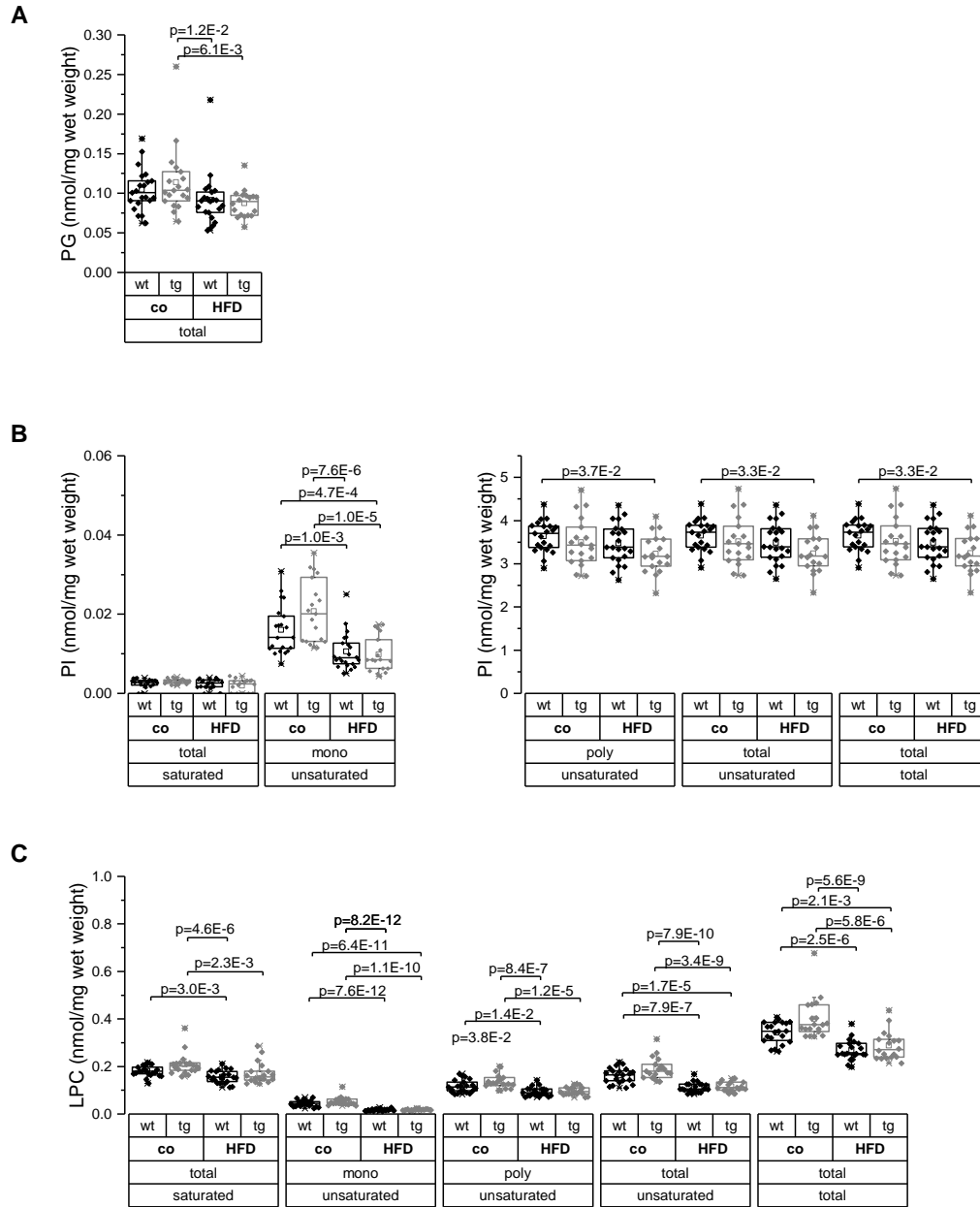
Supplemental figure 7-3: *Lipidomic analysis via ESI-MS/MS of wild-type (wt) and p62 transgenic (tg) animals fed a control (co) or high-fat diet (HFD) (n=18-21). A: Phosphatidylglycerol (PG). B: Phosphatidylinositol (PI). C: Lysophosphatidylcholine (LPC). P-values were calculated by Mann Whitney U test with Bonferroni correction (significance level set at p≤1.25E-2). One-way ANOVA for determination of statistical significance was used for the following species: PI polyunsaturated, total unsaturated, total; LPC polyunsaturated. Results are shown as box plots with 25th/75th percentile boxes, geometric medians (line), means (square), and 10th/90th percentile as whiskers.*
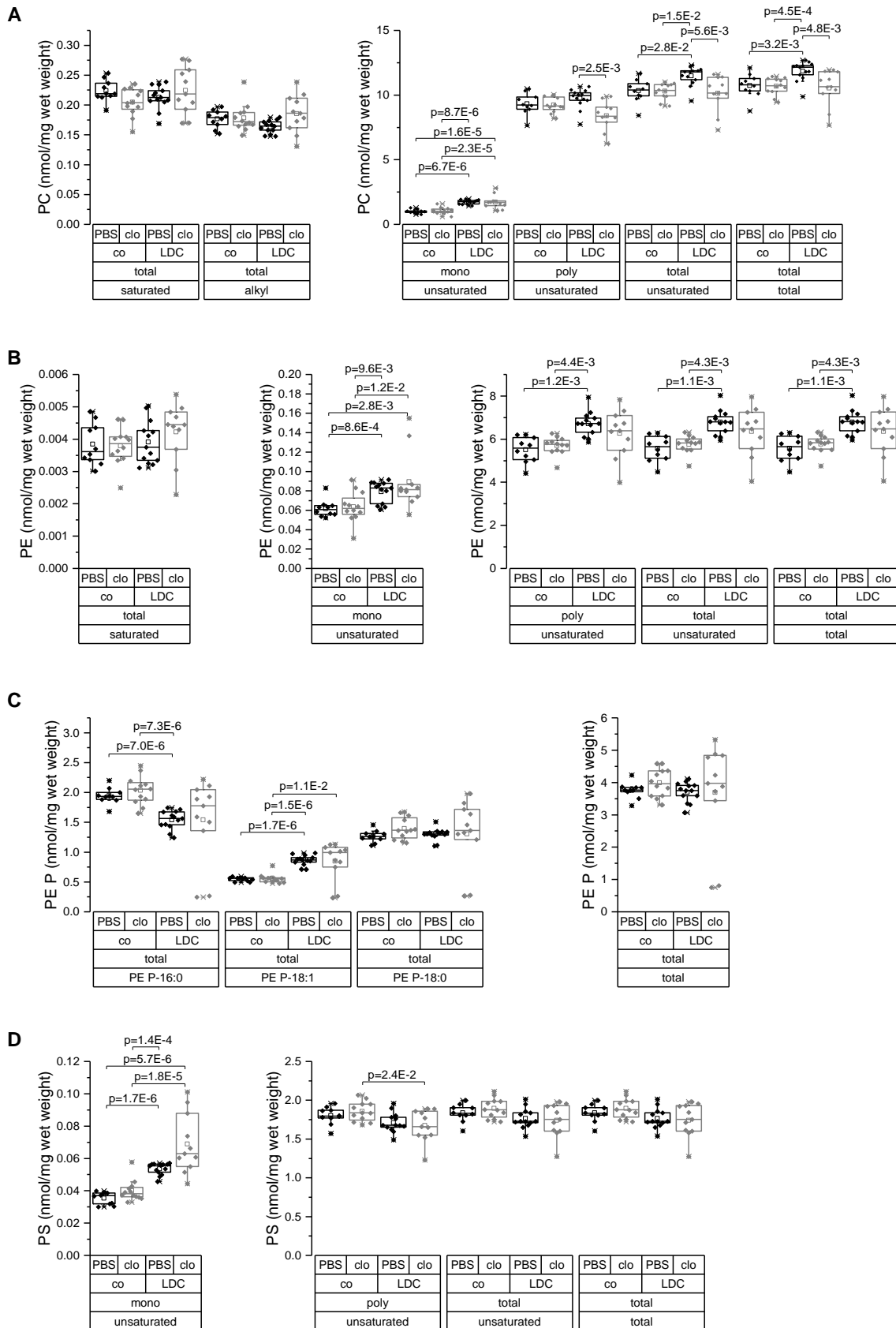
7.2 Lipidomic analysis: livers from animals on control or LDC diet with or without Kupffer cell depletion (Chapter III-1)

Supplemental table 7-2: Simplified table of significantly increased or decreased lipid classes in livers of animals fed a control (co) or Lieber-DeCarli (LDC) diet in the absence (clo) or presence (PBS) of Kupffer cells. (n=10-13 per group). Increased levels of lipid classes are highlighted in dark grey and decreased levels in light grey color. Corresponding figures are shown in Supplemental figure 7-4 - Supplemental figure 7-6. CE: cholesteryl ester, CER: ceramide, SM: sphingomyelin, PC: phosphatidylcholine, PE: phosphatidylethanolamine, PE P: PE based plasmalogens, PS: phosphatidylserine, PG: phosphatidylglycerol, PI: phosphatidylinositol, LPC: lysophosphatidylcholine, sat: saturated species, mono: monounsaturated species, poly: polyunsaturated species, total: all species. Clo: clodronate liposomes.

			LDC+PBS compared to co+PBS	LDC+clo compared to co+clo	co+clo compared to co+PBS	LDC+clo compared to LDC+PBS
Sterol lipids	CE	sat	↑	↑		
		mono	↑	↑		
		poly	↑	↑		
		unsat	↑	↑		
		total	↑	↑		
	FC	total	↑	↑		↑
Sphingolipids	CER	sat	↑	↓	↑	
		unsat	↓	↓	↑	↑
		total			↑	
		HexCer	↑			
	SM	sat	↑	↑		
		mono	↓	↓		
		poly	↓			
		unsat	↓	↓		
		total	↑			
		dihydro	↑	↑		
Glycero-phospholipids	PC	mono	↑	↑		
		poly				↓
		unsat	↑			↓
		alkyl				
		total	↑			↓
	PE	mono	↑	↑		
		poly	↑			
		unsat	↑			
		total	↑			
	PE P	PE P-16:0	↓			
		PE P-18:1	↑	↑		
	PS	mono	↑	↑		
		poly		↓		
	PI	mono	↑	↑		
		poly	↑			↓
		unsat	↑			↓
		total	↑			↓
	LPC	sat	↑	↑		
		mono	↑	↑		
		total		↑		
all		sat	↑	↑		
		unsat	↑			↓
		sat/unsat	↑	↑		↑

Supplemental figure 7-4: *Lipidomic analysis of whole livers from animals fed a Lieber-DeCarli (LDC) or control diet (co) and treated with PBS or clodronate liposomes (clo) for 5 weeks (n=10-13 each). A: All saturated, unsaturated species and the saturated to unsaturated ratio. B: Cholesteryl ester (CE) and free cholesterol (FC). C: ceramide (CER) and hexosyl ceramide (HexCER). D: Sphingomyelin (SM) and dihydrosphingomyelin. P-values were calculated by one-way ANOVA. Mann Whitney U test with Bonferroni correction was used for the following species: ratio saturated to unsaturated; CE: mono- and polyunsaturated; CER saturated, total and hexosyl ceramide; SM: polyunsaturated and dihydrosphingomyelin. Results are shown as box plots with 25th/75th percentile boxes, geometric medians (line), means (square), and 10th/90th percentile as whiskers.*

Supplemental figure 7-5: Lipidomic analysis via ESI-MS/MS of whole livers from animals fed a Lieber-DeCarli (LDC) or control (co) diet and treated with PBS or clodronate liposomes (clo) for 5 weeks (n=10-13 per group). A: Phosphatidylcholine (PC). B: Phosphatidylethanolamine (PE). C: PE based plasmalogens (PE P). D: Phosphatidylserine (PS). P-values were calculated by one-way ANOVA. Mann Whitney U test with Bonferroni correction (significance level set at p≤1.25E-2) for determining statistical significance was used for the following species: PC polyunsaturated, alkyl species and total; PE monounsaturated; PE P; PS monounsaturated. Results are shown as box plots with 25th/75th percentile boxes, geometric medians (line), means (square), and 10th/90th percentile as whiskers.
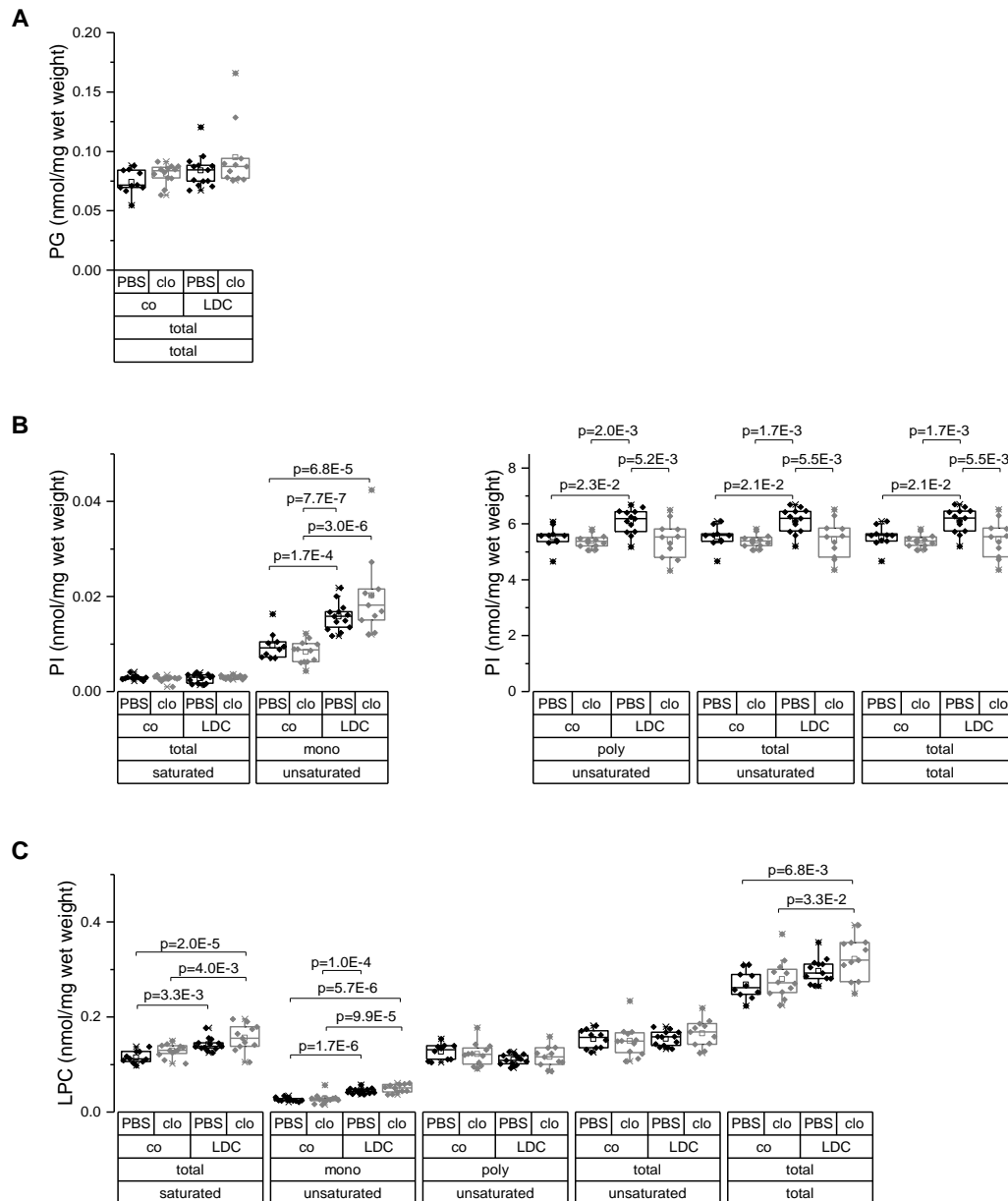
Supplemental figure 7-6: Lipidomic analysis via ESI-MS/MS of whole livers from animals fed a Lieber-DeCarli (LDC) or control (co) diet and treated with PBS or clodronate liposomes (clo) for 5weeks (n=10-13). A: Phosphatidylglycerol (PG). B: Phosphatidylinositol (PI). C: Lysophosphatidylcholine (LPC). P-values were calculated by one-way ANOVA. Mann Whitney U test with Bonferroni correction (statistical significance was set at p≤1.25E-2) was calculated for the following species: PG; PI saturated, monounsaturated; LPC monounsaturated. Results are shown as box plots with 25th/75th percentile boxes, geometric medians (line), means (square), and 10th/90th percentile as whiskers.
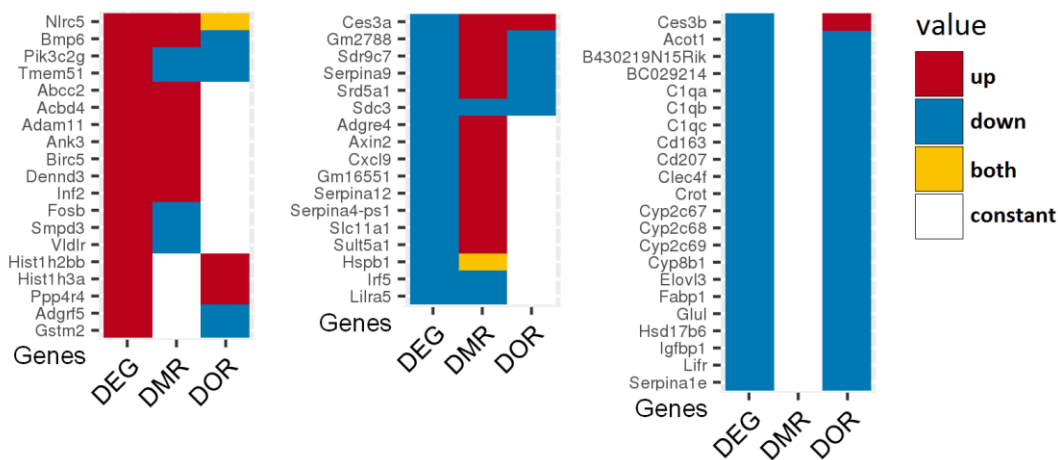
7.3 GO enrichment analysis and heatmaps of DEGs associated with epigenetic changes (Chapter III-1)

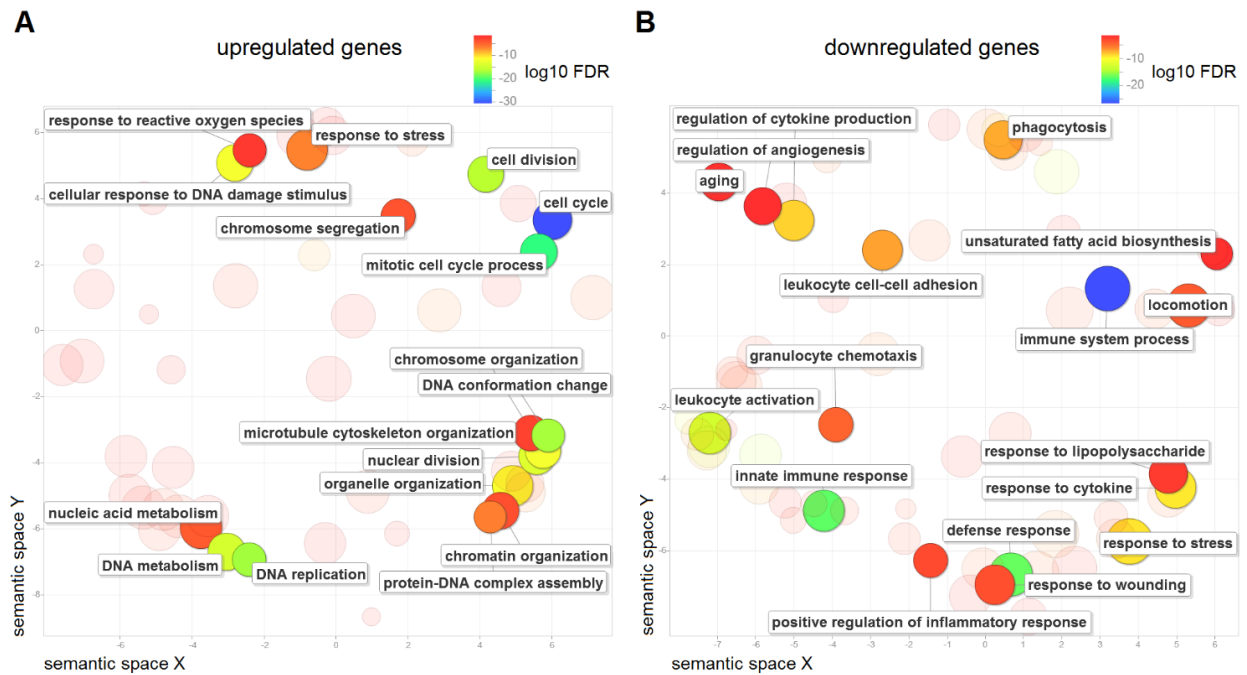### 7.3.1 Hepatocytes: co+clo compared to co+PBS
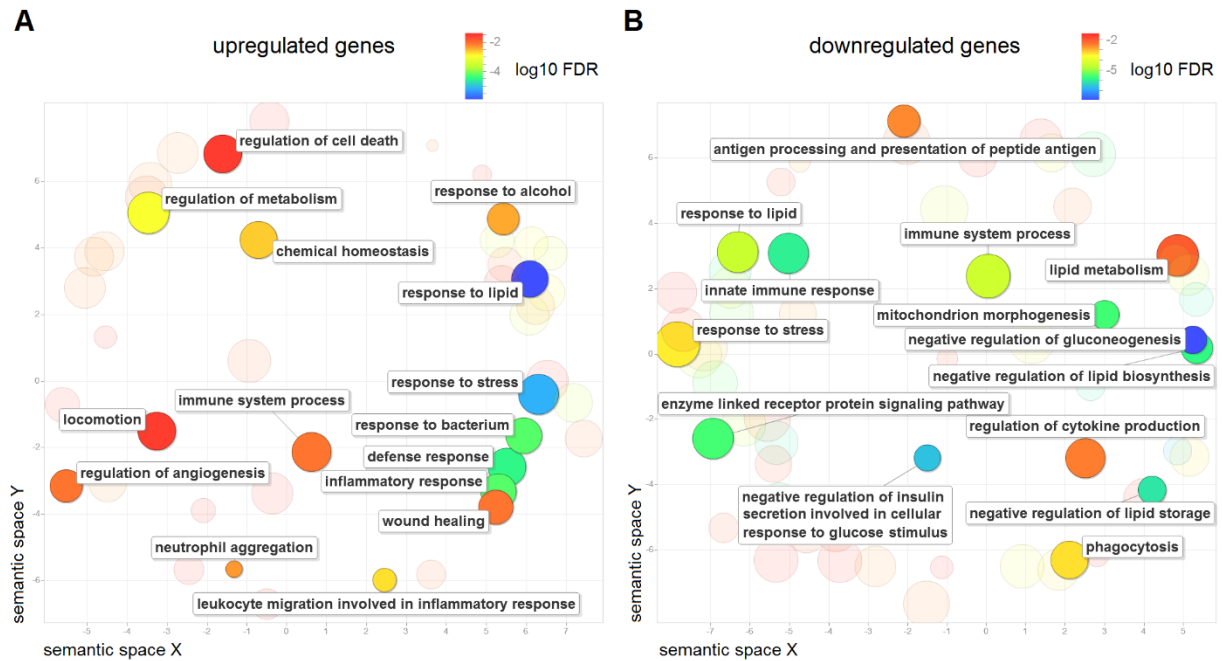
Supplemental figure 7-7: GO enrichment analysis of upregulated (A) and downregulated (B) genes of hepatocytes from clodronate-treated animals. GO terms for biological processes were categorized using semantic clustering and plotted by the REVIGO tool to identify similar GO terms among the enriched terms. Semantically similar GO terms remain closer together. Examples of genes included in the GO terms are shown in brackets. The circles represent individual GO terms or cluster of GO terms related to similar processes. The circle size corresponds to the percentage of genes annotated with the term in the reference database (UniProt for mus musculus) (larger means more general and smaller more specific GO term). The circle color illustrates the false discovery rate (in log10 FDR) of the GO enrichment analysis: red indicates the lowest and blue the highest significance.
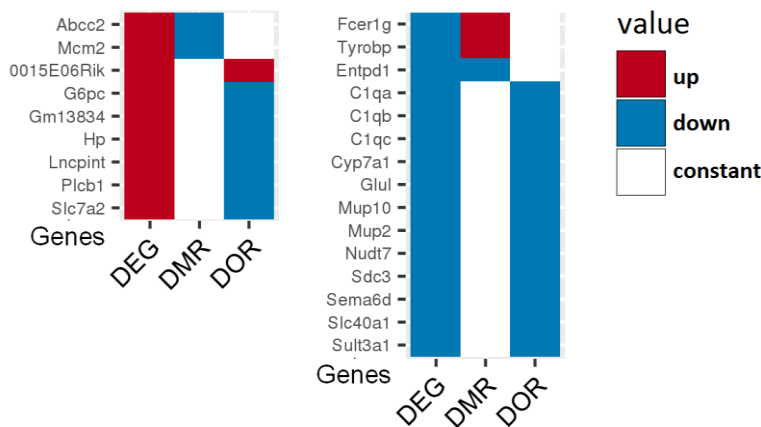

Supplemental figure 7-8: Simplified heatmap of the 58 differentially expressed genes (DEGs) associated with differentially methylated regions (DMRs) and/or differentially open chromatin regions (DORs) for the comparison of hepatocytes isolated from animals treated with clodronate to animals treated with PBS as a control. DEGs were determined by RNA-sequencing, DMRs by RRBS, and DORs by DNaseI-sequencing.
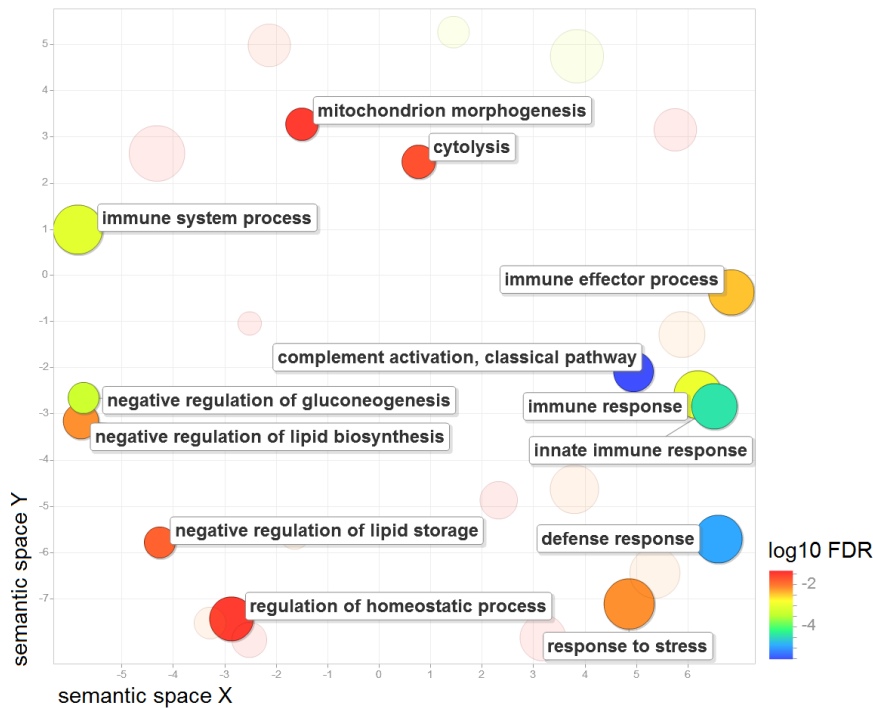
7.3.2 Hepatocytes: LDC+clo compared to LDC+PBS

Supplemental figure 7-9: *GO enrichment analysis of upregulated (A) and downregulated (B) genes in hepatocytes isolated from Kupffer cell-depleted animals fed an LDC diet compared to the LDC-fed control. GO terms for biological processes were categorized using semantic clustering and plotted by the REVIGO tool to identify similar GO terms among the enriched terms. Semantically similar GO terms remain closer together. The circles represent individual GO terms or cluster of GO terms related to similar processes. The circle size corresponds to the percentage of genes annotated with the term in the reference database (UniProt for mus musculus) (larger means more general and smaller more specific GO term). The circle color illustrates the false discovery rate (in log10 FDR) of the GO enrichment analysis: red indicates the lowest and blue the highest significance.*

Supplemental figure 7-10: *Differentially expressed genes (DEG) associated with epigenetic changes in clodronate-treated LCD-fed mice compared to control LDC-fed mice. DEGs were determined by RNA-sequencing, differentially methylated regions (DMRs) by reduced representative bisulfite sequencing, and differentially open chromatin regions (DORs) by DNaseI-sequencing.*

7.3.3   Hepatocytes: LDC+clo compared to co+clo

Supplemental figure 7-11*: GO enrichment analysis of downregulated genes in hepatocytes isolated from Kupffer cell-depleted LDC-fed mice compared to the control diet. GO terms for biological processes were categorized using semantic clustering and plotted by the REVIGO tool to identify similarities among the enriched terms. Semantically similar GO terms remain closer together. The circles represent individual GO terms or cluster of GO terms related to similar processes. The circle size corresponds to the percentage of genes annotated with the term in the reference database (UniProt) (larger means more general and smaller more specific GO term). The color illustrates the false discovery rate (in log10 FDR) of the GO enrichment analysis (red: lowest, blue: highest significance).*
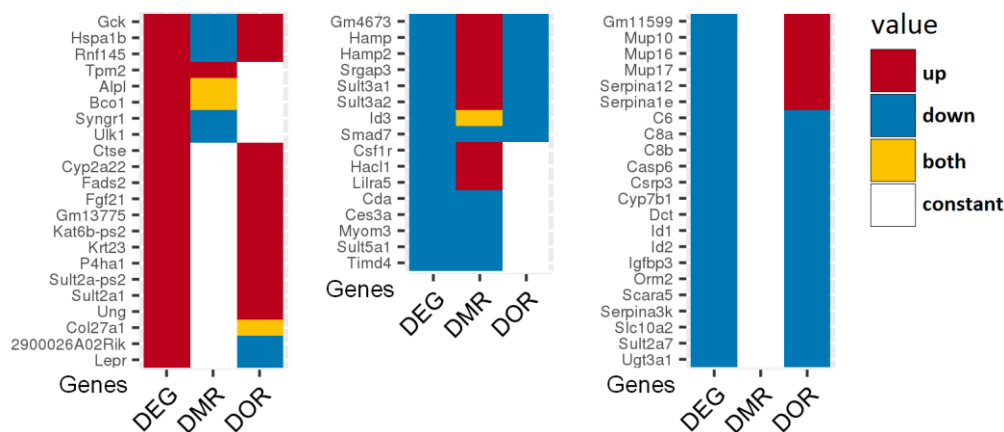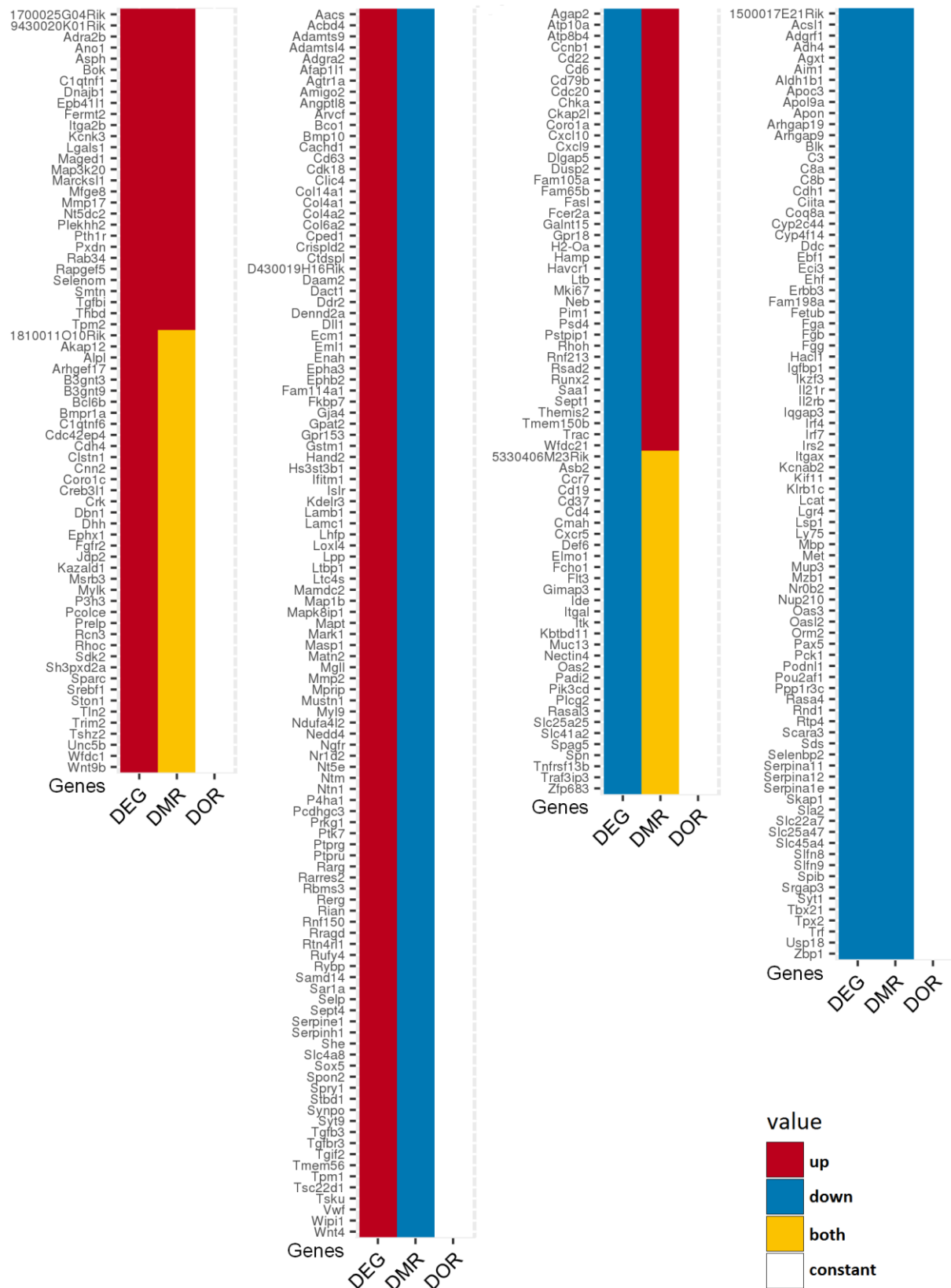

Supplemental figure 7-12*: Differentially expressed genes (DEG) associated with epigenetic changes in clodronate-treated LCD-fed mice compared to clodronate-treated mice on control diet. DEGs were determined by RNA-sequencing, differentially methylated regions (DMRs) by reduced representative bisulfite sequencing, and differentially open chromatin regions (DORs) by DNaseI-sequencing.*

7.3.4   NPCs: LDC+PBS compared to co+PBS

Supplemental figure 7-13: *Simplified heatmap of the 337 differentially expressed genes (DEGs) associated with differentially methylated regions (DMRs) and/or differentially open chromatin regions (DORs) for the comparison of non-parenchymal cells isolated from LDC fed animals to the control. DEGs were determined by RNA-sequencing, DMRs by reduced representative co bisulfite sequencing and DORs by DNaseI-sequencing.*
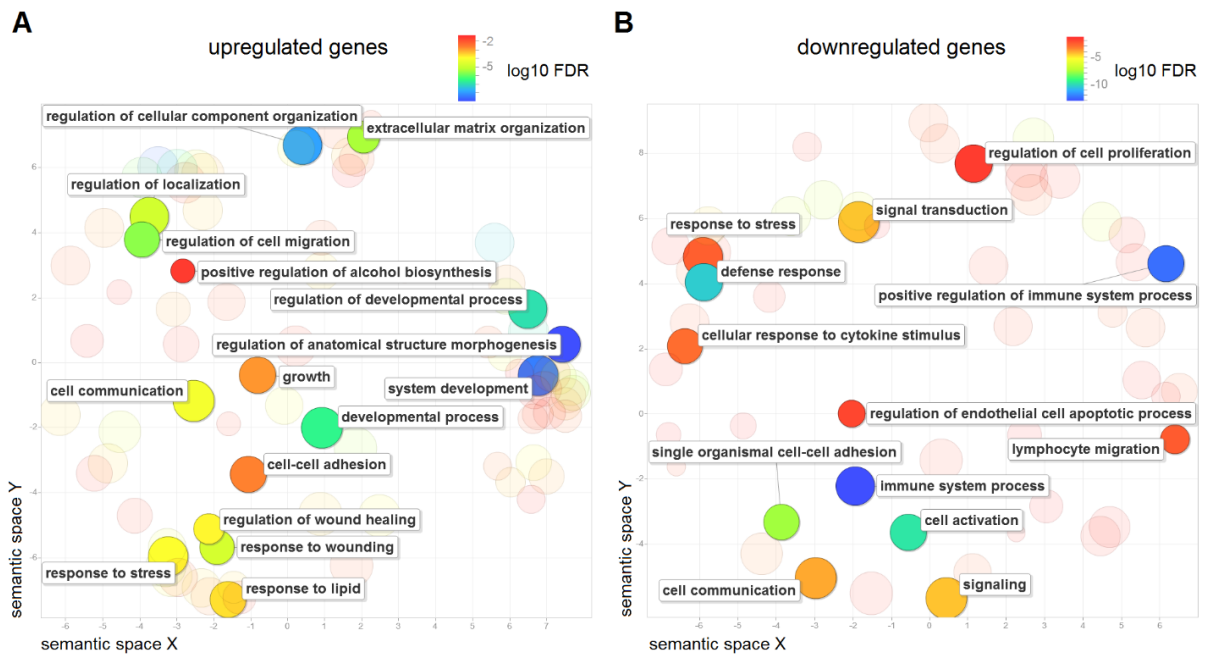
Supplemental figure 7-14: *GO enrichment analysis of upregulated (A) and downregulated (B) genes in non-parenchymal cells isolated from LDC-fed mice compared to the control. GO terms for biological processes were categorized using semantic clustering and plotted by the REVIGO tool to identify similar GO terms among the enriched terms. Semantically similar GO terms remain closer together. The circles represent individual GO terms or cluster of GO terms related to similar processes. The circle size corresponds to the percentage of genes annotated with the term in the reference database (UniProt for mus musculus) (larger means more general and smaller more specific GO term). The circle color illustrates the false discovery rate (in log10 FDR) of the GO enrichment analysis: red indicates the lowest and blue the highest significance.*

7.3.5 NPCs: LDC+clo compared to LDC+PBS
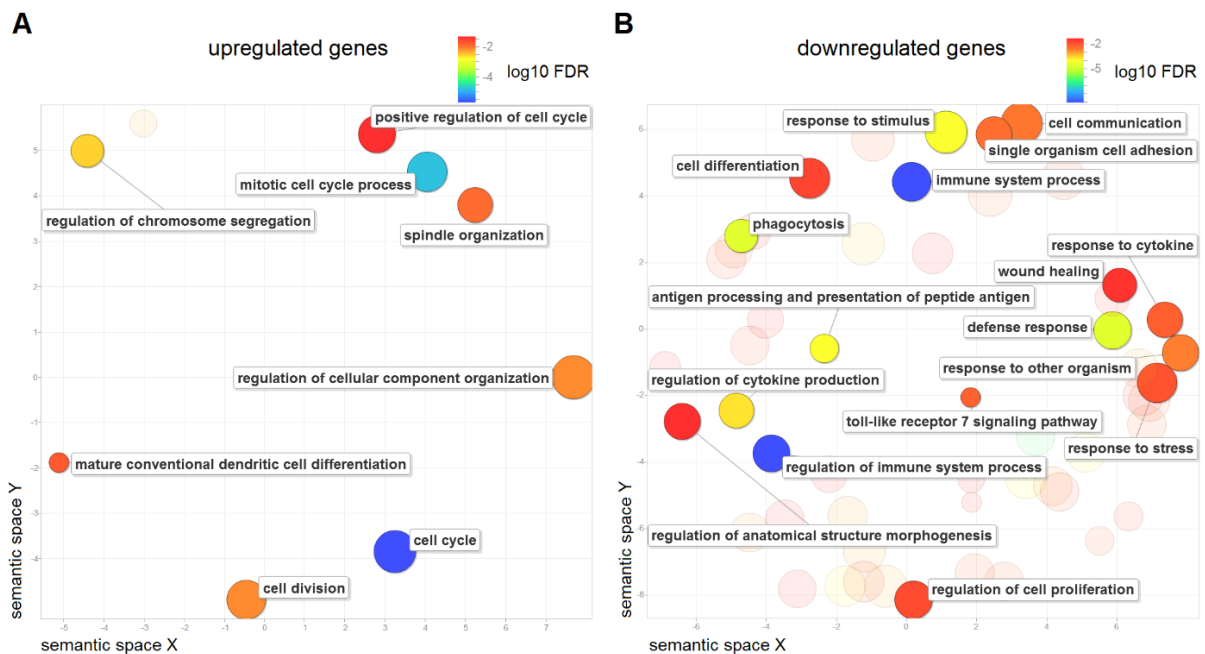
Supplemental figure 7-15: *GO enrichment analysis of upregulated (A) and downregulated (B) genes in NPCs isolated from clodronate-treated LDC-fed mice with PBS-treated LDC-fed mice. GO terms for biological processes were categorized using semantic clustering and plotted by the REVIGO tool to identify similar GO terms among the enriched terms. The circles represent individual GO terms or cluster of GO terms related to similar processes. The circle size corresponds to the percentage of genes annotated with the term in the reference database (UniProt for mus musculus) (larger means more general and smaller more specific GO term). The circle color illustrates the false discovery rate (in log10 FDR) of the GO enrichment analysis (red: lowest, blue: highest significance).*
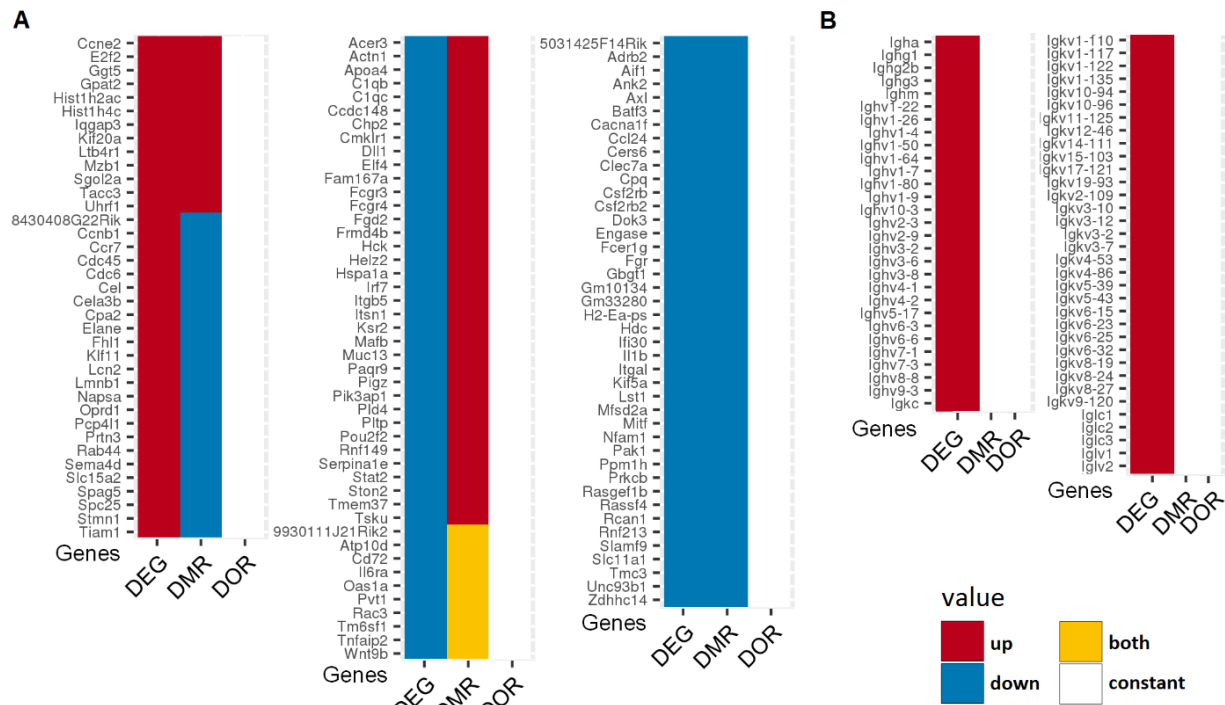
Supplemental figure 7-16: *Simplified heatmap of the differentially expressed genes (DEGs) in fractions of non-parenchymal cells of Kupffer cell-depleted animals fed an LDC diet (n=2) compared to animals fed the same diet in the presence of Kupffer cells (n=2). A: DEGs associated with differentially methylated regions (DMRs) and/or differentially open chromatin regions (DORs). B: Differentially expressed immunoglobulin genes.*

7.4 Serum analysis: wild-type and p62 transgenic animals on control or LDC diet with or without Kupffer cells (Chapter III-2)
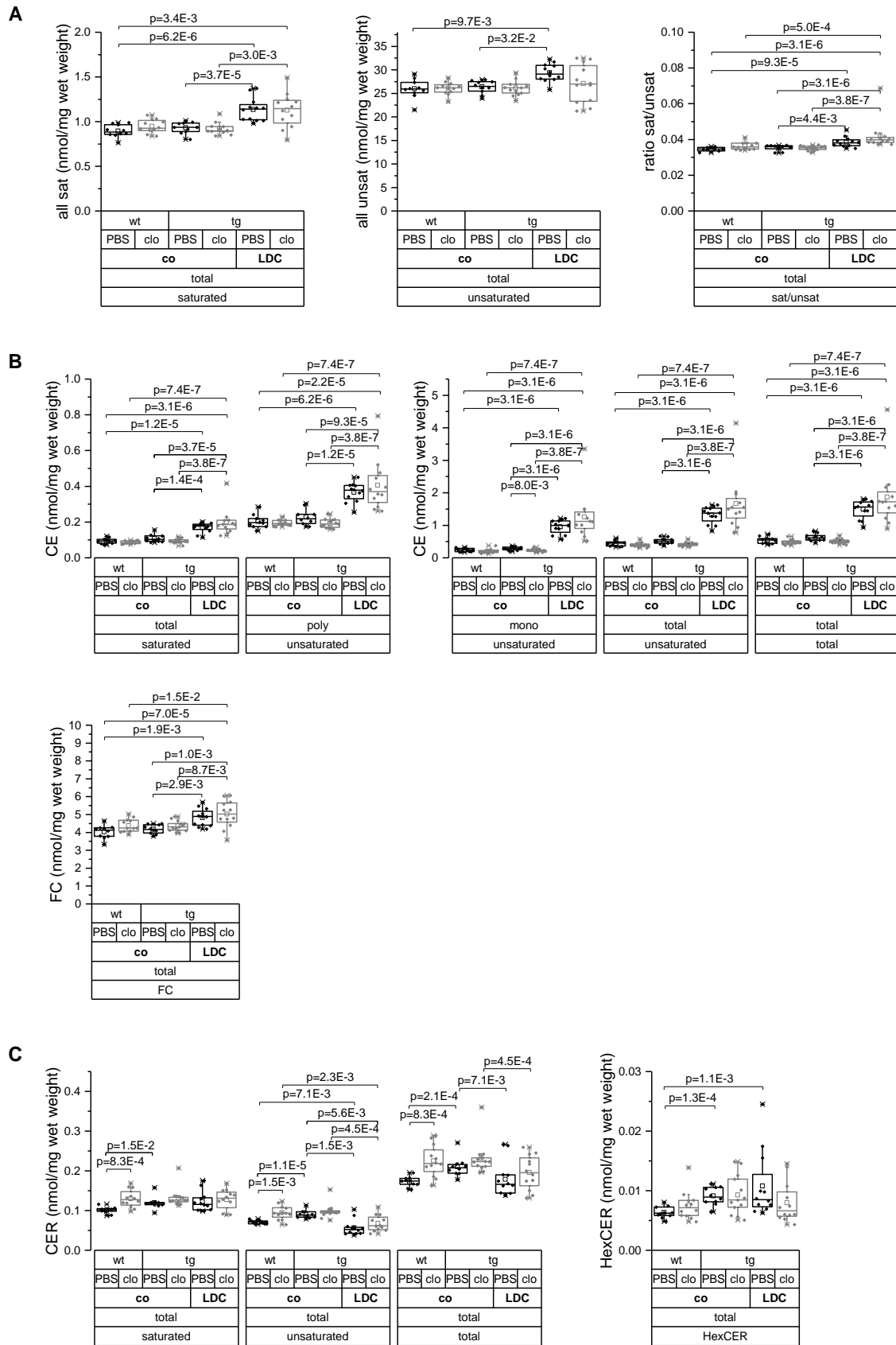
Supplemental table 7-3: *Serum levels of wildtype (wt) and p62 transgenic (tg) animals fed a normal chow (co) or a Lieber-DeCarli (LDC) diet in combination with PBS or clodronate liposome (clo) injections. Data are shown as mean ± SEM. P-values of were determined by Mann Whitney U test: **p<1.66E-3 compared to co+PBS wt; ††<1.66E-3 compared to co+PBS tg; ‡p<8.33E-3, ‡‡p<1.66E-3 compared to LDC+PBS tg.*

	wt		tg		tg	
	PBS	clo	PBS	clo	PBS	clo
	co		co		LDC	
number animals (n)	10	12	10	13	12	12
serum ALT [U/l]	49.5 ± 5.60	102 ± 20.6 **	50.0 ± 5.11	280 ± 107 ††	55.3 ± 6.69	99.6 ± 14.6 ** †† ‡
serum AST [U/l]	325 ± 42.3	555 ± 70.7	349 ± 43.8	1002 ± 228	345 ± 33.7	694 ± 72.6 ** †† ‡‡
serum cholesterol [mg/dl]	70.0 ± 4.65	77.9 ± 4.98	73.0 ± 3.51	76.5 ± 3.60	82.1 ± 4.86	86.7 ± 5.09
serum glucose [mg/dl]	381 ± 30.9	328 ± 36.2	331 ± 19.2	287 ± 10.3	343 ± 28.5	323 ± 17.3
serum triglycerides [mg/dl]	131 ± 11.9	131 ± 13.7	123 ± 12.1	130 ± 7.73	122 ± 10.3	125 ± 9.22
serum HDL [mg/dl]	60.5 ± 4.04	64.2 ± 4.76	62.5 ± 2.81	62.7 ± 2.63	77.5 ± 6.29	76.3 ± 5.68

7.5 Lipidomic analysis: wild-type and *p62* transgenic animals on control or LDC diet with or without Kupffer cells (Chapter III-2)

Supplemental table 7-4: Simplified table of significantly increased or decreased lipid classes in livers of wild-type (wt) or p62 transgenic (tg) animals fed a control or Lieber-DeCarli (LDC) diet in the absence (clo) or presence (PBS) of Kupffer cells (n=10-13). Increased levels of lipid classes are highlighted in dark grey and decreased levels in light grey color. Corresponding figures are shown in Supplemental figure 7-17 - Supplemental figure 7-20. CE: cholesteryl ester, CER: ceramide, SM: sphingomyelin, PC: phosphatidylcholine, PE: phosphatidylethanolamine, PE P: PE based plasmalogens, PS: phosphatidylserine, PG: phosphatidylglycerol, PI: phosphatidylinositol, LPC: lysophosphatidylcholine, sat: saturated species, mono: monounsaturated species, poly: polyunsaturated species, total: all species. Clo: clodronate liposomes.

|			LDC+PBS tg compared to co+PBS tg	co+PBS tg compared to co+PBS wt	co+clo tg compared to co+clo wt	co+clo tg compared to co+PBS tg	LDC+clo tg compared to co+clo tg	LDC+clo tg compared to LDC+PBS tg
Sterol lipids	**CE and FC**	sat	↑				↑	
		mono	↑			↓	↑	
		poly	↑				↑	
		unsat	↑				↑	
		total	↑				↑	
		FC	↑				↑	
Sphingo-lipids	**CER**	sat		↑				
		unsat	↓	↑			↓	
		total	↓	↑				
		HexCer		↑				
	SM	sat	↑					
		mono					↓	
		poly	↓				↓	
		unsat					↓	
		total	↑					
		dihydro					↑	
Glycero-phospho-lipids	**PC**	sat				↓		
		mono	↑				↑	
		alkyl					↓	
	PE	mono			↑			
		poly	↑					
		unsat	↑					
		total	↑					
	PE P	PE P-16:0	↓				↓	↓
		PE P-18:1	↑				↓	↓
		PE P-18:0					↓	↓
		Total					↓	↓
	PS	mono	↑				↑	
		poly					↓	↓
		unsat					↓	↓
		total					↓	↓
	PI	mono			↑			
	LPC	sat	↑				↑	
		mono	↑				↑	↑
		poly	↓				↑	↑
		unsat					↑	↑
		total					↑	↑
All		sat	↑					
		unsat	↑					
		sat/unsat	↑				↑	

Supplemental figure 7-17*: Lipidomic analysis of whole livers from wild-type (wt) or p62 transgenic (tg) animals fed a Lieber-DeCarli (LDC) or control diet (co) and treated with PBS or clodronate liposomes (clo) for 5 weeks (n=10-13). A: All saturated, unsaturated species and the saturated to unsaturated ratio. B: Cholesteryl ester (CE) and free cholesterol (FC). C: ceramide (CER) and hexosyl ceramide (HexCER). P-values were calculated by Mann Whitney U test with Bonferroni correction (significance level set at p≤8.33E-3). One-way ANOVA was used for the following species: all unsaturated; FC. Results are shown as box plots with 25th/75th percentile boxes, geometric medians (line), means (square), and 10th/90th percentile as whiskers.*

A

B
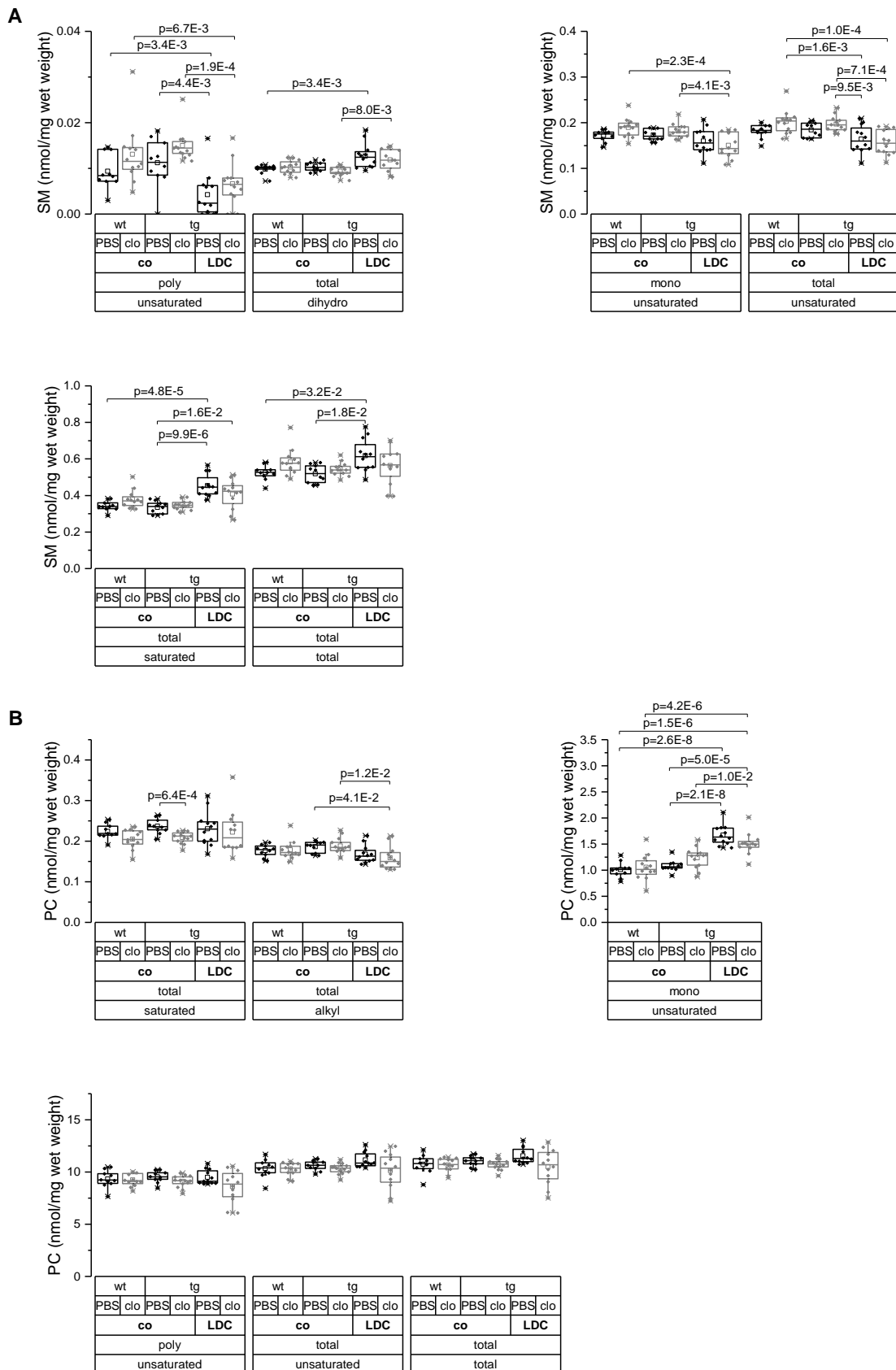
Supplemental figure 7-18: Lipidomic analysis via ESI-MS/MS of whole livers from wild-type (wt) or p62 transgenic (tg) animals fed a Lieber-DeCarli (LDC) or control diet (co) and treated with PBS or clodronate liposomes (clo) for 5 weeks (n=10-13). A: Sphingomyelin (SM) and dihydrosphingomyelin B: Phosphatidylcholine (PC). P-values were calculated by Mann Whitney U test with Bonferroni correction (significance level set at p≤8.33E-3). P-values were determined by one-way ANOVA for the following species: SM polyunsaturated, dihydrosphingomyelin; PC saturated, polyunsaturated. Results are shown as box plots with 25th/75th percentile boxes, geometric medians (line), means (square), and 10th/90th percentile as whiskers.
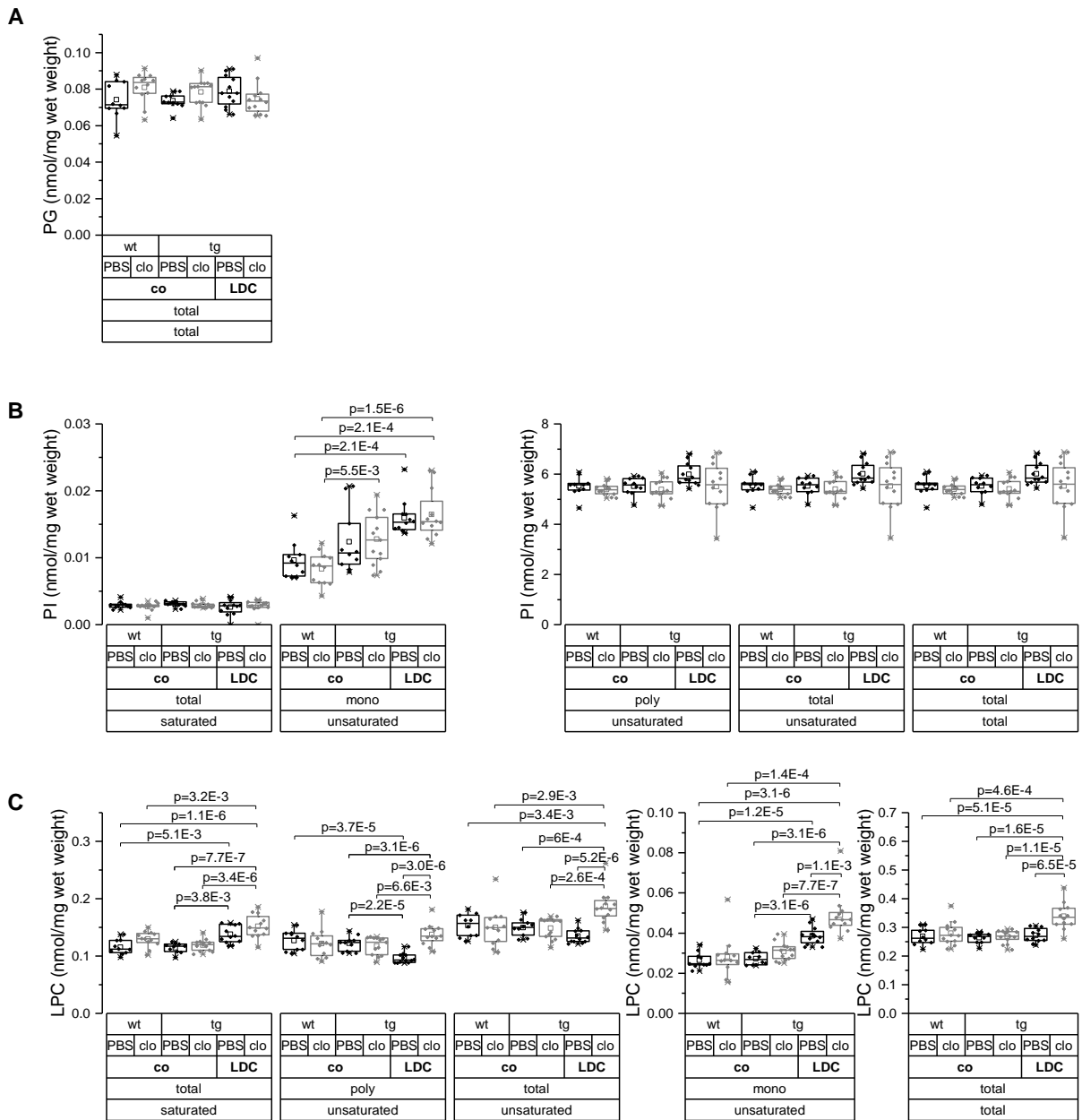
A

B

C
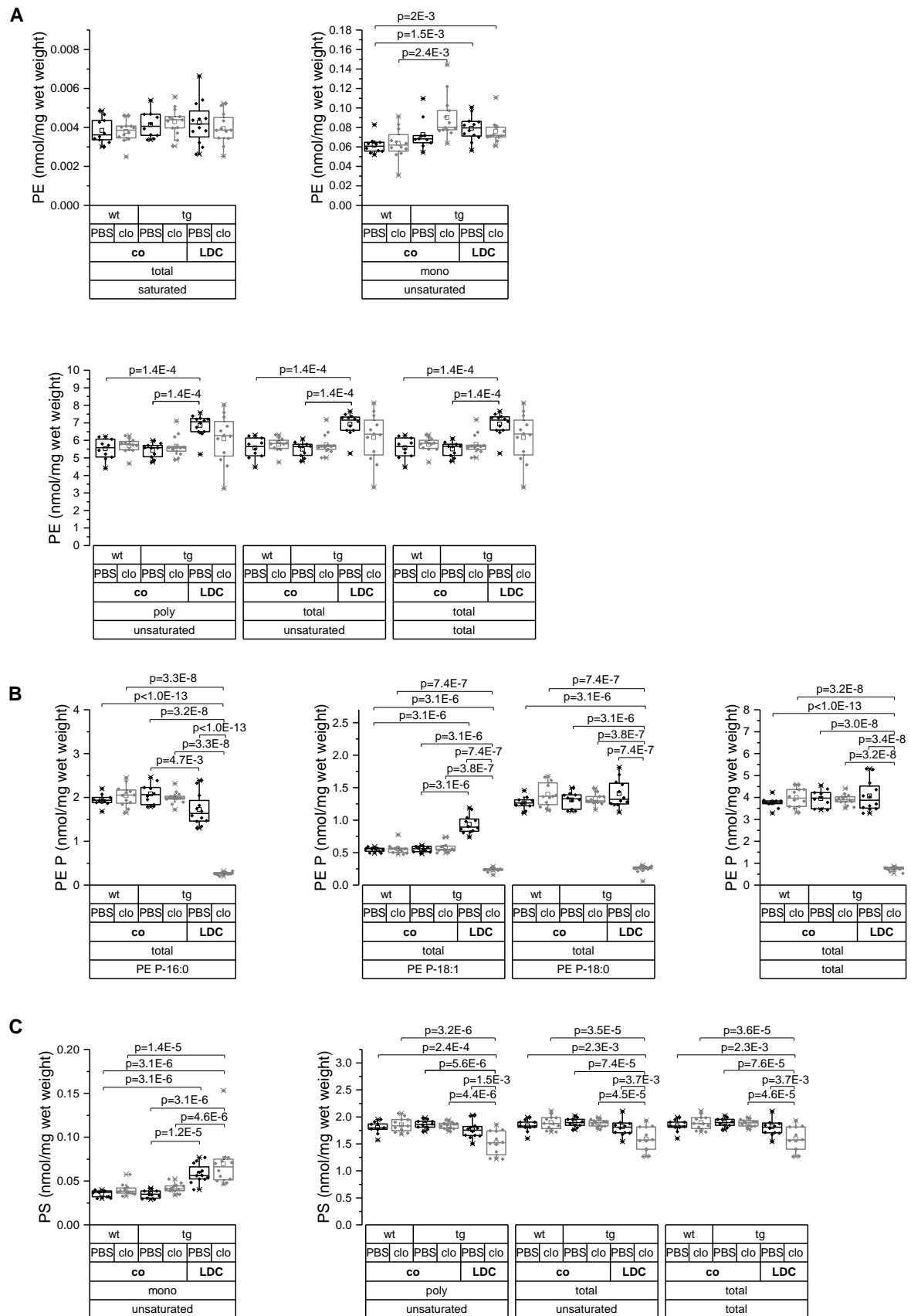
Supplemental figure 7-19: *Lipidomic analysis via ESI-MS/MS of whole livers from wild-type (wt) or p62 transgenic (tg) animals fed a Lieber-DeCarli (LDC) or control diet (co) and treated with PBS or clodronate liposomes (clo) for 5 weeks (n=10-13). A: Phosphatidylethanolamine (PE). B: PE based plasmalogens (PE P). C: Phosphatidylserine (PS). P-values were calculated by Mann Whitney U test with Bonferroni correction (significance level set at p≤8.33E-3). One-way ANOVA was used for the following species: PE saturated; PE P 16:0, and total; PS polyunsaturated, total unsaturated and total. Results are shown as box plots with 25th/75th percentile boxes, geometric medians (line), means (square), and 10th/90th percentile as whiskers.*

Supplemental figure 7-20: *Lipidomic analysis via ESI-MS/MS of whole livers from wild-type (wt) or p62 transgenic (tg) animals fed a Lieber-DeCarli (LDC) or control diet (co) and treated with PBS or clodronate liposomes (clo) for 5 weeks (n=10-13). A: Phosphatidylglycerol (PG). B: Phosphatidylinositol (PI). C: Lysophosphatidylcholine (LPC). P-values were calculated by one-way ANOVA. Or by Mann Whitney U test with Bonferroni correction (significance level set at p≤8.33E-3) for the following species: PI saturated, monounsaturated; LPC monounsaturated, polyunsaturated and total unsaturated. Results are shown as box plots with 25th/75th percentile boxes, geometric medians (line), means (square), and 10th/90th percentile as whiskers.*

7.6 Expression analysis in *H19*ko and *H19*wt mice
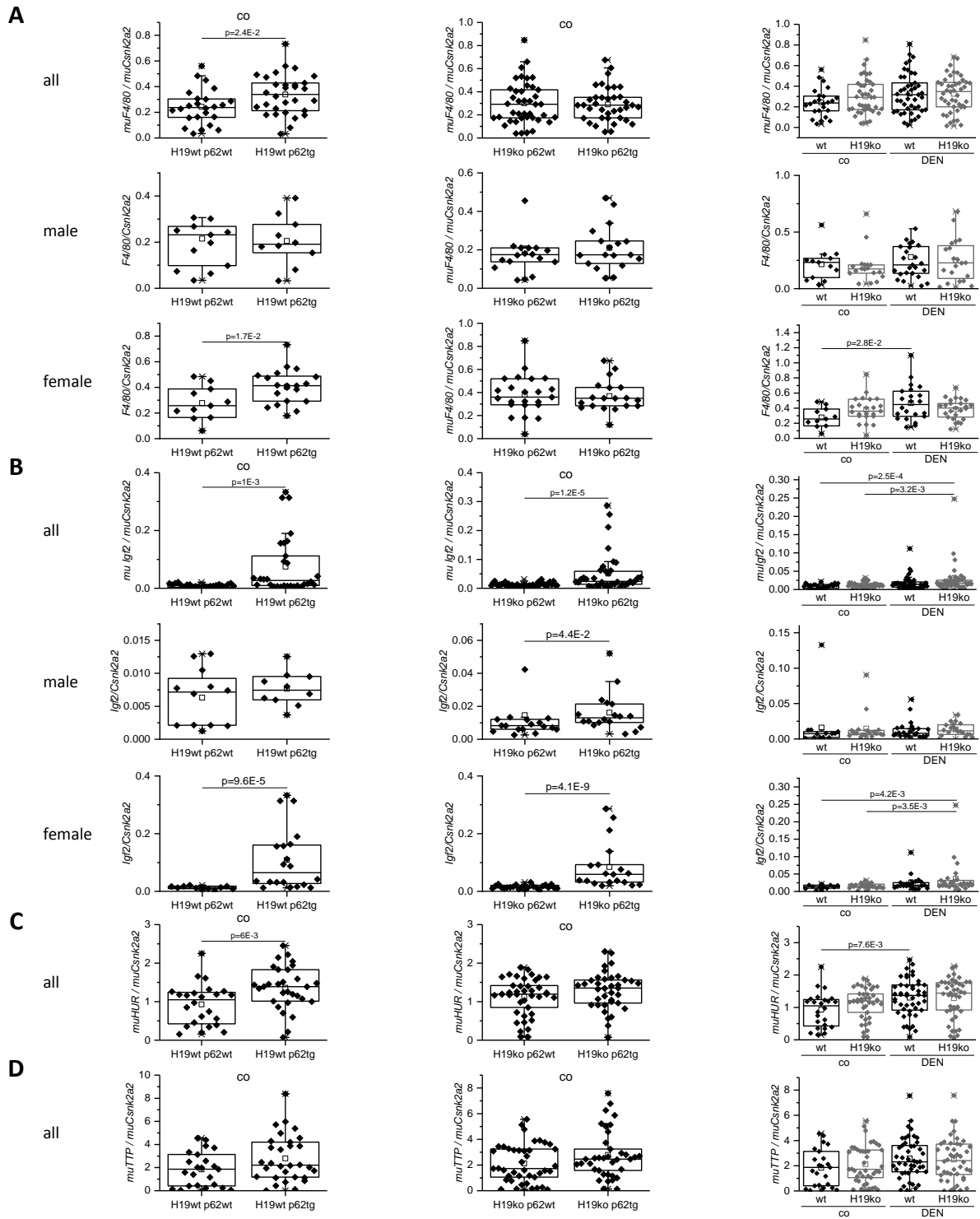
Supplemental figure 7-21: *Expression analysis of* F4/80*(A),* Igf2*(B),* HUR*(C), and* TTP*(D) in livers of female, male, and all (female + male) control (co) and DEN treated (DEN) mice, having a* H19 *knockout (*H19*ko), expressing* p62 *(*p62 *tg) or the respective wild-type (wt). Injection (i.p.) of NaCl or DEN with 5mg/kg body weight at the age of 2 weeks and sacrificed 24 weeks after injection (see Schultheiss et al., 2017). Left + middle: impact of* p62 *expression in* H19*wt and* H19*ko mice. Right:* H19*ko or* H19*wt mice in* p62*wt treated with control (co) or DEN. Data are shown as the ratio of mRNA expression of the gene of interest to the reference gene* Csnk2a2*. Results are shown as box plots with 25th/75th percentile boxes, geometric medians (line), means (square), and 10th/90th percentile as whiskers. Statistical significance was determined by t-test, one-way ANOVA or Mann-Whitney U test (with Bonferroni correction when comparing more than two groups) depending on normal distribution (all: co − H19*wt p62*wt n=24, co − H19*wt p62*tg n=30, co − H19*ko p62*wt n=41, co − H19*ko p62*tg n=37, DEN − H19*wt p62*wt n=47, DEN − H19*ko p62*wt n=45; male: co − H19*wt p62*wt n=13, co − H19*wt p62*tg n=10, co − H19*ko p62*wt n=18, co − H19*ko p62*tg n=18, DEN − H19*wt p62*wt n=25, DEN − H19*ko p62*wt n=20; female: co − H19*wt p62*wt n=11, co − H19*wt p62*tg n=20, co − H19*ko p62*wt n=23, co − H19*ko p62*tg n=19, DEN − H19*wt p62*wt n=22, DEN − H19*ko p62*wt n=25).*

8 REFERENCES

ADACHI M, and BRENNER DA Clinical Syndromes of Alcoholic Liver Disease. *Digestive diseases (Basel, Switzerland)* **2005**, *23* (3–4), 255–63.

ADACHI Y, BRADFORD BU, GAO W, BOJES HK, and THURMAN RG Inactivation of Kupffer Cells Prevents Early Alcohol-Induced Liver Injury. *Hepatology* **1994**, *20* (2), 453–460.

ALTAMIRANO J, MIQUEL R, KATOONIZADEH A, ABRALDES JG, DUARTE-ROJO A, LOUVET A, AUGUSTIN S, MOOKERJEE RP, MICHELENA J, SMYRK TC, BUOB D, LETEURTRE E, RINCÓN D, RUIZ P, GARCÍA-PAGÁN JC, GUERRERO-MARQUEZ C, JONES PD, BARRITT AS, ARROYO V, ET AL. A Histologic Scoring System for Prognosis of Patients with Alcoholic Hepatitis. *Gastroenterology* **2014**, *146* (5), 1231-9.e1–6.

ANDERSEN CL, JENSEN JL, and ØRNTOFT TF Normalization of Real-Time Quantitative Reverse Transcription-PCR Data: A Model-Based Variance Estimation Approach to Identify Genes Suited for Normalization, Applied to Bladder and Colon Cancer Data Sets. *Cancer Research* **2004**, *64* (15), 5245–5250.

ANGULO P Nonalcoholic Fatty Liver Disease. *New England Journal of Medicine* **2002**, *346* (16), 1221–1231.

ANSTEE QM, and GOLDIN RD Mouse Models in Non-Alcoholic Fatty Liver Disease and Steatohepatitis Research. *International journal of experimental pathology* **2006**, *87* (1), 1–16.

ASIMAKOPOULOU A, WEISKIRCHEN S, and WEISKIRCHEN R Lipocalin 2 (LCN2) Expression in Hepatic Malfunction and Therapy. *Frontiers in Physiology* **2016**, *7*.

BADER JE, ENOS RT, VELÁZQUEZ KT, CARSON MS, SOUGIANNIS AT, MCGUINNESS OP, ROBINSON CM, and MURPHY EA Repeated Clodronate-Liposome Treatment Results in Neutrophilia and Is Not Effective in Limiting Obesity-Linked Metabolic Impairments. *American Journal of Physiology-Endocrinology and Metabolism* **2019**, *316* (3), E358–E372.

BAJAJ JS Alcohol, Liver Disease and the Gut Microbiota. *Nature Reviews Gastroenterology & Hepatology* **2019**, *16* (4), 235–246.

BAKER SS, BAKER RD, LIU W, NOWAK NJ, and ZHU L Role of Alcohol Metabolism in Non-Alcoholic Steatohepatitis. *PLoS ONE* **2010**. Edited by C. Gluud, *5* (3), e9570.

BALA S, MARCOS M, KODYS K, CSAK T, CATALANO D, MANDREKAR P, and SZABO G Up-Regulation of microRNA-155 in Macrophages Contributes to Increased Tumor Necrosis Factor α (TNFα) Production via Increased mRNA Half-Life in Alcoholic Liver Disease. *Journal of Biological Chemistry* **2011**, *286* (2), 1436–1444.

BALA S, and SZABO G MicroRNA Signature in Alcoholic Liver Disease. *International journal of hepatology* **2012**, *2012*, 498232.

BELL JESSICA L., WÄCHTER K, MÜHLECK B, PAZAITIS N, KÖHN M, LEDERER M, and HÜTTELMAIER S Insulin-like Growth Factor 2 mRNA-Binding Proteins (IGF2BPs): Post-Transcriptional Drivers of Cancer Progression? *Cellular and Molecular Life Sciences* **2013**, *70* (15), 2657–2675.

BENJAMINI Y, and HOCHBERG Y Controlling the False Discovery Rate: A Practical and Powerful Approach to Multiple Testing. *Journal of the Royal Statistical Society. Series B (Methodological)* **1995**, 289–300.

BERREBI D, BRUSCOLI S, COHEN N, FOUSSAT A, MIGLIORATI G, BOUCHET-DELBOS L, MAILLOT M-C, PORTIER A, COUDERC J, GALANAUD P, PEUCHMAUR M, RICCARDI C, and EMILIE D Synthesis of Glucocorticoid-Induced Leucine Zipper (GILZ) by Macrophages: An Anti-Inflammatory and Immunosuppressive Mechanism Shared by Glucocorticoids and IL-10. *Blood* **2003**, *101* (2), 729–738.

BERRY KAZ, and MURPHY RC Electrospray Ionization Tandem Mass Spectrometry of Glycerophosphoethanolamine Plasmalogen Phospholipids. *Journal of the American Society for Mass Spectrometry* **2004**, *15* (10), 1499–1508.

Bertola A, Mathews S, Ki SH, Wang H, and Gao B Mouse Model of Chronic and Binge Ethanol Feeding (the NIAAA Model). *Nature Protocols* **2013**, *8* (3), 627–637.

Bertola A Rodent Models of Fatty Liver Diseases. *Liver Research* **2018**, *2* (1), 3–13.

Bertola A, Park O, and Gao B Chronic plus Binge Ethanol Feeding Synergistically Induces Neutrophil Infiltration and Liver Injury in Mice: A Critical Role for E-Selectin. *Hepatology* **2013**, *58* (5), 1814–1823.

Bhagwandeen BS, Apte M, Manwarring L, and Dickeson J Endotoxin Induced Hepatic Necrosis in Rats on an Alcohol Diet. *The Journal of Pathology* **1987**, *152* (1), 47–53.

Biewenga J, van der Ende MB, Krist LFG, Borst A, Ghufron M, and van Rooijen N Macrophage Depletion in the Rat after Intraperitoneal Administration of Liposome-Encapsulated Clodronate: Depletion Kinetics and Accelerated Repopulation of Peritoneal and Omental Macrophages by Administration of Freund's Adjuvant. *Cell and Tissue Research* **1995**, *280* (1), 189–196.

Binder M, Liebisch G, Langmann T, and Schmitz G Metabolic Profiling of Glycerophospholipid Synthesis in Fibroblasts Loaded with Free Cholesterol and Modified Low Density Lipoproteins. *The Journal of biological chemistry* **2006**, *281* (31), 21869–77.

Blizard DA Sweet and Bitter Taste of Ethanol in C57BL/6J and DBA2/J Mouse Strains. *Behavior Genetics* **2007**, *37* (1), 146–159.

Borkham-Kamphorst E, van de Leur E, Zimmermann HW, Karlmark KR, Tihaa L, Haas U, Tacke F, Berger T, Mak TW, and Weiskirchen R Protective Effects of Lipocalin-2 (LCN2) in Acute Liver Injury Suggest a Novel Function in Liver Homeostasis. *Biochimica et Biophysica Acta (BBA) - Molecular Basis of Disease* **2013**, *1832* (5), 660–673.

Bradbury MW, and Berk PD Lipid Metabolism in Hepatic Steatosis. *Clinics in Liver Disease* **2004**, *8* (3), 639–671.

Brandon-Warner E, Walling TL, Schrum LW, and McKillop IH Chronic Ethanol Feeding Accelerates Hepatocellular Carcinoma Progression in a Sex-Dependent Manner in a Mouse Model of Hepatocarcinogenesis. *Alcoholism, clinical and experimental research* **2012**, *36* (4), 641–53.

Brandon-Warner E, Schrum LW, Schmidt CM, and McKillop IH Rodent Models of Alcoholic Liver Disease: Of Mice and Men. *Alcohol (Fayetteville, N.Y.)* **2012**, *46* (8), 715–25.

Bu L, Gao M, Qu S, and Liu D Intraperitoneal Injection of Clodronate Liposomes Eliminates Visceral Adipose Macrophages and Blocks High-Fat Diet-Induced Weight Gain and Development of Insulin Resistance. *The AAPS Journal* **2013**, *15* (4), 1001–1011.

Burcelin R, Crivelli V, Dacosta A, Roy-Tirelli A, and Thorens B Heterogeneous Metabolic Adaptation of C57BL/6J Mice to High-Fat Diet. *American Journal of Physiology-Endocrinology and Metabolism* **2002**, *282* (4), E834–E842.

Bykov I, Junnikkala S, Pekna M, Lindros KO, and Meri S Complement C3 Contributes to Ethanol-induced Liver Steatosis in Mice. *Annals of Medicine* **2006**, *38* (4), 280–286.

Byrne CD, and Targher G NAFLD: A Multisystem Disease. *Journal of hepatology* **2015**, *62* (1 Suppl), S47-64.

Byun J-S, Suh Y-G, Yi H-S, Lee Y-S, and Jeong W-I Activation of Toll-like Receptor 3 Attenuates Alcoholic Liver Injury by Stimulating Kupffer Cells and Stellate Cells to Produce Interleukin-10 in Mice. *Journal of Hepatology* **2013**, *58* (2), 342–349.

Caballero F, Fernández A, De Lacy AM, Fernández-Checa JC, Caballería J, and García-Ruiz C Enhanced Free Cholesterol, SREBP-2 and StAR Expression in Human NASH. *Journal of Hepatology* **2009**, *50* (4), 789–796.

Cai Y, Jogasuria A, Yin H, Xu M-J, Hu X, Wang J, Kim C, Wu J, Lee K, Gao B, and You M The Detrimental Role Played by Lipocalin-2 in Alcoholic Fatty Liver in Mice. *The American journal of pathology* **2016**, *186* (9), 2417–28.

Cao J, Mu Q, and Huang H The Roles of Insulin-Like Growth Factor 2 MRNA-Binding Protein 2 in Cancer and Cancer Stem Cells. *Stem Cells International* **2018**, *2018*, 1–15.

Carballo E, Lai WS, and Blackshear PJ Feedback Inhibition of Macrophage Tumor Necrosis Factor-Alpha Production by Tristetraprolin. *Science (New York, N.Y.)* **1998**, *281* (5379), 1001–5.

Chalasani N, Younossi Z, Lavine JE, Charlton M, Cusi K, Rinella M, Harrison SA, Brunt EM, and Sanyal AJ The Diagnosis and Management of Nonalcoholic Fatty Liver Disease: Practice Guidance from the American Association for the Study of Liver Diseases. *Hepatology* **2018**, *67* (1), 328–357.

Chang B, Xu M-J, Zhou Z, Cai Y, Li M, Wang W, Feng D, Bertola A, Wang H, Kunos G, and Gao B Short- or Long-Term High-Fat Diet Feeding plus Acute Ethanol Binge Synergistically Induce Acute Liver Injury in Mice: An Important Role for CXCL1. *Hepatology (Baltimore, Md.)* **2015**, *62* (4), 1070–85.

Charkoftaki G, Wang Y, McAndrews M, Bruford EA, Thompson DC, Vasiliou V, and Nebert DW Update on the Human and Mouse Lipocalin (LCN) Gene Family, Including Evidence the Mouse Mup Cluster Is Result of an

"Evolutionary Bloom". *Human genomics* **2019**, *13* (1), 11.

CHEN P, MIYAMOTO Y, MAZAGOVA M, LEE K-C, ECKMANN L, and SCHNABL B Microbiota Protects Mice Against Acute Alcohol-Induced Liver Injury. *Alcoholism, clinical and experimental research* **2015**, *39* (12), 2313–23.

CHEN Y, GULDIKEN N, SPURNY M, MOHAMMED HH, HAYBAECK J, POLLHEIMER MJ, FICKERT P, GASSLER N, JEON MK, TRAUTWEIN C, and STRNAD P Loss of Keratin 19 Favours the Development of Cholestatic Liver Disease through Decreased Ductular Reaction. *The Journal of Pathology* **2015**, *237* (3), 343–354.

CHENG Y-S, ZHENG Y, and VANDERGHEYNST JS Rapid Quantitative Analysis of Lipids Using a Colorimetric Method in a Microplate Format. *Lipids* **2011**, *46* (1), 95–103.

CHRISTIANSEN J, KOLTE AM, HANSEN TVO, and NIELSEN FC IGF2 mRNA-Binding Protein 2: Biological Function and Putative Role in Type 2 Diabetes. *Journal of Molecular Endocrinology* **2009**, *43* (5), 187–195.

CLAASSEN I, VAN ROOIJEN N, and CLAASSEN E A New Method for Removal of Mononuclear Phagocytes from Heterogeneous Cell Populations in Vitro, Using the Liposome-Mediated Macrophage 'Suicide' Technique. *Journal of Immunological Methods* **1990**, *134* (2), 153–161.

CLEMENTI AH, GAUDY AM, VAN ROOIJEN N, PIERCE RH, and MOONEY RA Loss of Kupffer Cells in Diet-Induced Obesity Is Associated with Increased Hepatic Steatosis, STAT3 Signaling, and Further Decreases in Insulin Signaling. *Biochimica et Biophysica Acta (BBA) - Molecular Basis of Disease* **2009**, *1792* (11), 1062–1072.

CLUGSTON RD, JIANG H, LEE MX, PIANTEDOSI R, YUEN JJ, RAMAKRISHNAN R, LEWIS MJ, GOTTESMAN ME, HUANG L-S, GOLDBERG IJ, BERK PD, and BLANER WS Altered Hepatic Lipid Metabolism in C57BL/6 Mice Fed Alcohol: A Targeted Lipidomic and Gene Expression Study. *Journal of lipid research* **2011**, *52* (11), 2021–31.

COHEN JI, ROYCHOWDHURY S, MCMULLEN MR, STAVITSKY AB, and NAGY LE Complement and Alcoholic Liver Disease: Role of C1q in the Pathogenesis of Ethanol-Induced Liver Injury in Mice. *Gastroenterology* **2010**, *139* (2), 664–74, 674.e1.

COOK RT, SCHLUETER AJ, COLEMAN RA, TYGRETT L, BALLAS ZK, JERRELLS TR, NASHELSKY MB, RAY NB, HAUGEN TH, and WALDSCHMIDT TJ Thymocytes, Pre-B Cells, and Organ Changes in a Mouse Model of Chronic Ethanol Ingestion-Absence of Subset-Specific Glucocorticoid-Induced Immune Cell Loss. *Alcoholism, clinical and experimental research* **2007**, *31* (10), 1746–58.

COOMBES JD, SWIDERSKA-SYN M, DOLLÉ L, REID D, EKSTEEN B, CLARIDGE L, BRIONES-ORTA MA, SHETTY S, OO YH, RIVA A, CHOKSHI S, PAPA S, MI Z, KUO PC, WILLIAMS R, CANBAY A, ADAMS DH, DIEHL AM, VAN GRUNSVEN LA, ET AL. Osteopontin Neutralisation Abrogates the Liver Progenitor Cell Response and Fibrogenesis in Mice. *Gut* **2015**, *64* (7), 1120–31.

COPE K, RISBY T, and DIEHL AM Increased Gastrointestinal Ethanol Production in Obese Mice: Implications for Fatty Liver Disease Pathogenesis. *Gastroenterology* **2000**, *119* (5), 1340–1347.

CORTEZ-PINTO H, JESUS L, BARROS H, LOPES C, MOURA MC, and CAMILO ME How Different Is the Dietary Pattern in Non-Alcoholic Steatohepatitis Patients? *Clinical Nutrition* **2006**, *25* (5), 816–823.

D'SOUZA EL-GUINDY NB, KOVACS EJ, DE WITTE P, SPIES C, LITTLETON JM, DE VILLIERS WJS, LOTT AJ, PLACKETT TP, LANZKE N, and MEADOWS GG Laboratory Models Available to Study Alcohol-Induced Organ Damage and Immune Variations: Choosing the Appropriate Model. *Alcoholism: Clinical and Experimental Research* **2010**, *34* (9), 1489–1511.

DAI N, RAPLEY J, ANGEL M, YANIK MF, BLOWER MD, and AVRUCH J MTOR Phosphorylates IMP2 to Promote IGF2 mRNA Translation by Internal Ribosomal Entry. *Genes & Development* **2011**, *25* (11), 1159–1172.

DAI N, ZHAO L, WRIGHTING D, KRÄMER D, MAJITHIA A, WANG Y, CRACAN V, BORGES-RIVERA D, MOOTHA VK, NAHRENDORF M, THORBURN DR, MINICHIELLO L, ALTSHULER D, and AVRUCH J IGF2BP2/IMP2-Deficient Mice Resist Obesity through Enhanced Translation of Ucp1 mRNA and Other mRNAs Encoding Mitochondrial Proteins. *Cell Metabolism* **2015**, *21* (4), 609–621.

DANNENBERG LO, CHEN H-J, TIAN H, and EDENBERG HJ Differential Regulation of the Alcohol Dehydrogenase 1B (ADH1B) and ADH1C Genes by DNA Methylation and Histone Deacetylation. *Alcoholism: Clinical and Experimental Research* **2006**, *30* (6), 928–937.

DAY CP Pathogenesis of Steatohepatitis. *Best Practice & Research Clinical Gastroenterology* **2002**, *16* (5), 663–678.

DAY CP Genes or Environment to Determine Alcoholic Liver Disease and Non-Alcoholic Fatty Liver Disease. *Liver International* **2006**, *26* (9), 1021–1028.

DAY CP, and JAMES OFW Steatohepatitis: A Tale of Two "Hits"? *Gastroenterology* **1998**, *114* (4), 842–845.

DECARLI LM, and LIEBER CS Fatty Liver in the Rat after Prolonged Intake of Ethanol with a Nutritionally Adequate New Liquid Diet. *The Journal of Nutrition* **1967**, *91* (3_suppl), 331–336.

DHAHBI JM, KIM H-J, MOTE PL, BEAVER RJ, and SPINDLER SR Temporal Linkage between the Phenotypic and Genomic Responses to Caloric Restriction. *Proceedings of the National Academy of Sciences of the United States of America* **2004**, *101* (15), 5524–9.

DIEHL AM, POTTER J, BOITNOTT J, DUYN MA VAN, HERLONG HF, and MEZEY E Relationship Between Pyridoxal 5'-Phosphate Deficiency and Aminotransferase Levels in Alcoholic Hepatitis. *Gastroenterology* **1984**, *86* (4), 632–636.

DING JL, and HO B A New Era in Pyrogen Testing. *Trends in Biotechnology* **2001**, *19* (8), 277–281.

DIXON LJ, BARNES M, TANG H, PRITCHARD MT, and NAGY LE Kupffer Cells in the Liver. *Comprehensive Physiology* **2013**, *3* (2), 785–97.

VAN DONGEN J, NIVARD MG, WILLEMSEN G, HOTTENGA J-J, HELMER Q, DOLAN C V., EHLI EA, DAVIES GE, VAN ITERSON M, BREEZE CE, BECK S, HOEN PAC'., POOL R, VAN GREEVENBROEK MMJ, STEHOUWER CDA, KALLEN CJH VAN DER, SCHALKWIJK CG, WIJMENGA C, ZHERNAKOVA S, ET AL. Genetic and Environmental Influences Interact with Age and Sex in Shaping the Human Methylome. *Nature Communications* **2016**, *7*, 11115.

DUVAL C, THISSEN U, KESHTKAR S, ACCART B, STIENSTRA R, BOEKSCHOTEN M V, ROSKAMS T, KERSTEN S, and MÜLLER M Adipose Tissue Dysfunction Signals Progression of Hepatic Steatosis towards Nonalcoholic Steatohepatitis in C57BL/6 Mice. *Diabetes* **2010**, *59* (12), 3181–91.

EAGON PK Alcoholic Liver Injury: Influence of Gender and Hormones. *World journal of gastroenterology* **2010**, *16* (11), 1377–84.

EBE Y, HASEGAWA G, TAKATSUKA H, UMEZU H, MITSUYAMA M, ARAKAWA M, MUKAIDA N, and NAITO M The Role of Kupffer Cells and Regulation of Neutrophil Migration into the Liver by Macrophage Inflammatory Protein-2 in Primary Listeriosis in Mice. *Pathology International* **1999**, *49* (6), 519–532.

EDWARDS JR, O'DONNELL AH, ROLLINS RA, PECKHAM HE, LEE C, MILEKIC MH, CHANRION B, FU Y, SU T, HIBSHOOSH H, GINGRICH JA, HAGHIGHI F, NUTTER R, and BESTOR TH Chromatin and Sequence Features That Define the Fine and Gross Structure of Genomic Methylation Patterns. *Genome research* **2010**, *20* (7), 972–80.

ELLACOTT KLJ, MORTON GJ, WOODS SC, TSO P, and SCHWARTZ MW Assessment of Feeding Behavior in Laboratory Mice. *Cell metabolism* **2010**, *12* (1), 10–7.

ESLAM M, and GEORGE J Genetic and Epigenetic Mechanisms of NASH. *Hepatology International* **2016**, *10* (3), 394–406.

ESLAM M, VALENTI L, and ROMEO S Genetics and Epigenetics of NAFLD and NASH: Clinical Impact. *Journal of hepatology* **2018**, *68* (2), 268–279.

ESPAÑOL–SUÑER R, CARPENTIER R, VAN HUL N, LEGRY V, ACHOURI Y, CORDI S, JACQUEMIN P, LEMAIGRE F, and LECLERCQ IA Liver Progenitor Cells Yield Functional Hepatocytes in Response to Chronic Liver Injury in Mice. *Gastroenterology* **2012**, *143* (6), 1564-1575.e7.

EUROPEAN ASSOCIATION FOR THE STUDY OF THE LIVER EASL Clinical Practical Guidelines: Management of Alcoholic Liver Disease. *Journal of Hepatology* **2012**, *57* (2), 399–420.

EUROPEAN ASSOCIATION FOR THE STUDY OF THE LIVER (EASL), EUROPEAN ASSOCIATION FOR THE STUDY OF DIABETE (EASD), and EUROPEAN ASSOCIATION FOR THE STUDY OF OBESITY (EASO) EASL–EASD–EASO Clinical Practice Guidelines for the Management of Non-Alcoholic Fatty Liver Disease. *Journal of Hepatology* **2016**, *64* (6), 1388–1402.

FARHADI A, GUNDLAPALLI S, SHAIKH M, FRANTZIDES C, HARRELL L, KWASNY MM, and KESHAVARZIAN A Susceptibility to Gut Leakiness: A Possible Mechanism for Endotoxaemia in Non-Alcoholic Steatohepatitis. *Liver international : official journal of the International Association for the Study of the Liver* **2008**, *28* (7), 1026–33.

FARINA KL, HUTTELMAIER S, MUSUNURU K, DARNELL R, and SINGER RH Two ZBP1 KH Domains Facilitate Beta-Actin mRNA Localization, Granule Formation, and Cytoskeletal Attachment. *The Journal of cell biology* **2003**, *160* (1), 77–87.

FENG B, JIAO P, NIE Y, KIM T, JUN D, ROOIJEN N VAN, YANG Z, and XU H Clodronate Liposomes Improve Metabolic Profile and Reduce Visceral Adipose Macrophage Content in Diet-Induced Obese Mice. *PLoS ONE* **2011**, *6* (9).

FENGLER VERA HI, MACHEINER T, KESSLER SM, CZEPUKOJC B, GEMPERLEIN K, MÜLLER R, KIEMER AK, MAGNES C, HAYBAECK J, LACKNER C, and SARGSYAN K Susceptibility of Different Mouse Wild Type Strains to Develop Diet-Induced NAFLD/AFLD-Associated Liver Disease. *PLoS ONE* **2016**, *11* (5), e0155163.

FERRAMOSCA A, and ZARA V Modulation of Hepatic Steatosis by Dietary Fatty Acids. *World journal of gastroenterology* **2014**, *20* (7), 1746–55.

Ferreira DMS, Simão AL, Rodrigues CMP, and Castro RE Revisiting the Metabolic Syndrome and Paving the Way for microRNAs in Non-Alcoholic Fatty Liver Disease. *FEBS Journal* **2014**, *281* (11), 2503–2524.

Ferrere G, Wrzosek L, Cailleux F, Turpin W, Puchois V, Spatz M, Ciocan D, Rainteau D, Humbert L, Hugot C, Gaudin F, Noordine M-L, Robert V, Berrebi D, Thomas M, Naveau S, Perlemuter G, and Cassard A-M Fecal Microbiota Manipulation Prevents Dysbiosis and Alcohol-Induced Liver Injury in Mice. *Journal of Hepatology* **2017**, *66* (4), 806–815.

Fracanzani AL, Valenti L, Bugianesi E, Andreoletti M, Colli A, Vanni E, Bertelli C, Fatta E, Bignamini D, Marchesini G, and Fargion S Risk of Severe Liver Disease in Nonalcoholic Fatty Liver Disease with Normal Aminotransferase Levels: A Role for Insulin Resistance and Diabetes. *Hepatology* **2008**, *48* (3), 792–798.

Frezza M, di Padova C, Pozzato G, Terpin M, Baraona E, and Lieber CS High Blood Alcohol Levels in Women. *New England Journal of Medicine* **1990**, *322* (2), 95–99.

Furuyama K, Kawaguchi Y, Akiyama H, Horiguchi M, Kodama S, Kuhara T, Hosokawa S, Elbahrawy A, Soeda T, Koizumi M, Masui T, Kawaguchi M, Takaori K, Doi R, Nishi E, Kakinoki R, Deng JM, Behringer RR, Nakamura T, et al. Continuous Cell Supply from a Sox9-Expressing Progenitor Zone in Adult Liver, Exocrine Pancreas and Intestine. *Nature Genetics* **2011**, *43* (1), 34–41.

Gadd VL, Skoien R, Powell EE, Fagan KJ, Winterford C, Horsfall L, Irvine K, and Clouston AD The Portal Inflammatory Infiltrate and Ductular Reaction in Human Nonalcoholic Fatty Liver Disease. *Hepatology* **2014**, *59* (4), 1393–1405.

Gao B, Jeong W-I, and Tian Z Liver: An Organ with Predominant Innate Immunity. *Hepatology* **2007**, *47* (2), 729–736.

Gao B, and Tsukamoto H Inflammation in Alcoholic and Nonalcoholic Fatty Liver Disease: Friend or Foe? *Gastroenterology* **2016**, *150* (8), 1704–1709.

Giller K, Huebbe P, Doering F, Pallauf K, and Rimbach G Major Urinary Protein 5, a Scent Communication Protein, Is Regulated by Dietary Restriction and Subsequent Re-Feeding in Mice. *Proceedings of the Royal Society B: Biological Sciences* **2013**, *280* (1757).

Gnauck A, Lentle RG, and Kruger MC The Limulus Amebocyte Lysate Assay May Be Unsuitable for Detecting Endotoxin in Blood of Healthy Female Subjects. *Journal of Immunological Methods* **2015**, *416*, 146–156.

Godoy P, Hewitt NJ, Albrecht U, Andersen ME, Ansari N, Bhattacharya S, Bode JG, Bolleyn J, Borner C, Böttger J, Braeuning A, Budinsky RA, Burkhardt B, Cameron NR, Camussi G, Cho C-S, Choi Y-J, Craig Rowlands J, Dahmen U, et al. Recent Advances in 2D and 3D in Vitro Systems Using Primary Hepatocytes, Alternative Hepatocyte Sources and Non-Parenchymal Liver Cells and Their Use in Investigating Mechanisms of Hepatotoxicity, Cell Signaling and ADME. *Archives of toxicology* **2013**, *87* (8), 1315–530.

Gorden DL, Ivanova PT, Myers DS, McIntyre JO, VanSaun MN, Wright JK, Matrisian LM, and Brown HA Increased Diacylglycerols Characterize Hepatic Lipid Changes in Progression of Human Nonalcoholic Fatty Liver Disease; Comparison to a Murine Model. *PLoS ONE* **2011**. Edited by J. F. Turrens, *6* (8), e22775.

Gordy C, Pua H, Sempowski GD, and He Y-W Regulation of Steady-State Neutrophil Homeostasis by Macrophages. *Blood* **2011**, *117* (2), 618–29.

Gouw ASH, Clouston AD, and Theise ND Ductular Reactions in Human Liver: Diversity at the Interface. *Hepatology* **2011**, *54* (5), 1853–1863.

Gramenzi A, Caputo F, Biselli M, Kuria F, Loggi E, Andreone P, and Bernardi M Review Article: Alcoholic Liver Disease -Pathophysiological Aspects and Risk Factors. *Alimentary Pharmacology and Therapeutics* **2006**, *24* (8), 1151–1161.

Hahn RT, Hoppstädter J, Hirschfelder K, Hachenthal N, Diesel B, Kessler SM, Huwer H, and Kiemer AK Downregulation of the Glucocorticoid-Induced Leucine Zipper (GILZ) Promotes Vascular Inflammation. *Atherosclerosis* **2014**, *234* (2), 391–400.

Hamdi H, Bigorgne A, Naveau S, Balian A, Bouchet-Delbos L, Cassard-Doulcier A-M, Maillot M-C, Durand-Gasselin I, Prévot S, Delaveaucoupet J, Emilie D, and Perlemuter G Glucocorticoid-Induced Leucine Zipper: A Key Protein in the Sensitization of Monocytes to Lipopolysaccharide in Alcoholic Hepatitis. *Hepatology* **2007**, *46* (6), 1986–1992.

Hammer NA, Hansen T vO, Byskov AG, Rajpert-De Meyts E, Grøndahl ML, Bredkjær HE, Wewer UM, Christiansen J, and Nielsen FC Expression of IGF-II mRNA-Binding Proteins (IMPs) in Gonads and Testicular Cancer. *Reproduction* **2005**, *130* (2), 203–212.

REFERENCES

HAN MS, PARK SY, SHINZAWA K, KIM S, CHUNG KW, LEE JI-HYUN, KWON CH, LEE K-W, LEE JOON-HYOEK, PARK CK, CHUNG WJ, HWANG JS, YAN J-J, SONG D-K, TSUJIMOTO Y, and LEE M-S Lysophosphatidylcholine as a Death Effector in the Lipoapoptosis of Hepatocytes. *Journal of lipid research* **2008**, *49* (1), 84–97.

HANNUN YA, and OBEID LM Principles of Bioactive Lipid Signalling: Lessons from Sphingolipids. *Nature Reviews Molecular Cell Biology* **2008**, *9* (2), 139–150.

HARA A, and RADIN NS Lipid Extraction of Tissues with a Low-Toxicity Solvent. *Analytical Biochemistry* **1978**, *90* (1), 420–426.

HARTE AL, DA SILVA NF, CREELY SJ, MCGEE KC, BILLYARD T, YOUSSEF-ELABD EM, TRIPATHI G, ASHOUR E, ABDALLA MS, SHARADA HM, AMIN AI, BURT AD, KUMAR S, DAY CP, MCTERNAN PG, DAY C, BELLENTANI S, SACCOCCIO G, MASUTTI F, ET AL. Elevated Endotoxin Levels in Non-Alcoholic Fatty Liver Disease. *Journal of Inflammation* **2010**, *7* (1), 15.

HARTMANN P, CHU H, DUAN Y, and SCHNABL B Gut Microbiota in Liver Disease: *Too Much Is Harmful, Nothing at All Is Not Helpful Either*. *American Journal of Physiology-Gastrointestinal and Liver Physiology* **2019**, ajpgi.00370.2018.

HIRSOVA P, IBRAHIM SH, GORES GJ, and MALHI H Lipotoxic Lethal and Sublethal Stress Signaling in Hepatocytes: Relevance to NASH Pathogenesis. *Journal of lipid research* **2016**, *57* (10), 1758–1770.

HOPPSTÄDTER J, and KIEMER AK Glucocorticoid-Induced Leucine Zipper (GILZ) in Immuno Suppression: Master Regulator or Bystander? *Oncotarget* **2015**, *6* (36), 38446–57.

HRITZ I, MANDREKAR P, VELAYUDHAM A, CATALANO D, DOLGANIUC A, KODYS K, KURT-JONES E, and SZABO G The Critical Role of Toll-like Receptor (TLR) 4 in Alcoholic Liver Disease Is Independent of the Common TLR Adapter MyD88. *Hepatology* **2008**, *48* (4), 1224–1231.

HUANG W, METLAKUNTA A, DEDOUSIS N, ZHANG P, SIPULA I, DUBE JJ, SCOTT DK, and O'DOHERTY RM Depletion of Liver Kupffer Cells Prevents the Development of Diet-Induced Hepatic Steatosis and Insulin Resistance. *Diabetes* **2010**, *59* (2), 347–57.

HUANG ZY, STABLER T, PEI FX, and KRAUS VB Both Systemic and Local Lipopolysaccharide (LPS) Burden Are Associated with Knee OA Severity and Inflammation. *Osteoarthritis and cartilage* **2016**, *24* (10), 1769–1775.

HUI X, ZHU W, WANG Y, LAM KSL, ZHANG J, WU D, KRAEGEN EW, LI Y, and XU A Major Urinary Protein-1 Increases Energy Expenditure and Improves Glucose Intolerance through Enhancing Mitochondrial Function in Skeletal Muscle of Diabetic Mice. *The Journal of biological chemistry* **2009**, *284* (21), 14050–7.

VAN HUL NKM, ABARCA-QUINONES J, SEMPOUX C, HORSMANS Y, and LECLERCQ IA Relation between Liver Progenitor Cell Expansion and Extracellular Matrix Deposition in a CDE-Induced Murine Model of Chronic Liver Injury. *Hepatology* **2009**, *49* (5), 1625–1635.

HUWILER A, JOHANSEN B, SKARSTAD A, and PFEILSCHIFTER J Ceramide Binds to the CaLB Domain of Cytosolic Phospholipase A 2 and Facilitates Its Membrane Docking and Arachidonic Acid Release. *The FASEB Journal* **2001**, *15* (1), 7–9.

HUYPENS P, SASS S, WU M, DYCKHOFF D, TSCHÖP M, THEIS F, MARSCHALL S, DE ANGELIS MH, and BECKERS J Epigenetic Germline Inheritance of Diet-Induced Obesity and Insulin Resistance. *Nature Genetics* **2016**, *48* (5), 497–499.

IOANNOU GN The Role of Cholesterol in the Pathogenesis of NASH. *Trends in Endocrinology & Metabolism* **2016**, *27* (2), 84–95.

JAGAVELU K, ROUTRAY C, SHERGILL U, O'HARA SP, FAUBION W, and SHAH VH Endothelial Cell Toll-like Receptor 4 Regulates Fibrosis-Associated Angiogenesis in the Liver. *Hepatology (Baltimore, Md.)* **2010**, *52* (2), 590–601.

JANISZEWSKA M, SUVÀ ML, RIGGI N, HOUTKOOPER RH, AUWERX J, CLÉMENT-SCHATLO V, RADOVANOVIC I, RHEINBAY E, PROVERO P, and STAMENKOVIC I Imp2 Controls Oxidative Phosphorylation and Is Crucial for Preserving Glioblastoma Cancer Stem Cells. *Genes & development* **2012**, *26* (17), 1926–44.

JIANG S-Y, LI H, TANG J-J, WANG J, LUO J, LIU B, WANG J-K, SHI X-J, CUI H-W, TANG J, YANG F, QI W, QIU W-W, and SONG B-L Discovery of a Potent HMG-CoA Reductase Degrader That Eliminates Statin-Induced Reductase Accumulation and Lowers Cholesterol. *Nature Communications* **2018**, *9* (1), 5138.

JUÁREZ-HERNÁNDEZ E, CHÁVEZ-TAPIA NC, URIBE M, and BARBERO-BECERRA VJ Role of Bioactive Fatty Acids in Nonalcoholic Fatty Liver Disease. *Nutrition journal* **2016**, *15* (1), 72.

KALLIS YN, ROBSON AJ, FALLOWFIELD JA, THOMAS HC, ALISON MR, WRIGHT NA, GOLDIN RD, IREDALE JP, and FORBES SJ Remodelling of Extracellular Matrix Is a Requirement for the Hepatic Progenitor Cell Response. *Gut* **2011**, *60* (4), 525–33.

KEEGAN A, MARTINI R, and BATEY R Ethanol-Related Liver Injury in the Rat: A Model of Steatosis, Inflammation and Pericentral Fibrosis. *Journal of Hepatology* **1995**, *23* (5), 591–600.

KESSLER S, SIMON Y, GEMPERLEIN K, GIANMOENA K, CADENAS C, ZIMMER V, POKORNY J, BARGHASH A, HELMS V, VAN ROOIJEN N, BOHLE R, LAMMERT F, HENGSTLER J, MUELLER R, HAYBAECK J, and KIEMER A Fatty Acid Elongation in Non-Alcoholic Steatohepatitis and Hepatocellular Carcinoma. *International Journal of Molecular Sciences* **2014**, *15* (4), 5762–5773.

KESSLER SM, POKORNY J, ZIMMER V, LAGGAI S, LAMMERT F, BOHLE RM, and KIEMER AK IGF2 mRNA Binding Protein P62/IMP2-2 in Hepatocellular Carcinoma: Antiapoptotic Action Is Independent of IGF2/PI3K Signaling. *American Journal of Physiology - Gastrointestinal and Liver Physiology* **2013**, *304* (4).

KESSLER SM, LAGGAI S, BARGHASH A, SCHULTHEISS CS, LEDERER E, ARTL M, HELMS V, HAYBAECK J, and KIEMER AK IMP2/P62 Induces Genomic Instability and an Aggressive Hepatocellular Carcinoma Phenotype. *Cell death & disease* **2015**, *6* (10), e1894.

KHARBANDA KK, TODERO SL, WARD BW, CANNELLA JJ, and TUMA DJ Betaine Administration Corrects Ethanol-Induced Defective VLDL Secretion. *Molecular and Cellular Biochemistry* **2009**, *327* (1–2), 75–78.

KOZA RA, NIKONOVA L, HOGAN J, RIM J-S, MENDOZA T, FAULK C, SKAF J, and KOZAK LP Changes in Gene Expression Foreshadow Diet-Induced Obesity in Genetically Identical Mice. *PLoS genetics* **2006**, *2* (5), e81.

KURAMITSU K, SVERDLOV DY, LIU SB, CSIZMADIA E, BURKLY L, SCHUPPAN D, HANTO DW, OTTERBEIN LE, and POPOV Y Failure of Fibrotic Liver Regeneration in Mice Is Linked to a Severe Fibrogenic Response Driven by Hepatic Progenitor Cell Activation. *The American Journal of Pathology* **2013**, *183* (1), 182–194.

KUTAY H, KLEPPER C, WANG B, HSU S, DATTA J, YU L, ZHANG X, MAJUMDER S, MOTIWALA T, KHAN N, BELURY M, MCCLAIN C, JACOB S, and GHOSHAL K Reduced Susceptibility of DNA Methyltransferase 1 Hypomorphic (Dnmt1N/+) Mice to Hepatic Steatosis upon Feeding Liquid Alcohol Diet. *PloS one* **2012**, *7* (8), e41949.

LAGGAI S, SIMON Y, RANSSWEILER T, KIEMER AK, and KESSLER SM Rapid Chromatographic Method to Decipher Distinct Alterations in Lipid Classes in NAFLD/NASH. *World journal of hepatology* **2013**, *5* (10), 558–67.

LAGGAI S, KESSLER SM, BOETTCHER S, LEBRUN V, GEMPERLEIN K, LEDERER E, LECLERCQ I A., MUELLER R, HARTMANN RW, HAYBAECK J, and KIEMER A. K The IGF2 mRNA Binding Protein P62/IGF2BP2-2 Induces Fatty Acid Elongation as a Critical Feature of Steatosis. *The Journal of Lipid Research* **2014**, *55* (6), 1087–1097.

LAI WS, CARBALLO E, STRUM JR, KENNINGTON EA, PHILLIPS RS, and BLACKSHEAR PJ Evidence That Tristetraprolin Binds to AU-Rich Elements and Promotes the Deadenylation and Destabilization of Tumor Necrosis Factor Alpha mRNA. *Molecular and cellular biology* **1999**, *19* (6), 4311–23.

LANTHIER N, MOLENDI-COSTE O, HORSMANS Y, VAN ROOIJEN N, CANI PD, and LECLERCQ IA Kupffer Cell Activation Is a Causal Factor for Hepatic Insulin Resistance. *American Journal of Physiology-Gastrointestinal and Liver Physiology* **2010**, *298* (1), G107–G116.

LANTHIER N, MOLENDI-COSTE O, CANI PD, VAN ROOIJEN N, HORSMANS Y, and LECLERCQ IA Kupffer Cell Depletion Prevents but Has No Therapeutic Effect on Metabolic and Inflammatory Changes Induced by a High-Fat Diet. *The FASEB Journal* **2011**, *25* (12), 4301–4311.

LANTHIER N, RUBBIA-BRANDT L, LIN-MARQ N, CLÉMENT S, FROSSARD J-L, GOOSSENS N, HADENGUE A, and SPAHR L Hepatic Cell Proliferation Plays a Pivotal Role in the Prognosis of Alcoholic Hepatitis. *Journal of hepatology* **2015**, *63* (3), 609–21.

LANTHIER N, HORSMANS Y, and LECLERCQ IA Clodronate Liposomes: All Sites of Injection Are Not Equal. *Hepatology* **2010**, *51* (2), 721–722.

LARTER CZ Not All Models of Fatty Liver Are Created Equal: Understanding Mechanisms of Steatosis Development Is Important. *Journal of Gastroenterology and Hepatology* **2007**, *22* (9), 1353–1354.

LAVIN Y, WINTER D, BLECHER-GONEN R, DAVID E, KEREN-SHAUL H, MERAD M, JUNG S, and AMIT I Tissue-Resident Macrophage Enhancer Landscapes Are Shaped by the Local Microenvironment. *Cell* **2014**, *159* (6), 1312–1326.

LÊ AD, KO J, CHOW S, and QUAN B Alcohol Consumption by C57BL/6, BALB/c, and DBA/2 Mice in a Limited Access Paradigm. *Pharmacology Biochemistry and Behavior* **1994**, *47* (2), 375–378.

LEE B, QIAO L, KINNEY B, FENG G-S, and SHAO J Macrophage Depletion Disrupts Immune Balance and Energy Homeostasis. *PloS one* **2014**, *9* (6), e99575.

LEE J, FRISO S, CHOI S-W, LEE JH, FRISO S, and CHOI S-W Epigenetic Mechanisms Underlying the Link between Non-Alcoholic Fatty Liver Diseases and Nutrition. *Nutrients* **2014**, *6* (8), 3303–3325.

LEENDERTSE M, WILLEMS RJL, GIEBELEN IAJ, ROELOFS JJTH, VAN ROOIJEN N, BONTEN MJM, and VAN DER POLL T Peritoneal Macrophages Are Important for the Early Containment of Enterococcus Faecium Peritonitis in Mice. *Innate Immunity* **2009**, *15* (1), 3–12.

LIEBER CS, and DECARLI LM The Feeding of Alcohol in Liquid Diets: Two Decades of Applications and 1982 Update. *Alcoholism: Clinical and Experimental Research* **1982**, *6* (4), 523–531.

LIEBER CS, DECARLI LM, and SORRELL MF Experimental Methods of Ethanol Administration. *Hepatology* **1989**, *10* (4), 501–510.

LIEBISCH G, DROBNIK W, REIL M, TRÜMBACH B, ARNECKE R, OLGEMÖLLER B, ROSCHER A, and SCHMITZ G Quantitative Measurement of Different Ceramide Species from Crude Cellular Extracts by Electrospray Ionization Tandem Mass Spectrometry (ESI-MS/MS). *Journal of lipid research* **1999**, *40* (8), 1539–46.

LIEBISCH G, DROBNIK W, LIESER B, and SCHMITZ G High-Throughput Quantification of Lysophosphatidylcholine by Electrospray Ionization Tandem Mass Spectrometry. *Clinical Chemistry* **2002**, *48* (12).

LIEBISCH G, LIESER B, RATHENBERG J, DROBNIK W, and SCHMITZ G High-Throughput Quantification of Phosphatidylcholine and Sphingomyelin by Electrospray Ionization Tandem Mass Spectrometry Coupled with Isotope Correction Algorithm. *Biochimica et Biophysica Acta (BBA) - Molecular and Cell Biology of Lipids* **2004**, *1686* (1–2), 108–117.

LIEBISCH G, BINDER M, SCHIFFERER R, LANGMANN T, SCHULZ B, and SCHMITZ G High Throughput Quantification of Cholesterol and Cholesteryl Ester by Electrospray Ionization Tandem Mass Spectrometry (ESI-MS/MS). *Biochimica et Biophysica Acta (BBA) - Molecular and Cell Biology of Lipids* **2006**, *1761* (1), 121–128.

LING C, and GROOP L Epigenetics: A Molecular Link between Environmental Factors and Type 2 Diabetes. *Diabetes* **2009**, *58* (12), 2718–25.

LIPPAI D, BALA S, CATALANO D, KODYS K, and SZABO G Micro-RNA-155 Deficiency Prevents Alcohol-Induced Serum Endotoxin Increase and Small Bowel Inflammation in Mice. *Alcoholism: Clinical and Experimental Research* **2014**, *38* (8), 2217–2224.

LIU S, GALLO DJ, GREEN AM, WILLIAMS DL, GONG X, SHAPIRO RA, GAMBOTTO AA, HUMPHRIS EL, VODOVOTZ Y, and BILLIAR TR Role of Toll-like Receptors in Changes in Gene Expression and NF-Kappa B Activation in Mouse Hepatocytes Stimulated with Lipopolysaccharide. *Infection and immunity* **2002**, *70* (7), 3433–42.

LLOPIS M, CASSARD AM, WRZOSEK L, BOSCHAT L, BRUNEAU A, FERRERE G, PUCHOIS V, MARTIN JC, LEPAGE P, ROY T LE, LEFÈVRE L, LANGELIER B, CAILLEUX F, GONZÁLEZ-CASTRO AM, RABOT S, GAUDIN F, AGOSTINI H, PRÉVOT S, BERREBI D, ET AL. Intestinal Microbiota Contributes to Individual Susceptibility to Alcoholic Liver Disease. *Gut* **2016**, *65* (5), 830–839.

LORENZINI S, BIRD TG, BOULTER L, BELLAMY C, SAMUEL K, AUCOTT R, CLAYTON E, ANDREONE P, BERNARDI M, GOLDING M, ALISON MR, IREDALE JP, and FORBES SJ Characterisation of a Stereotypical Cellular and Extracellular Adult Liver Progenitor Cell Niche in Rodents and Diseased Human Liver. *Gut* **2010**, *59* (5), 645–54.

LOWES KN, BRENNAN BA, YEOH GC, and OLYNYK JK Oval Cell Numbers in Human Chronic Liver Diseases Are Directly Related to Disease Severity. *The American Journal of Pathology* **1999**, *154* (2), 537–541.

LU SC, HUANG Z-Z, YANG H, MATO JM, AVILA MA, and TSUKAMOTO H Changes in Methionine Adenosyltransferase and *S* -Adenosylmethionine Homeostasis in Alcoholic Rat Liver. *American Journal of Physiology-Gastrointestinal and Liver Physiology* **2000**, *279* (1), G178–G185.

LU SC, MARTINEZ-CHANTAR ML, and MATO JM Methionine Adenosyltransferase and S-Adenosylmethionine in Alcoholic Liver Disease. *Journal of Gastroenterology and Hepatology* **2006**, *21* (s3), S61–S64.

LU W-Y, BIRD TG, BOULTER L, TSUCHIYA A, COLE AM, HAY T, GUEST R V., WOJTACHA D, MAN TY, MACKINNON A, RIDGWAY RA, KENDALL T, WILLIAMS MJ, JAMIESON T, RAVEN A, HAY DC, IREDALE JP, CLARKE AR, SANSOM OJ, ET AL. Hepatic Progenitor Cells of Biliary Origin with Liver Repopulation Capacity. *Nature Cell Biology* **2015**, *17* (8), 971–983.

LUDWIG J, VIGGIANO TR, MCGILL DB, and OH BJ Nonalcoholic Steatohepatitis: Mayo Clinic Experiences with a Hitherto Unnamed Disease. *Mayo Clinic proceedings* **1980**, *55* (7), 434–8.

LUKACS-KORNEK V, and LAMMERT F The Progenitor Cell Dilemma: Cellular and Functional Heterogeneity in Assistance or Escalation of Liver Injury. *Journal of hepatology* **2017**, *66* (3), 619–630.

MALAKOUTI M, KATARIA A, ALI SK, and SCHENKER S Elevated Liver Enzymes in Asymptomatic Patients - What Should I Do? *Journal of clinical and translational hepatology* **2017**, *5* (4), 394–403.

MANN RE, SMART RG, and GOVONI R The Epidemiology of Alcoholic Liver Disease. *Alcohol research & health : the journal of the National Institute on Alcohol Abuse and Alcoholism* **2003**, *27* (3), 209–19.

MATHERS JC, STRATHDEE G, and RELTON CL Induction of Epigenetic Alterations by Dietary and Other Environmental Factors. *Advances in Genetics* **2010**, *71*, 3–39.

MATO JM, and LU SC Role of S-Adenosyl-L-Methionine in Liver Health and Injury. *Hepatology* **2007**, *45* (5), 1306–1312.

MATYASH V, LIEBISCH G, KURZCHALIA T V, SHEVCHENKO A, and SCHWUDKE D Lipid Extraction by Methyl-Tert-Butyl Ether

for High-Throughput Lipidomics. *Journal of lipid research* **2008**, *49* (5), 1137–46.

McClain C, and Barve S A Tale of Two Institutions. *Journal of hepatology* **2017**, *66* (4), 682–684.

McVicker BL, Rasineni K, Tuma DJ, McNiven MA, and Casey CA Lipid Droplet Accumulation and Impaired Fat Efflux in Polarized Hepatic Cells: Consequences of Ethanol Metabolism. *International Journal of Hepatology* **2012**, *2012*, 1–8.

de Medeiros IC, and de Lima JG Is Nonalcoholic Fatty Liver Disease an Endogenous Alcoholic Fatty Liver Disease? – A Mechanistic Hypothesis. *Medical Hypotheses* **2015**, *85* (2), 148–152.

Miele L, Valenza V, La Torre G, Montalto M, Cammarota G, Ricci R, Mascianà R, Forgione A, Gabrieli ML, Perotti G, Vecchio FM, Rapaccini G, Gasbarrini G, Day CP, and Grieco A Increased Intestinal Permeability and Tight Junction Alterations in Nonalcoholic Fatty Liver Disease. *Hepatology* **2009**, *49* (6), 1877–1887.

Miller RA, Chang Y, Galecki AT, Al-Regaiey K, Kopchick JJ, and Bartke A Gene Expression Patterns in Calorically Restricted Mice: Partial Overlap with Long-Lived Mutant Mice. *Molecular Endocrinology* **2002**, *16* (11), 2657–2666.

Min H-K, Kapoor A, Fuchs M, Mirshahi F, Zhou H, Maher J, Kellum J, Warnick R, Contos MJ, and Sanyal AJ Increased Hepatic Synthesis and Dysregulation of Cholesterol Metabolism Is Associated with the Severity of Nonalcoholic Fatty Liver Disease. *Cell metabolism* **2012**, *15* (5), 665–74.

Miyajima A, Tanaka M, and Itoh T Stem/Progenitor Cells in Liver Development, Homeostasis, Regeneration, and Reprogramming. *Cell Stem Cell* **2014**, *14* (5), 561–574.

Momen-Heravi F, Saha B, Kodys K, Catalano D, Satishchandran A, and Szabo G Increased Number of Circulating Exosomes and Their MicroRNA Cargos Are Potential Novel Biomarkers in Alcoholic Hepatitis. *Journal of Translational Medicine* **2015**, *13* (1), 261.

Moore EM, Mariani JN, Linsenbardt DN, Melón LC, and Boehm SL Adolescent C57BL/6J (but Not DBA/2J) Mice Consume Greater Amounts of Limited-Access Ethanol Compared to Adults and Display Continued Elevated Ethanol Intake into Adulthood. *Alcoholism: Clinical and Experimental Research* **2010**, *34* (4), 734–742.

Mota M, Banini BA, Cazanave SC, and Sanyal AJ Molecular Mechanisms of Lipotoxicity and Glucotoxicity in Nonalcoholic Fatty Liver Disease. *Metabolism* **2016**, *65* (8), 1049–1061.

Murphy SK, Yang H, Moylan CA, Pang H, Dellinger A, Abdelmalek MF, Garrett ME, Ashley–Koch A, Suzuki A, Tillmann HL, Hauser MA, and Diehl AM Relationship Between Methylome and Transcriptome in Patients With Nonalcoholic Fatty Liver Disease. *Gastroenterology* **2013**, *145* (5), 1076–1087.

Nair S, Cope K, Terence RH, and Diehl AM Obesity and Female Gender Increase Breath Ethanol Concentration: Potential Implications for the Pathogenesis of Nonalcoholic Steatohepatitis. *The American Journal of Gastroenterology* **2001**, *96* (4), 1200–1204.

Neuschwander-Tetri BA Nonalcoholic Steatohepatitis and the Metabolic Syndrome. *American Journal of the Medical Sciences* **2005**, *330* (6), 326–335.

Neyrinck AM, Cani PD, Dewulf EM, De Backer F, Bindels LB, and Delzenne NM Critical Role of Kupffer Cells in the Management of Diet-Induced Diabetes and Obesity. *Biochemical and Biophysical Research Communications* **2009**, *385* (3), 351–356.

Nielsen J, Christiansen J, Lykke-Andersen J, Johnsen AH, Wewer UM, and Nielsen FC A Family of Insulin-like Growth Factor II mRNA-Binding Proteins Represses Translation in Late Development. *Molecular and cellular biology* **1999**, *19* (2), 1262–70.

Ogilvie RL, Sternjohn JR, Rattenbacher B, Vlasova IA, Williams DA, Hau HH, Blackshear PJ, and Bohjanen PR Tristetraprolin Mediates Interferon-Gamma mRNA Decay. *The Journal of biological chemistry* **2009**, *284* (17), 11216–23.

Pagadala M, Kasumov T, McCullough AJ, Zein NN, and Kirwan JP Role of Ceramides in Nonalcoholic Fatty Liver Disease. *Trends in endocrinology and metabolism: TEM* **2012**, *23* (8), 365–71.

Page A, Paoli PP, Hill SJ, Howarth R, Wu R, Kweon S-M, French J, White S, Tsukamoto H, Mann DA, and Mann J Alcohol Directly Stimulates Epigenetic Modifications in Hepatic Stellate Cells. *Journal of hepatology* **2015**, *62* (2), 388–97.

Papandreou D, Rousso I, and Mavromichalis I Update on Non-Alcoholic Fatty Liver Disease in Children. *Clinical Nutrition* **2007**, *26* (4), 409–415.

Park P-H, Lim RW, and Shukla SD Involvement of Histone Acetyltransferase (HAT) in Ethanol-Induced Acetylation of Histone H3 in Hepatocytes: Potential Mechanism for Gene Expression. *American Journal of Physiology-Gastrointestinal and Liver Physiology* **2005**, *289* (6), G1124–G1136.

Peng Z-W, Ikenaga N, Liu SB, Sverdlov DY, Vaid KA, Dixit R, Weinreb PH, Violette S, Sheppard D, Schuppan D, and Popov Y Integrin Avβ6 Critically Regulates Hepatic Progenitor Cell Function and Promotes Ductular Reaction, Fibrosis, and Tumorigenesis. *Hepatology* **2016**, *63* (1), 217–232.

Pirola CJ, Fernández Gianotti T, Castaño GO, Mallardi P, San Martino J, Mora Gonzalez Lopez Ledesma M, Flichman D, Mirshahi F, Sanyal AJ, and Sookoian S Circulating MicroRNA Signature in Non-Alcoholic Fatty Liver Disease: From Serum Non-Coding RNAs to Liver Histology and Disease Pathogenesis. *Gut* **2015**, *64* (5), 800–12.

Pritchard MT, McMullen MR, Stavitsky AB, Cohen JI, Lin F, Medof ME, and Nagy LE Differential Contributions of C3, C5 and Decay Accelerating Factor to Ethanol-Induced Fatty Liver in Mice. *Gastroenterology* **2007**, *132* (3), 1117.

Pritchett J, Harvey E, Athwal V, Berry A, Rowe C, Oakley F, Moles A, Mann DA, Bobola N, Sharrocks AD, Thomson BJ, Zaitoun AM, Irving WL, Guha IN, Hanley NA, and Hanley KP Osteopontin Is a Novel Downstream Target of SOX9 with Diagnostic Implications for Progression of Liver Fibrosis in Humans. *Hepatology (Baltimore, Md.)* **2012**, *56* (3), 1108–16.

Puri P, Baillie RA, Wiest MM, Mirshahi F, Choudhury J, Cheung O, Sargeant C, Contos MJ, and Sanyal AJ A Lipidomic Analysis of Nonalcoholic Fatty Liver Disease. *Hepatology* **2007**, *46* (4), 1081–1090.

Puri P, Wiest MM, Cheung O, Mirshahi F, Sargeant C, Min H-K, Contos MJ, Sterling RK, Fuchs M, Zhou H, Watkins SM, and Sanyal AJ The Plasma Lipidomic Signature of Nonalcoholic Steatohepatitis. *Hepatology (Baltimore, Md.)* **2009**, *50* (6), 1827–38.

Qian Q, Jutila MA, Van Rooijen N, and Cutler JE Elimination of Mouse Splenic Macrophages Correlates with Increased Susceptibility to Experimental Disseminated Candidiasis. *Journal of immunology (Baltimore, Md. : 1950)* **1994**, *152* (10), 5000–8.

Ramaiah SK, and Jaeschke H Role of Neutrophils in the Pathogenesis of Acute Inflammatory Liver Injury. *Toxicologic Pathology* **2007**, *35* (6), 757–766.

Rao R Endotoxemia and Gut Barrier Dysfunction in Alcoholic Liver Disease. *Hepatology* **2009**, *50* (2), 638–644.

Ratziu V, Bellentani S, Cortez-Pinto H, Day C, and Marchesini G A Position Statement on NAFLD/NASH Based on the EASL 2009 Special Conference. *Journal of hepatology* **2010**, *53* (2), 372–84.

Rehm J, Samokhvalov A V., and Shield KD Global Burden of Alcoholic Liver Diseases. *Journal of Hepatology* **2013**, *59* (1), 160–168.

Richardson MM, Jonsson JR, Powell EE, Brunt EM, Neuschwander–Tetri BA, Bhathal PS, Dixon JB, Weltman MD, Tilg H, Moschen AR, Purdie DM, Demetris AJ, and Clouston AD Progressive Fibrosis in Nonalcoholic Steatohepatitis: Association With Altered Regeneration and a Ductular Reaction. *Gastroenterology* **2007**, *133* (1), 80–90.

Rinella ME, Elias MS, Smolak RR, Fu T, Borensztajn J, and Green RM Mechanisms of Hepatic Steatosis in Mice Fed a Lipogenic Methionine Choline-Deficient Diet. *Journal of Lipid Research* **2008**, *49* (5), 1068–1076.

Rivals I, Personnaz L, Taing L, and Potier M-C Enrichment or Depletion of a GO Category within a Class of Genes: Which Test? *Bioinformatics* **2007**, *23* (4), 401–407.

Rivera CA, Adegboyega P, van Rooijen N, Tagalicud A, Allman M, and Wallace M Toll-like Receptor-4 Signaling and Kupffer Cells Play Pivotal Roles in the Pathogenesis of Non-Alcoholic Steatohepatitis. *Journal of hepatology* **2007**, *47* (4), 571–9.

Robert O, Boujedidi H, Bigorgne A, Ferrere G, Voican CS, Vettorazzi S, Tuckermann JP, Bouchet-Delbos L, Tran T, Hemon P, Puchois V, Dagher I, Douard R, Gaudin F, Gary-Gouy H, Capel F, Durand-Gasselin I, Prévot S, Rousset S, et al. Decreased Expression of the Glucocorticoid Receptor-GILZ Pathway in Kupffer Cells Promotes Liver Inflammation in Obese Mice. *Journal of hepatology* **2016**, *64* (4), 916–24.

Van Rooijen N The Liposome-Mediated Macrophage 'Suicide' Technique. *Journal of Immunological Methods* **1989**, *124* (1), 1–6.

Van Rooijen N, and Sanders A Liposome Mediated Depletion of Macrophages: Mechanism of Action, Preparation of Liposomes and Applications. *Journal of Immunological Methods* **1994**, *174* (1–2), 83–93.

van Rooijen N, Sanders A, and van den Berg TK Apoptosis of Macrophages Induced by Liposome-Mediated Intracellular Delivery of Clodronate and Propamidine. *Journal of Immunological Methods* **1996**, *193* (1), 93–99.

Roskams T, Yang SQ, Koteish A, Durnez A, DeVos R, Huang X, Achten R, Verslype C, and Diehl AM Oxidative Stress and Oval Cell Accumulation in Mice and Humans with Alcoholic and Nonalcoholic Fatty Liver Disease. *The American journal of pathology* **2003**, *163* (4), 1301–11.

Roskams T Liver Stem Cells and Their Implication in Hepatocellular and Cholangiocarcinoma. *Oncogene* **2006**, *25* (27), 3818–3822.

Roskams TA, Theise ND, Balabaud C, Bhagat G, Bhathal PS, Bioulac-Sage P, Brunt EM, Crawford JM, Crosby HA, Desmet V, Finegold MJ, Geller SA, Gouw ASH, Hytiroglou P, Knisely AS, Kojiro M, Lefkowitch JH, Nakanuma Y, Olynyk JK, et al. Nomenclature of the Finer Branches of the Biliary Tree: Canals, Ductules, and Ductular Reactions in Human Livers. *Hepatology* **2004**, *39* (6), 1739–1745.

Roychowdhury S, McMullen MR, Pritchard MT, Hise AG, van Rooijen N, Medof ME, Stavitsky AB, and Nagy LE An Early Complement-Dependent and TLR-4-Independent Phase in the Pathogenesis of Ethanol-Induced Liver Injury in Mice. *Hepatology (Baltimore, Md.)* **2009**, *49* (4), 1326–34.

Runge S, Nielsen FC, Nielsen J, Lykke-Andersen J, Wewer UM, and Christiansen J H19 RNA Binds Four Molecules of Insulin-like Growth Factor II mRNA-Binding Protein. *The Journal of biological chemistry* **2000**, *275* (38), 29562–9.

Sancho-Bru P, Altamirano J, Rodrigo-Torres D, Coll M, Millán C, José Lozano J, Miquel R, Arroyo V, Caballería J, Ginès P, and Bataller R Liver Progenitor Cell Markers Correlate with Liver Damage and Predict Short-Term Mortality in Patients with Alcoholic Hepatitis. *Hepatology* **2012**, *55* (6), 1931–1941.

Sanduja S, Blanco FF, Young LE, Kaza V, and Dixon DA The Role of Tristetraprolin in Cancer and Inflammation. *Frontiers in bioscience (Landmark edition)* **2012**, *17*, 174–88.

Sauer I, Schaljo B, Vogl C, Gattermeier I, Kolbe T, Müller M, Blackshear PJ, and Kovarik P Interferons Limit Inflammatory Responses by Induction of Tristetraprolin. *Blood* **2006**, *107* (12), 4790–7.

Sawicki KT, Chang H-C, Shapiro JS, Bayeva M, Jesus A De, Finck BN, Wertheim JA, Blackshear PJ, and Ardehali H Hepatic Tristetraprolin Promotes Insulin Resistance through RNA Destabilization of FGF21. *JCI Insight* **2018**, *3* (13).

Schmitz G, and Ruebsaamen K Metabolism and Atherogenic Disease Association of Lysophosphatidylcholine. *Atherosclerosis* **2010**, *208* (1), 10–18.

Schnabl B, and Brenner DA Interactions between the Intestinal Microbiome and Liver Diseases. *Gastroenterology* **2014**, *146* (6), 1513–24.

Schultheiss CS, Laggai S, Czepukojc B, Hussein UK, List M, Barghash A, Tierling S, Hosseini K, Golob-Schwarzl N, Pokorny J, Hachenthal N, Schulz M, Helms V, Walter J, Zimmer V, Lammert F, Bohle RM, Dandolo L, Haybaeck J, et al. The Long Non-Coding RNA H19 Suppresses Carcinogenesis and Chemoresistance in Hepatocellular Carcinoma. *Cell Stress* **2017**, *1* (1), 37–54.

Schuppan D, and Schattenberg JM Non-Alcoholic Steatohepatitis: Pathogenesis and Novel Therapeutic Approaches. *Journal of Gastroenterology and Hepatology* **2013**, *28*, 68–76.

Seki E, De Minicis S, Österreicher CH, Kluwe J, Osawa Y, Brenner DA, and Schwabe RF TLR4 Enhances TGF-β Signaling and Hepatic Fibrosis. *Nature Medicine* **2007**, *13* (11), 1324–1332.

Seki E, and Schnabl B Role of Innate Immunity and the Microbiota in Liver Fibrosis: Crosstalk between the Liver and Gut. *The Journal of physiology* **2012**, *590* (3), 447–58.

Shimata K, Yoshii D, Yokouchi Y, Komohara Y, Sugawara Y, Inomata Y, and Hibi T Effect of SOX9 on Ductular Reaction and Fibrogenesis. *Transplantation* **2018**, *102*, S729.

da Silva RP, Kelly KB, Al Rajabi A, and Jacobs RL Novel Insights on Interactions between Folate and Lipid Metabolism. *BioFactors* **2014**, *40* (3), 277–283.

Simon Y The Insulin-like Growth Factor 2 (IGF2) mRNA Binding Protein P62/IGF2BP2-2 Amplifies Steatosis, Inflammation, and Fibrosis in Murine Non-Alcoholic Steatohepatitis (NASH). *Doctoral dissertation, Saarland University, Saarbrücken, Germany* **2013**.

Simon Y, Kessler Sonja M., Gemperlein K, Bohle RM, Müller R, Haybaeck J, and Kiemer AK Elevated Free Cholesterol in a P62 Overexpression Model of Non-Alcoholic Steatohepatitis. *World Journal of Gastroenterology* **2014**, *20* (47), 17839–17850.

Simon Y, Kessler Sonja M, Bohle RM, Haybaeck J, and Kiemer AK The Insulin-like Growth Factor 2 (IGF2) mRNA-Binding Protein P62/IGF2BP2-2 as a Promoter of NAFLD and HCC? *Gut* **2014**, *63* (5), 861–3.

Stadler MB, Murr R, Burger L, Ivanek R, Lienert F, Schöler A, Wirbelauer C, Oakeley EJ, Gaidatzis D, Tiwari VK, Schübeler D, and Schübeler D DNA-Binding Factors Shape the Mouse Methylome at Distal Regulatory Regions. *Nature* **2011**, *480* (7378), 490.

STIENSTRA R, SAUDALE F, DUVAL C, KESHTKAR S, GROENER JEM, VAN ROOIJEN N, STAELS B, KERSTEN S, and MÜLLER M Kupffer Cells Promote Hepatic Steatosis via Interleukin-1β-Dependent Suppression of Peroxisome Proliferator-Activated Receptor α Activity. *Hepatology* **2010**, *51* (2), 511–522.

SU L, LI N, TANG H, LOU Z, CHONG X, ZHANG C, SU J, and DONG X Kupffer Cell-Derived TNF-α Promotes Hepatocytes to Produce CXCL1 and Mobilize Neutrophils in Response to Necrotic Cells. *Cell Death & Disease* **2018**, *9* (3), 323.

SUPEK F, BOŠNJAK M, ŠKUNCA N, and ŠMUC T REVIGO Summarizes and Visualizes Long Lists of Gene Ontology Terms. *PLoS ONE* **2011**. Edited by C. Gibas, *6* (7), e21800.

SUTTER A, GENG T, LEWIN DN, CHAVIN KD, and COWART LA Dietary Fat Composition and Liver Disease: A Model OfProgressive NAFLD In Diet-Induced Obesity. *Hepatology* **2012**, *56* (S1), 191A-1144A.

SYN W-K, CHOI SS, LIASKOU E, KARACA GF, AGBOOLA KM, OO YH, MI Z, PEREIRA TA, ZDANOWICZ M, MALLADI P, CHEN Y, MOYLAN C, JUNG Y, BHATTACHARYA SD, TEABERRY V, OMENETTI A, ABDELMALEK MF, GUY CD, ADAMS DH, ET AL. Osteopontin Is Induced by Hedgehog Pathway Activation and Promotes Fibrosis Progression in Nonalcoholic Steatohepatitis. *Hepatology (Baltimore, Md.)* **2011**, *53* (1), 106–15.

SYN W-K, AGBOOLA KM, SWIDERSKA M, MICHELOTTI GA, LIASKOU E, PANG H, XIE G, PHILIPS G, CHAN IS, KARACA GF, PEREIRA T DE A, CHEN Y, MI Z, KUO PC, CHOI SS, GUY CD, ABDELMALEK MF, and DIEHL AM NKT-Associated Hedgehog and Osteopontin Drive Fibrogenesis in Non-Alcoholic Fatty Liver Disease. *Gut* **2012**, *61* (9), 1323–9.

SZABO G, BALA S, PETRASEK J, and GATTU A Gut-Liver Axis and Sensing Microbes. *Digestive diseases (Basel, Switzerland)* **2010**, *28* (6), 737–44.

SZABO G, and BALA S MicroRNAs in Liver Disease. *Nature reviews. Gastroenterology & hepatology* **2013**, *10* (9), 542–52.

SZABO G, and MANDREKAR P A Recent Perspective on Alcohol, Immunity, and Host Defense. *Alcoholism, clinical and experimental research* **2009**, *33* (2), 220–32.

SZABO G, and PETRASEK J Inflammasome Activation and Function in Liver Disease. *Nature Reviews Gastroenterology & Hepatology* **2015**, *12* (7), 387–400.

SZKLARCZYK D, FRANCESCHINI A, WYDER S, FORSLUND K, HELLER D, HUERTA-CEPAS J, SIMONOVIC M, ROTH A, SANTOS A, TSAFOU KP, KUHN M, BORK P, JENSEN LJ, and VON MERING C STRING V10: Protein-Protein Interaction Networks, Integrated over the Tree of Life. *Nucleic acids research* **2015**, *43* (Database issue), D447-52.

SZKLARCZYK D, MORRIS JH, COOK H, KUHN M, WYDER S, SIMONOVIC M, SANTOS A, DONCHEVA NT, ROTH A, BORK P, JENSEN LJ, and VON MERING C The STRING Database in 2017: Quality-Controlled Protein-Protein Association Networks, Made Broadly Accessible. *Nucleic acids research* **2017**, *45* (D1), D362–D368.

TARLOW BD, PELZ C, NAUGLER WE, WAKEFIELD L, WILSON EM, FINEGOLD MJ, and GROMPE M Bipotential Adult Liver Progenitors Are Derived from Chronically Injured Mature Hepatocytes. *Cell stem cell* **2014**, *15* (5), 605–18.

TAYLOR GA, CARBALLO E, LEE DM, LAI WS, THOMPSON MJ, PATEL DD, SCHENKMAN DI, GILKESON GS, BROXMEYER HE, HAYNES BF, and BLACKSHEAR PJ A Pathogenetic Role for TNFα in the Syndrome of Cachexia, Arthritis, and Autoimmunity Resulting from Tristetraprolin (TTP) Deficiency. *Immunity* **1996**.

TERATANI T, TOMITA K, SUZUKI T, OSHIKAWA T, YOKOYAMA H, SHIMAMURA K, TOMINAGA S, HIROI S, IRIE R, OKADA Y, KURIHARA C, EBINUMA H, SAITO H, HOKARI R, SUGIYAMA K, KANAI T, MIURA S, and HIBI T A High-Cholesterol Diet Exacerbates Liver Fibrosis in Mice via Accumulation of Free Cholesterol in Hepatic Stellate Cells. *Gastroenterology* **2012**, *142* (1), 152-164.e10.

TILG H, and MOSCHEN AR Evolution of Inflammation in Nonalcoholic Fatty Liver Disease: The Multiple Parallel Hits Hypothesis. *Hepatology* **2010**, *52* (5), 1836–1846.

TOSELLO-TRAMPONT A-C, LANDES SG, NGUYEN V, NOVOBRANTSEVA TI, and HAHN YS Kupffer Cells Trigger Nonalcoholic Steatohepatitis Development in Diet-Induced Mouse Model through Tumor Necrosis Factor-α Production. *The Journal of biological chemistry* **2012**, *287* (48), 40161–72.

TRIPATHI A, DEBELIUS J, BRENNER DA, KARIN M, LOOMBA R, SCHNABL B, and KNIGHT R The Gut–Liver Axis and the Intersection with the Microbiome. *Nature Reviews Gastroenterology & Hepatology* **2018**, *15* (7), 397–411.

TRIPATHI D, WELCH E, CHEEKATLA SS, RADHAKRISHNAN RK, VENKATASUBRAMANIAN S, PAIDIPALLY P, VAN A, SAMTEN B, DEVALRAJU KP, NEELA VSK, VALLURI VL, MASON C, NELSON S, and VANKAYALAPATI R Alcohol Enhances Type 1 Interferon-α Production and Mortality in Young Mice Infected with Mycobacterium Tuberculosis. *PLOS Pathogens* **2018**. Edited by D. M. Lewinsohn, *14* (8), e1007174.

TSUCHIDA T, and FRIEDMAN SL Mechanisms of Hepatic Stellate Cell Activation. *Nature Reviews Gastroenterology & Hepatology* **2017**, *14* (7), 397–411.

TSUCHIYA M, JI C, KOSYK O, SHYMONYAK S, MELNYK S, KONO H, TRYNDYAK V, MUSKHELISHVILI L, POGRIBNY IP, KAPLOWITZ N,

and Rusyn I Interstrain Differences in Liver Injury and One-Carbon Metabolism in Alcohol-Fed Mice. *Hepatology (Baltimore, Md.)* **2012**, *56* (1), 130–9.

Van Tubergen E, Vander Broek R, Lee J, Wolf G, Carey T, Bradford C, Prince M, Kirkwood KL, and D'Silva NJ Tristetraprolin Regulates Interleukin-6, Which Is Correlated with Tumor Progression in Patients with Head and Neck Squamous Cell Carcinoma. *Cancer* **2011**, *117* (12), 2677–89.

Turnbaugh PJ, Ley RE, Mahowald MA, Magrini V, Mardis ER, and Gordon JI An Obesity-Associated Gut Microbiome with Increased Capacity for Energy Harvest. *Nature* **2006**, *444* (7122), 1027–131.

Tybl E, Shi F-D, Kessler SM, Tierling S, Walter J, Bohle RM, Wieland S, Zhang J, Tan EM, and Kiemer AK Overexpression of the IGF2-mRNA Binding Protein P62 in Transgenic Mice Induces a Steatotic Phenotype. *Journal of Hepatology* **2011**, *54* (5), 994–1001.

Vance JE, and Vance DE The Role of Phosphatidylcholine Biosynthesis in the Secretion of Lipoproteins from Hepatocytes. *Canadian Journal of Biochemistry and Cell Biology* **1985**, *63* (8), 870–881.

Vandesompele J, De Preter K, Pattyn F, Poppe B, Van Roy N, De Paepe A, and Speleman F Accurate Normalization of Real-Time Quantitative RT-PCR Data by Geometric Averaging of Multiple Internal Control Genes. *Genome biology* **2002**, *3* (7), RESEARCH0034.

Varlinskaya EI, and Spear LP Ontogeny of Acute Tolerance to Ethanol-Induced Social Inhibition in Sprague?Dawley Rats. *Alcoholism: Clinical and Experimental Research* **2006**, *30* (11), 1833–1844.

van der Veen JN, Lingrell S, and Vance DE The Membrane Lipid Phosphatidylcholine Is an Unexpected Source of Triacylglycerol in the Liver. *The Journal of biological chemistry* **2012**, *287* (28), 23418–26.

Venkatesan S, Ward RJ, and Peters TJ Effect of Chronic Ethanol Feeding on the Hepatic Secretion of Very-Low-Density Lipoproteins. *Biochimica et Biophysica Acta (BBA) - Lipids and Lipid Metabolism* **1988**, *960* (1), 61–66.

VerHague MA, Cheng D, Weinberg RB, and Shelness GS Apolipoprotein A-IV Expression in Mouse Liver Enhances Triglyceride Secretion and Reduces Hepatic Lipid Content by Promoting Very Low Density Lipoprotein Particle ExpansionSignificance. *Arteriosclerosis, Thrombosis, and Vascular Biology* **2013**, *33* (11), 2501–2508.

Vernon G, Baranova A, and Younossi ZM Systematic Review: The Epidemiology and Natural History of Non-Alcoholic Fatty Liver Disease and Non-Alcoholic Steatohepatitis in Adults. *Alimentary Pharmacology & Therapeutics* **2011**, *34* (3), 274–285.

Wahlsten D, Bachmanov A, Finn DA, and Crabbe JC Stability of Inbred Mouse Strain Differences in Behavior and Brain Size between Laboratories and across Decades. *Proceedings of the National Academy of Sciences of the United States of America* **2006**, *103* (44), 16364–9.

Wan J, Benkdane M, Teixeira-Clerc F, Bonnafous S, Louvet A, Lafdil F, Pecker F, Tran A, Gual P, Mallat A, Lotersztajn S, and Pavoine C M2 Kupffer Cells Promote M1 Kupffer Cell Apoptosis: A Protective Mechanism against Alcoholic and Nonalcoholic Fatty Liver Disease. *Hepatology* **2014**, *59* (1), 130–142.

Wang HJ, Zakhari S, and Jung MK Alcohol, Inflammation, and Gut-Liver-Brain Interactions in Tissue Damage and Disease Development. *World journal of gastroenterology* **2010**, *16* (11), 1304–13.

Wang M, You Q, Lor K, Chen F, Gao B, and Ju C Chronic Alcohol Ingestion Modulates Hepatic Macrophage Populations and Functions in Mice. *Journal of Leukocyte Biology* **2014**, *96* (4), 657–665.

Wehr H, Rodo M, Lieber CS, and Baraona E Acetaldehyde Adducts and Autoantibodies against VLDL and LDL in Alcoholics. *Journal of lipid research* **1993**, *34* (7), 1237–44.

Wieser V, Tymoszuk P, Adolph TE, Grander C, Grabherr F, Enrich B, Pfister A, Lichtmanegger L, Gerner R, Drach M, Moser P, Zoller H, Weiss G, Moschen AR, Theurl I, and Tilg H Lipocalin 2 Drives Neutrophilic Inflammation in Alcoholic Liver Disease. *Journal of Hepatology* **2016**, *64* (4), 872–880.

Wieser V, Adolph TE, Enrich B, Kuliopulos A, Kaser A, Tilg H, and Kaneider NC Reversal of Murine Alcoholic Steatohepatitis by Pepducin-Based Functional Blockade of Interleukin-8 Receptors. *Gut* **2017**, *66* (5), 930–938.

Wong VW-S, Wong GL-H, Chan H-Y, Yeung DK-W, Chan RS-M, Chim AM-L, Chan CK-M, Tse Y-K, Woo J, Chu WC-W, and Chan HL-Y Bacterial Endotoxin and Non-Alcoholic Fatty Liver Disease in the General Population: A Prospective Cohort Study. *Alimentary Pharmacology & Therapeutics* **2015**, *42* (6), 731–740.

Wu C-L, McNeill J, Goon K, Little D, Kimmerling K, Huebner J, Kraus V, and Guilak F Conditional Macrophage Depletion Increases Inflammation and Does Not Inhibit the Development of Osteoarthritis in Obese Macrophage Fas-Induced Apoptosis-Transgenic Mice. *Arthritis & Rheumatology* **2017**, *69* (9), 1772–1783.

Xiao X, Yeoh BS, and Vijay-Kumar M Lipocalin 2: An Emerging Player in Iron Homeostasis and Inflammation. *Annual Review of Nutrition* **2017**, *37* (1), 103–130.

Xu M-J, Feng D, Wu H, Wang H, Chan Y, Kolls J, Borregaard N, Porse B, Berger T, Mak TW, Cowland JB, Kong X, and Gao B Liver Is the Major Source of Elevated Serum Lipocalin-2 Levels after Bacterial Infection or Partial Hepatectomy: A Critical Role for IL-6/STAT3. *Hepatology (Baltimore, Md.)* **2015**, *61* (2), 692–702.

Yamaguchi K, Yang L, McCall S, Huang J, Yu XX, Pandey SK, Bhanot S, Monia BP, Li Y-X, and Diehl AM Inhibiting Triglyceride Synthesis Improves Hepatic Steatosis but Exacerbates Liver Damage and Fibrosis in Obese Mice with Nonalcoholic Steatohepatitis. *Hepatology* **2007**, *45* (6), 1366–1374.

Yan AW, Fouts DE, Brandl J, Stärkel P, Torralba M, Schott E, Tsukamoto H, Nelson KE, Brenner DA, and Schnabl B Enteric Dysbiosis Associated with a Mouse Model of Alcoholic Liver Disease. *Hepatology (Baltimore, Md.)* **2011**, *53* (1), 96–105.

Yang C-Y, Chen J-B, Tsai T-F, Tsai Y-C, Tsai C-Y, Liang P-H, Hsu T-L, Wu C-Y, Netea MG, Wong C-H, and Hsieh S-L CLEC4F Is an Inducible C-Type Lectin in F4/80-Positive Cells and Is Involved in Alpha-Galactosylceramide Presentation in Liver. *PloS one* **2013**, *8* (6), e65070.

Yanger K, Zong Y, Maggs LR, Shapira SN, Maddipati R, Aiello NM, Thung SN, Wells RG, Greenbaum LE, and Stanger BZ Robust Cellular Reprogramming Occurs Spontaneously during Liver Regeneration. *Genes & development* **2013**, *27* (7), 719–24.

Yao Z, and Vance DE Reduction in VLDL, but Not HDL, in Plasma of Rats Deficient in Choline. *Biochemistry and Cell Biology* **1990**, *68* (2), 552–558.

Yilmaz Y Review Article: Is Non-Alcoholic Fatty Liver Disease a Spectrum, or Are Steatosis and Non-Alcoholic Steatohepatitis Distinct Conditions? *Alimentary Pharmacology & Therapeutics* **2012**, *36* (9), 815–823.

Yoneyama N, Crabbe JC, Ford MM, Murillo A, and Finn DA Voluntary Ethanol Consumption in 22 Inbred Mouse Strains. *Alcohol* **2008**, *42* (3), 149–160.

Younossi ZM, Stepanova M, Afendy M, Fang Y, Younossi Y, Mir H, and Srishord M Changes in the Prevalence of the Most Common Causes of Chronic Liver Diseases in the United States From 1988 to 2008. *Clinical Gastroenterology and Hepatology* **2011**, *9* (6), 524-530.e1.

Younossi ZM, Koenig AB, Abdelatif D, Fazel Y, Henry L, and Wymer M Global Epidemiology of Nonalcoholic Fatty Liver Disease-Meta-Analytic Assessment of Prevalence, Incidence, and Outcomes. *Hepatology* **2016**, *64* (1), 73–84.

Yue F, Cheng Y, Breschi A, Vierstra J, Wu W, Ryba T, Sandstrom R, Ma Z, Davis C, Pope BD, Shen Y, Pervouchine DD, Djebali S, Thurman RE, Kaul R, Rynes E, Kirilusha A, Marinov GK, Williams BA, et al. A Comparative Encyclopedia of DNA Elements in the Mouse Genome. *Nature* **2014**, *515* (7527), 355–364.

Zeybel M, Hardy T, Robinson SM, Fox C, Anstee QM, Ness T, Masson S, Mathers JC, French J, White S, and Mann J Differential DNA Methylation of Genes Involved in Fibrosis Progression in Non-Alcoholic Fatty Liver Disease and Alcoholic Liver Disease. *Clinical epigenetics* **2015**, *7* (1), 25.

Zhang JY, Chan EK, Peng XX, and Tan EM A Novel Cytoplasmic Protein with RNA-Binding Motifs Is an Autoantigen in Human Hepatocellular Carcinoma. *The Journal of experimental medicine* **1999**, *189* (7), 1101–10.

Zhang X-H, Lu X, Long X-B, You X-J, Gao Q-X, Cui Y-H, and Liu Z Chronic Rhinosinusitis with and without Nasal Polyps Is Associated with Decreased Expression of Glucocorticoid-Induced Leucine Zipper. *Clinical & Experimental Allergy* **2009**, *39* (5), 647–654.

Zhao W, Liu M, D'Silva NJ, and Kirkwood KL Tristetraprolin Regulates Interleukin-6 Expression through P38 MAPK-Dependent Affinity Changes with mRNA 3' Untranslated Region. *Journal of interferon & cytokine research : the official journal of the International Society for Interferon and Cytokine Research* **2011**, *31* (8), 629–37.

Zhou H-Z, Karliner JS, and Gray MO Moderate Alcohol Consumption Induces Sustained Cardiac Protection by Activating PKC-ε and Akt. *American Journal of Physiology-Heart and Circulatory Physiology* **2002**, *283* (1), H165–H174.

Zhou Y, Jiang L, and Rui L Identification of MUP1 as a Regulator for Glucose and Lipid Metabolism in Mice. *The Journal of biological chemistry* **2009**, *284* (17), 11152–9.

Zhu L, Baker SS, Gill C, Liu W, Alkhouri R, Baker RD, and Gill SR Characterization of Gut Microbiomes in Nonalcoholic Steatohepatitis (NASH) Patients: A Connection between Endogenous Alcohol and NASH. *Hepatology* **2013**, *57* (2), 601–609.

PUBLICATIONS

Publications

Submitted to *Frontiers in medicine:* CZEPUKOJC B, BARGHASH A, TIERLING S, NAß N, SIMON Y, KÖRBEL C, CADENAS C, VAN HUL NKM, SACHINIDIS A, HENGSTLER JG, HELMS V, LASCHKE MW, WALTER J, HAYBAECK J, LECLERCQ I, KIEMER AK, and KESSLER SM IGF2 mRNA binding protein 2 transgenic mice are more prone to develop a ductular reaction and to progress towards cirrhosis.

RAMISCH A, HEINRICH V, GLASER L V., FUCHS A, YANG X, BENNER P, SCHOEPFLIN R, LI N, KINKLEY S, HILLMANN A, LONGINOTTO J, HEYNE S, CZEPUKOJC B, KESSLER SM, KIEMER AK, CADENAS C, ARRIGONI L, GASPARONI N, MANKE T, ET AL. CRUP: A Comprehensive Framework to Predict Condition-Specific Regulatory Units. *bioRxiv* **2018**, 501601.

SCHULTHEISS CS, LAGGAI S, CZEPUKOJC B, HUSSEIN UK, LIST M, BARGHASH A, TIERLING S, HOSSEINI K, GOLOB-SCHWARZL N, POKORNY J, HACHENTHAL N, SCHULZ M, HELMS V, WALTER J, ZIMMER V, LAMMERT F, BOHLE RM, DANDOLO L, HAYBAECK J, ET AL. The Long Non-Coding RNA H19 Suppresses Carcinogenesis and Chemoresistance in Hepatocellular Carcinoma. *Cell Stress* **2017**, *1* (1), 37–54.

DEMBEK A, LAGGAI S, KESSLER SM, CZEPUKOJC B, SIMON Y, KIEMER AK, and HOPPSTÄDTER J Hepatic Interleukin-6 Production Is Maintained during Endotoxin Tolerance and Facilitates Lipid Accumulation. *Immunobiology* **2017**, *222* (6), 786–796.

FENGLER VHI, MACHEINER T, KESSLER SM, CZEPUKOJC B, GEMPERLEIN K, MÜLLER R, KIEMER AK, MAGNES C, HAYBAECK J, LACKNER C, and SARGSYAN K Susceptibility of Different Mouse Wild Type Strains to Develop Diet-Induced NAFLD/AFLD-Associated Liver Disease. *PLoS ONE* **2016**, *11* (5), e0155163.

Abstracts for conferences / poster presentation

CZEPUKOJC B, KESSLER SM, CADENAS C, GIANMOENA K, GASPARONI N, NORDSTRÖM K, GASPARONI G, SINHA A, FALK-PAULSEN M, ROSENSTIEL P, HENGSTLER JG, WALTER J, and KIEMER AK P01-10YI: Epigenomic Profiling of Hepatocytes Overexpressing the Lipogenic and Tumor-Promoting mRNA Binding Protein *p62/IMP2-2*. *Poster presentation at the 1ˢᵗ EASL NAFLD Summit: Target-oriented approach to diagnosis and pharmacotherapy of NASH: a dialogue between academia and industry,* Rome, Italy, **2017**. Supported by an EASL Young Investigator's Bursary

CZEPUKOJC B, KESSLER SM, CADENAS C, GIANMOENA K, GASPARONI N, NORDSTRÖM K, GASPARONI G, SINHA A, FALK-PAULSEN M, LIEBISCH G, HAYBAECK J, ROSENSTIEL P, HENGSTLER JG, WALTER J, KIEMER AK, and DEEP CONSORTIUM (GERMAN EPIGENOME PROGRAMME) Differential Gene Expression Associated with Epigenetic Changes in Steatohepatitis Is Kupffer Cell Dependent. *Poster presentation at the Annual Meeting & Science days of the International Human Epigenome Consortium (IHEC),* Berlin, Germany, **2017.** Supported by the German epigenome program (DEEP) and the Bundesministerium für Bildung und Forschung (BMBF).

Acknowledgements